High Content Screening and Proteomic Analysis Identify a Kinase Inhibitor that rescues pathological phenotypes in a Patient-Derived Model of Parkinson's Disease

Nasia Antoniou[1, 2], Kanella Prodromidou[1], Georgia Kouroupi[1], Martina Samiotaki[3], George Panayotou[3], Maria Xilouri[4], Leonidas Stefanis[4, 5], Regis Grailhe[6], Era Taoufik[1*] and Rebecca Matsas[1*#]

[1]Laboratory of Cellular and Molecular Neurobiology-Stem Cells, Hellenic Pasteur Institute, 127 Vassilissis Sofias Avenue, 11521 Athens, Greece

[2]Division of Animal and Human Physiology, Department of Biology, National & Kapodistrian University of Athens, Panepistimioupolis, Ilisia, Greece.

[3]Institute of Bioinnovation, Biomedical Sciences Research Center "Alexander Fleming", Vari 16672, Greece

[4]Center of Clinical Research, Experimental Surgery and Translational Research, Biomedical Research Foundation of the Academy of Athens (BRFAA), 4 Soranou Efesiou Street, 11527 Athens, Greece

[5]1st Department of Neurology, Eginition Hospital, Medical School, National and Kapodistrian University of Athens, Athens, Greece

[6]Technology Development Platform, Screening Sciences & Novel Assay Technology, Institut Pasteur Korea, Bundang-gu, Seongnam-si, Gyeonggi-do, 463-400 Republic of Korea

*Co-senior authors

[#]Correspondence: Rebecca Matsas, Laboratory of Cellular and Molecular Neurobiology-Stem Cells, Hellenic Pasteur Institute, 127 Vassilissis Sofias Avenue, 11521 Athens, Greece; rmatsa@pasteur.gr

Abstract

Combining high throughput screening approaches with induced pluripotent stem cell (iPSC)-based disease modeling represents a promising unbiased strategy to identify therapies for neurodegenerative disorders. Here we applied high content imaging on iPSC-derived neurons from patients with familial Parkinson's disease bearing the G209A (p.A53T) α-synuclein (αSyn) mutation and launched a screening campaign on a small kinase inhibitor library. We thus identified the multi-kinase inhibitor BX795 that at a single dose effectively restores disease-associated neurodegenerative phenotypes. Proteomics profiling mapped the molecular pathways underlying the protective effects of BX795, comprising a cohort of 118 protein-mediators of the core biological processes of RNA metabolism, protein synthesis, modification and clearance, and stress response, all linked to the mTORC1 signaling hub. In agreement, expression of human p.A53T-αSyn in neuronal cells affected key components of the mTORC1 pathway resulting in aberrant protein synthesis that was restored in the presence of BX795 with concurrent facilitation of autophagy. Taken together, we have identified a promising small molecule with neuroprotective actions as candidate therapeutic for PD and other protein conformational disorders.

Key words: p.A53T α-synuclein mutation, high-content imaging, proteomics, drug screening, mTOR signaling, proteostasis

Introduction

Parkinson's disease (PD) is a complex neurodegenerative disorder affecting 2% of the world population over 65 years of age (1). PD is characterized by motor dysfunction related to the progressive loss of midbrain dopamine neurons (2) while a wide range of non-motor symptoms are also present such as psychiatric manifestations and cognitive impairment (3). The neuropathological hallmark of PD is the presence of intracytoplasmic inclusions in neuronal cell bodies and neurites, respectively termed Lewy bodies and Lewy neurites (4, 5). These are protein aggregates composed mainly of α-synuclein (αSyn), the major protein linked to sporadic PD (6). αSyn belongs to a class of intrinsically disordered amyloid proteins that form specific forms of oligomeric and fibrillar aggregates and exert neurotoxicity through various molecular pathways (7). Several point mutations (A30P, E46K, A53T, G51D) and multiplications of the *SNCA* locus encoding for αSyn cause autosomal dominant forms of PD (8-10). Among the different variants, the p.A53TαSyn mutation is generally considered to accelerate aggregation (11) resulting in widespread accumulation of insoluble α-syn deposits that have been identified in the post-mortem p.A53T human brain (12, 13). Despite extensive efforts in understanding PD pathogenesis, no disease modifying drugs exist. Currently only symptomatic or palliative treatments are available with none capable to prevent or slow-down disease progression. Dopamine-replacement drugs, such as levodopa, which was identified 53 years ago (14), are used to ameliorate motor symptoms and remain the primary and most effective treatment despite the undesired side-effects and deterioration of efficacy with disease progression. Therefore, the development of disease-modifying drugs is an urgent unmet need. Most present-day efforts in identifying novel PD therapeutics target the aggregation of misfolded αSyn as the major pathogenic factor that causes cellular toxicity (6, 15-17). Alternative strategies to tackle early steps in

neurodegeneration, particularly in an unbiased approach, have lagged behind. Recent advances in patient-derived induced pluripotent stem cell (iPSC)-based models for neurodegenerative diseases permit the detection of early, potentially triggering, pathologic phenotypes and provide amenable systems for drug discovery. In combination with high throughput high content screening technologies, these approaches open new perspectives for identification of disease-modifying compounds (18-21).

We have previously established a model of iPSC-derived neurons from patients with familial PD harboring the p.A53T αSyn mutation (G209A in the *SNCA* gene) that displays disease-relevant phenotypes at basal conditions (22).In this study, we successfully adapted this cellular system to perform the first small molecule screen on human p.A53T-neurons and discovered that the multi-kinase inhibitor BX795 significantly reverts disease-associated phenotypes. A single treatment of patient neurons with BX795 has sustainable effects in supporting neuritic growth, restoring axonal pathology and limiting αSyn protein aggregate formation. Protection from p.A53T-associated pathology was also confirmed in human iPSC-derived neurons in which the mutation was introduced by genome editing, against isogenic wild-type controls. Strikingly, proteomics profiling by quantitative mass spectrometry revealed that BX795 treatment results in significant downregulation of a cohort of 118 proteins that are abnormally upregulated in p.A53T-neurons. Enrichment analysis demonstrated that these proteins are associated with mRNA metabolism, mRNA transport and translation, protein metabolism and degradation processes. Using neuronal cells expressing the human p.A53T-αSyn, we demonstrate that BX795 affects the mTORC1 pathway to restrict excessive protein synthesis and facilitate autophagy. Taken together, our data highlight the BX795 kinase inhibitor as a compelling compound and candidate therapeutic that ameliorates p.A53T-related pathology.

Results

Assay development for high-content screening of p.A53T-iPSC derived neurons

iPSCs used in this study were previously generated from a PD patient bearing the p.A53T αSyn mutation and thoroughly characterized (22). For directed differentiation a dual SMAD inhibition protocol was used in the presence of Noggin and TGFβ inhibitor (22-24), which favors the generation and expansion of Pax6+/Nestin+ neural progenitor cells (NPCs; Fig. 1a). NPCs were further differentiated into βIII-tubulin (TUJ1)+ neurons (Fig. 1a) with 15-20% also expressing the dopaminergic marker TH at 21 DIV (Fig. 1a). The expression of dopaminergic lineage markers, such as Nurr1, TH, and aromatic amino acid decarboxylase (AADC) was confirmed by qRT-PCR (Fig. S1a). As readout for compound screening, we assessed TH immunofluorescence in iPSC-derived neurons adapted in miniature 384-well plates, seeking to identify putative neuroprotective compounds enhancing dopaminergic neuron output. To this end, the fluorescent signal for TH within a well was normalized to the fluorescent signal for the pan-neuronal marker βIII-tubulin (TUJ1) (Fig. 1b).

High content screening of a kinase inhibitor library identifies BX795 as a compound that increases TH immunofluorescence in p.A53T-neurons

Protein kinases represent central molecular hubs that regulate numerous cell processes, thus constituting potentially attractive clinical targets. Indeed, the success of kinase inhibitors in treating cancer has spurred the evaluation of such compounds in phase II/III clinical trials as candidates for treatment of various neurodegenerative diseases (25, 26). Since several kinases have been implicated in PD pathology (27), we screened a collection of 273 small molecule kinase inhibitors (Table S1) to identify compounds with prospective neuroprotective properties. p.A53T cells were exposed once (7 DIV) to the library of kinase

inhibitors at 1µM concentration and quantitative image analysis was performed at 21 DIV (Fig. 1a). Hits were defined as compounds that robustly conferred an increase in TH immunofluorescence compared to DMSO-treated p.A53T neurons within a well, normalized to the immunofluorescence of the pan-neuronal marker βIII-tubulin (TUJ1) (Fig. 1b). Toxic compounds were excluded by assessing cellular viability (total nuclei count) of compound-treated as compared to DMSO-treated cells (Fig. S2). Four hits were identified in the primary screen (Fig. 1b), which were re-tested for validation in a dose-response assay (Fig. 1d). Of these BX795, an aminopyrimidine compound that acts as a multi-kinase inhibitor with pro-survival and/or anti-inflammatory effects (28), significantly increased TH immunofluorescence at 1 µM (Figs. 1c, d). BX-795 was initially developed as an ATP-competitive inhibitor of 3-phosphoinositide-dependent kinase 1 (PDK1), but was later shown to inhibit the IKK-related kinase, TANK-binding kinase 1 (TBK1) and IKKε, as well as to have numerous additional targets (29-31). Based on the sustained effect of a single dose of BX795 on p.A53T dopaminergic neurons (Fig. 1d), we focused further on this compound to explore its function.

BX795 rescues neuropathological features of p.A53T neurons

The effects of BX795 on p.A53T-neurons were tested in cells that received a single treatment of the kinase inhibitor (1 µM) at 7 DIV and were analyzed at 21 DIV, in accordance with the protocol applied during the screening procedure. Prior to this, an initial set of experiments was performed using drug concentrations from 0.1-2 µM and repeated drug additions every 3 days, with the selected scheme ensuring optimal efficacy and minimal toxicity. Initially, we asked if the enhancement in TH immunofluorescence could be attributed to an increase in cell survival/proliferation or dopaminergic differentiation in p.A53T-cultures. We could not

detect BX795-driven changes in either proliferation, as assessed by the percentage of Ki67+ cells (Fig. S1b; % Ki67+ cells, DMSO: 43.3 ± 4.4; BX795: 50.3 ± 1.5, n=3), or in differentiation as estimated by the percentage of TH+ cells in the culture (% TH+ / TUJ1+ neurons , DMSO: 13.9 ± 3.1; BX795: 18.1.0 ± 3.9, n=3). These observations indicate that the effect of BX795 on dopaminergic neurons is not related to an increase in either survival/proliferation or differentiation.

Next, we investigated if treatment with BX795 could rescue neuropathological features previously identified in p.A53T-neurons, such as compromised neuritic growth, dystrophic or fragmented neurites and the presence of intracellular protein aggregates (22, 32). Overall, disease-associated phenotypes were assessed in iPSC-derived neurons from two p.A53T patients [22] and an iPSC gene-edited line in which the p.A53T mutation was inserted in one allele, against healthy or isogenic controls. Evaluation of total neurite length in TH+ dopaminergic neurons from the first p.A53T patient revealed a significant increase in response to BX795 compatible with the observed increase in TH immunofluorescence (length in µm, ctl: 221.7 ± 16.8, p.A53T:127.2 ± 13.5, p.A53T+ BX795: 196.8 ± 21.1, n=5, Fig.2a). Moreover, examination of the distinct pathological morphology of TUJ1+ p.A53T neurons revealed an almost 50% reduction in axonal degeneration (axon degeneration index: ctl: 2.945 ± 1.325, p.A53T:13.03 ± 1.491, p.A53T+ BX795: 7.276 ± 1.017 n=3; Fig. 2b). Finally, exposure to BX795 resulted in a notable 60% decrease in protein aggregate formation in p.A53T cells (number of aggregates per cell, p.A53T: 8.431 ± 0.77, n= 51, p.A53T+ BX795: 3.242 ± 0.40, n=62; Fig. 2c). This was accompanied by a consistent decline in the levels of (Ser129)-phosphorylated αSyn (Fig. 2d), a modification that renders αSyn prone to self-assembly and is commonly associated with synucleinopathy (33, 34). The

neuroprotective effects of BX795 were confirmed in p.A53T-neurons from a second patient (22, 32) (Fig. S3).

We also assessed the neuroprotective effects of BX795 in a highly enriched culture of mature human midbrain dopaminergic neurons (Fujifilm Cellular Dynamics Inc). These comprised an isogenic pair of wild-type (iCell DOPA) and gene-edited (iCell A53T DOPA) iPSC-derived neurons in which a heterozygous p.A53T mutation was inserted into one allele of the *SNCA* gene. After 14 days, more than 90% of cells were TUJ1+ and more than 80% were TH+ dopaminergic neurons (Fig3a). At this time and similarly to patient-derived cells, abundant protein aggregates were detected in the p.A53T iCell neurons compared to their isogenic control, and treatment with BX795 resulted in a significant reduction (number of aggregates per cell, ctl:2.7±0.49,n=57, p.A53T: 9.9 ± 1.1, n=76, p.A53T+ BX795:4.9 ±0.7, n=76; Fig3b,c). Taken together our results indicate that BX795 exerts prominent and sustainable neuroprotection in p.A53T neurons by improving neuritic growth, limiting the levels of pathological αSyn and restricting aggregate formation whilst maintaining axonal integrity. The beneficial effects of BX795 were noted whether it was added early during neuronal differentiation or at later stages of neuronal maturation when disease-associated phenotypes were was already established.

Proteomics analysis identifies cellular pathways targeted by BX795 in p.A53T neurons

Identification of the BX795 affected cellular pathways which vary according to the system investigated (30, 31, 35), is a challenging task. Therefore, we used an unbiased approach based on comparative proteomics. Similarly to the screening procedure, BX795 was added once at DIV 7 and proteomics analysis was performed at DIV 21 when rescue of neuropathological phenotypes was noted (Fig. 2). A total of 1652 proteins were identified

and quantified using the MaxQuant software (36, 37), followed by filtering of low quality protein hits with the Perseus software. Initial comparison between p.A53T versus control neurons in the absence of BX795, revealed differential expression of 640 proteins (Fig. S4a) from which only 67 were down-regulated whilst the rest 573 were up-regulated (Fig. S4b, Table S2). This large increase in protein expression was linked by GO enrichment analysis mainly to the biological processes of transcription, translation, protein synthesis and modification (Fig. S4b). Remarkably, the levels of a cohort of 118 proteins lying mostly within these biological processes and representing approximately 20% of the total dysregulated proteins in p.A53T neurons, were restored upon treatment with BX795 ($p<0.05$) (Fig. 4a, Table S3). Most important, this outcome was specific to p.A53T-neurons as BX795 had no significant effect on the proteome of control neurons.

Extensive data mining by GO enrichment analysis for biological processes, molecular function and cellular compartments ($p<0.01$), complemented by reactome pathway analysis ($p<0.01$), highlighted the dysregulated core pathways in p.A53T-neurons and, amongst them, those targeted by BX795 to restore neuronal physiology (Fig. 4b). These include proteins associated with RNA metabolism, protein synthesis, protein modification and transport, stress response, and neurodegeneration, as outlined below.

RNA metabolism. The p.A53T proteome showed enrichment for proteins in subcellular compartments known to be associated with αSyn (38), including membrane bound organelles (204 proteins), mitochondria (118), ribosomal complexes (29), nucleus (292), and neuron projection/axon cytoplasm (10) (Table S4). Processes such as cellular metabolism, translational initiation and regulation, tRNA aminoacetylation and export from nucleus, mRNA stability and export from nucleus, rRNA processing, formation of pre-initiation complex and protein folding were among the top pathways enriched in the p.A53T

proteome (Fig. S4). A previous study has identified mRNA binding proteins (RBPs) and those involved in protein biosynthesis within the protein network residing in immediate vicinity of αSyn, suggesting that perturbation of these pathways may be directly related to pathology (38). Herein, we provide evidence that these same pathways are altered when p.A53T is expressed in human neurons (Fig. S4). Specifically, a significant number of RBPs (60 proteins) were differentially expressed, including members with known neuronal localization and involvement in neuronal functions, such as ELAV-1, ELAV-3, RBBP7, RNPS1, RNMT, TARDBP, XPO1, XPO5, HNRNPA1, HNRNPA1L2, HNRNPF, HNRNPL, HNRPNPM, HRNNPUL1, PABPC1, PABPC4, PTBP2 and CELF1 (Table S2). Since even small changes in RBP expression or activity are amplified due to their broad impact on expression, splicing and translation of numerous RNA substrates, changes in such a large number of these RNA regulators suggest a severe perturbation in RNA homeostasis in p.A53T-neurons. A cluster of RBPs implicated in splicing and adenylation events in the nuclear compartment (DEK, MYEF2, UBTF, SNRPB, PCBP1, ZNF207, HINT1, RAE1, HNRNPUL1) was restored after BX795 treatment (Fig. 5a).

Protein Synthesis. Disturbances in RBP dosage have detrimental consequences also outside the nucleus, as they control the targeted localization of mRNAs, either proximally in the cell soma or distally in the projecting axon, affecting whether an mRNA will be translated or remain translationally silent and whether it will be stored for local mRNA translation or degraded (39). Aberrant expression of the translational machinery emerged in the p.A53T proteome with translational initiation and regulation processes being the most affected in mutant neurons (Fig. S4b, Table S2). A total of 18 proteins involved in the formation of the pre-initiation complex were identified and included EIF2, 3, 4 and 5, of which EIF4G2 that functions as a general suppressor of translation by forming translationally inactive stress granules, was targeted by BX795 (Fig. 5a). Ribosomal proteins (29 proteins), structural

components of ribosome subunits, were upregulated in p.A53T-neurons (Table S2) and a significant fraction returned to near-control levels after BX795 treatment (Fig. 5a). These included RPL31 and RPL12, which are involved in 60S biogenesis, and RPS6, a component of the 40S subunit and downstream effector of the mTORC1 signaling pathway. tRNA processing represents another important part of the translational cascade that was altered in p.A53T-neurons (Table S2), while a significant fraction was restored by BX795, including the aminoacyl-tRNA synthetases RARS (arginyl-tRNA synthase), VARS (valyl-tRNA synthase), and WARS (tryptophanyl-tRNA synthase) together with regulatory or accessory proteins such as PPA1, EEF1D PRMPT1, FAM98B and RTCB. Growing evidence associates changes in tRNA gene biogenesis and processing with neurodegenerative diseases (40). Our data reveal for the first time a link between p.A53T-αSyn expression and this molecular process (Fig. 5a, Table S2).

Protein modification and transport. p.A53T-αSyn toxicity has been attributed to problematic modifications at the ER membrane and disturbances in ER-Golgi and early endosomal/vesicle trafficking (33, 38, 41, 42). In accordance, p.A53T-neurons exhibit altered protein levels in components of these pathways (Table S2). Among these, five members of the adaptor protein complexes that function in transport-vesicle mediated transfer between membranous structures are increased by p.A53T-expression (AP1B1, AP2A2, AP3B1, AP3D1 and AP3M1). Another prominent category included members of the largest branch of Ras-like small GTPases involved in membrane trafficking (RAB2A, RAB2B, RAB6B). In addition, proteins participating in ER to Golgi transport and macroautophagy (SEC22B, SEC31A, RAB18, ARF1, ARF3) (43, 44), vesicle budding/uncoating in the Golgi apparatus (ARF1,ARF3) (45), SNARE-mediated autophagosome-lysosome fusion (RAB21) (46), retrograde Golgi to ER

transport (COPA, COPB, COPG) (Table S2) were also differentially expressed in p.A53T neurons.

BX795 had a selective effect on p.A53T-altered membrane transport proteins (SRP9, GDI2, ATP6VOD1, DAD1 subunit of oligosaccahryl transferase complex and OGT, and NAPB) and components of the SNARE complex (SAR1A, SEC22B and YKT6) (Fig. 5a) whilst alterations on molecules of the RAB, adaptor protein complex and coatomer remained largely unaffected.

Stress Response. p.A53T-αSyn protein expression acts as a primary neurotoxin triggering a battery of stress responses in human neurons (47). The proteomics analysis indicated that p.A53T neurons activate most of these mechanisms. Both the unfolded protein response (UPR), as evidenced by mis-expression of chaperones CCT2, 3, 4, 5, 7 and 8, as well as the heat shock protein response (HSP), with proteins such as DNAJA1, DNAJB11, DNAJC7, HSPA4L, HSP9 and HSPE1, were apparent in the p.A53T-proteome (Table S2). These stress response pathways were significantly downregulated in p.A53T neurons treated with BX795, which seems to target many stress response mediators (Fig. 5a). These included TCP-1, a member of the chaperonin TCP1 complex (CCT), PTPN1, a UPR regulator, STIP1, a coordinator of HSP70 and HSP90 function and the chaperone/ co-chaperone proteins DNAJB11, GCN1L1, CCT8, and DNAJA1.

Such a dysregulation of the UPR/HSP response systems in p.A53T neurons should result in the production of dangerous protein cargo and the formation of protein aggregates, as indeed identified by immunofluorescence (Fig. 2c). The p.A53T proteome also revealed alterations in protein clearance pathways with mediators of both proteasomal and autophagic systems being affected (Table S2). BX795 improved the expression of multiple ubiquitin-associated proteins suggesting partial restoration of proteasome targeting of aberrant protein products, in accordance with the decrease of protein aggregates in BX795-

treated p.A53T neurons (Fig. 2c). BX795 restored the expression of components of the proteasome complex and activators of the E2 and E3 ligase binding process (PSMA3, UCHL1, OTUB1, PSME3, CUL1, PSMD12 and UBA6), and VCP, an AAA ATPase that extracts ubiquitinated proteins from large protein complexes for degradation, previously shown to co-localize with protein aggregates in various neurodegenerative diseases (Fig. 5a).

Components of the lysosomal pathway of autophagy targeted by BX795 included vacuole transport components such as ATG4B and proteins required for multivesicular body (MVB) biogenesis and sorting (PDCD6IP, AP3M1 and DNM2) (Fig. 5a). Finally, BX795 also modulated oxidative stress response mechanisms, as the mitochondrial biosynthesis regulators TOMM70A and MDH2 were brought to near control levels. In addition, STOML2, a stimulator of cardiolipin biosynthesis recently shown to be associated with p.A53T neurotoxicity in human dopamine neurons was also positively targeted by BX795 (33).

When STRING analysis was used to assess the relatedness level of all 118 proteins affected by BX795, a network with strong functional linkage among the majority of these proteins was revealed (Fig. 5b).

Proteins associated with neurodegeneration. An important measure of the biological significance of the proteomic profile of p.A53T neurons comes from comparisons with human genetic studies. Enrichment analysis for PD and other neurodegenerative diseases identified several proteins comprising both known and novel converging targets that were modified by BX795 (Fig. 6a). Among those, UCHL1/PARK5 is linked to lower susceptibility for PD, while a point mutation co-segregating with the disease has been identified in one family (48) and VPS35/PARK17-D620N mutated protein causes late-onset autosomal dominant PD (49). FAM98B has been linked to SMA and ALS (50), VCP mutations can cause FTD, ALS and Charcot-Marie-Tooth diseases (51, 52), HINT1 autosomal recessive mutations lead to

neuromytotonia and axonal neuropathy (53), PAFAHB1 mutations and gene deletions lead to lissencephaly syndrome (54) and RBM4 is linked to Down's syndrome (55) (Fig. 6a, b). STRING analysis of the BX795-modified protein network to which αSyn was also incorporated, demonstrated a strong association between αSyn and other neurodegeneration-linked proteins (Fig. 6c).

These findings deepen our understanding of p.A53T-mediated neurotoxicity and reveal key biological processes that are targeted by BX795 to alleviate p.A53T-αSyn-related phenotypes in human neurons.

BX795 affects the mTORC1 signaling pathway to attenuate protein synthesis and facilitate autophagic flux in p.A53T neurons

The p.A53T proteome clearly indicates aberrant mRNA translation and protein clearance mechanisms, both linked to mammalian aging and neurodegenerative diseases that can be effectively restored by BX795. The mammalian target of rapamycin (mTOR) signaling pathway is a central regulator of proteostasis and the p.A53T proteome clearly indicates hyperfunctional overactive biosynthetic processes that could be associated with alterations in mTORC1 activation. Components of this signaling cascade have emerged in the proteomics analysis of p.A53T- neurons, including RPS6, a major downstream effector of mTORC1, together with several RAG GTPases like IQGAP1, required for efficient activation of mTORC1, which were largely restored after BX795 treatment (Table S3).

To confirm that the p.A53T mutation is causally related to dysregulation of protein metabolism and verify that BX795 can restore this effect in mature human neurons, we exploited the isogenic system of iCell DopaNeurons where we measured the levels of the activated form of RPS6, (phospho-RPS6; pRPS6), and the total protein synthesis rate. The

presence of the p.A53T mutation led to a significant increase in the levels of pRPS6 (Fig. 7a,b) that correlated with a significant increase of global protein synthesis in iCell Dopa p.A53T neurons (Fig. 7c, d). BX795 could lower significantly the levels of pRPS6 and reverse the aberrantly increased protein synthesis rate (Fig. 7a, d). This data suggests that BX795 targets and restores dysregulated mRNA translation and protein synthesis pathways instigated by the p.A53T mutation in neuronal cells.

To examine further the effect of the p.A53T mutation on mTORC1 activity and protein synthesis, we created stably transduced SH-SY5Y neuroblastoma cells co-expressing the human p.A53T-αSyn and the fluorescent protein DsRed or DsRed only as a control (Fig7e). Upon neuronal differentiation, SH-SY5Y cells expressing the human p.A53T-αSyn displayed a prominent upregulation in the levels of phosphorylated mTOR and pRPS6 as compared to control cells (Fig 7e, f), whilst BX795 had an acute effect in downregulating their levels (Fig. 7g), as determined by Western blot analysis.

mTORC1 also controls autophagy, the major degradation pathway essential for removing aggregation-prone αSyn (56, 57). To test if BX795 could also affect this clearance pathway, we utilized a previously established inducible SH-SY5Y cell line that expresses the human p.A53T-αSyn upon withdrawal of Doxycycline (-Dox). In this model, expression of mutant p.A53T has been shown to cause perturbation of the autophagy lysosomal pathway resulting in increased steady-state levels of LC3II and p62 ((58); Fig. 8 a, b). p62 is a receptor for ubiquitinated cargo destined to be degraded by autophagy and is associated with LC3-II, the processed form of LC3, within autophagosomes and autolysosomes (59, 60). To visualize LC3-II and quantify GFP-LC3-II+ puncta comprising brightly fluorescent autophagosomes and more weakly labeled autolysosomes (Fig. 8a), we transfected the inducible SH-SY5Y line with a fusion construct containing the green fluorescent protein tagged to LC3 (GFP-LC3) (61). In

agreement with the Western blot data, GFP-LC3-II+ puncta were scarce in p.A53T cells treated with DMSO while in the presence of BX795 there was a small, yet not significant increase (Fig. 8c, d). As expected, when DMSO-treated cells were exposed to bafilomycin, a blocker of autophagosome-lysosome fusion that prevents lysosome-mediated protein degradation, GFP-LC3-II+ puncta increased significantly (Fig. 8c, d)., Addition of both bafilomycin and BX795 further increased the number and brightness of GFP-LC3-II+ puncta, suggesting that BX795 acts as an autophagy inducer (Fig 8c, d).

To distinguish labeled autophagosomes from autolysosomes and monitor the autophagic flux, we used a dual fluorophore probe consisting of a tandem fluorescent mCherry-GFP-p62 construct (62). GFP fluorescence is sensitive to low-pH and labels only neutral-pH autophagosomes, while mCherry retains fluorescence in both autophagosomes and low-pH autolysosomes (60) (Fig. 8e). Calculation of the ratio of GFP+/mCherry+ puncta presents a measure of the autophagic flux, and a reduction in this ratio mirrors an increase in the progress of autophagy. Indeed, quantification of green and red puncta revealed a significantly lower GFP/mCherry ratio in the presence of BX795 as compared to DMSO-treated cells, indicating that BX795 facilitates the the autophagic flux (Fig. 8f, g). In agreement, a decrease in the total levels of p62 was noted upon treatment with BX95 (Fig. 8h).

Overall, our results indicate that BX795 can restore proteostasis in p.A53T cells by modulating aberrant protein synthesis and facilitating protein clearance mechanisms.

Discussion

The generation of novel human models based on patient-derived iPSCs has opened up new perspectives for investigation of disease mechanisms and discovery of new therapeutics. In this work, we used a well-characterized human model of p.A53T pathology (22) to screen for small molecules with protective function. We identified the multi-kinase inhibitor BX795 as a compound that exerts a consistent and sustainable beneficial effect on patient-derived p.A53T-neurons. Remarkably, we found that a single treatment with BX795 has long-lasting consequences in supporting neuritic growth, limiting αSyn protein aggregate formation and restoring axonal neuropathology, recorded two weeks after its addition in human p.A53T neurons.

To our knowledge, this study represents the first high-content drug discovery screen performed in human p.A53T iPSC-derived neurons to identify candidate therapeutics for PD. Using an unbiased screening approach in combination with quantitative proteomics profiling, we were able to show that treatment with BX795 restored proteins associated with key cellular processes, most notably RNA metabolism, protein synthesis and degradation processes, as well as stress response, suggesting that restoration of proteostasis is key for rescuing the neuropathological features in p.A53T-neurons. Dissecting further the pathways affected by BX795, we demonstrated that BX795 modulates the mTORC1 pathway to restrict excessive protein synthesis and facilitate autophagy. Taken together, our data highlight the BX795 kinase inhibitor as a promising compound and candidate therapeutic that ameliorates p.A53T-associated pathology.

Considerable progress in understanding the neurotoxic properties of α-Syn has been achieved by exploiting causal mutations resulting in rare familial forms of PD, most notably the p.A53T-αSyn mutation (G209A in the *SNCA* gene) (63, 64). We and others have shown

that disease-associated characteristics can be recapitulated in patient-derived p.A53T-neurons, including axonal degeneration and accumulation of protein inclusions resembling Lewy bodies and neurites (22). These have been linked to multiple molecular defects in mRNA processing and translation, endocytic and retrograde trafficking (38, 42), protein misfolding, redox homeostasis (20, 33) and the synaptic protein machinery (22). The p.A53T proteome examined here revealed a profound increase in proteins related to the biological processes of RNA metabolism, protein synthesis, modification and transport, protein clearance and stress response. Notably, the cohort of 118 proteins that was specifically restored in p.A53T-neurons upon treatment with BX795, was associated with these key cellular processes.

The pathways affected by mutant αSyn in our study have a high similarity with the αSyn connectome reported by Chung et al (38) for mouse neurons, and the predictions of the *in silico* "humanized" map of αSyn proteotoxicity reported in the accompanying study of Khurana et al (42). Our proteomics analysis, the first accomplished in p.A53T-human neurons, identified perturbations in RNA metabolic processes that started from the nucleus and reached the ribosome. Alternative mRNA processing greatly increases the dimensions of gene expression through splicing, polyadenylation, targeted localization and post-transcriptional silencing. Neurons take advantage of all these strategies as the brain has the highest levels of alternative splicing compared to any other human tissue (65). This process has recently been shown to be defective in the PS19 Tau model of Alzheimer's disease, where alternative splicing events affected genes particularly involved in synaptic transmission (66). Similarly, the p.A53T-proteome suggests that this process could be excessively induced in p.A53T-neurons as a number of RBPs known to be linked to αSyn aggregation have emerged, including ELAV1, ELAV3 and CELF, suggesting a possible

association with the abnormal expression of synaptic genes and the defective synaptic connectivity we have previously reported in p.A53T neurons- (22).

An excess of mRNAs coming out of the nucleus in p.A53T-neurons could explain the abnormal expression of proteins involved in translation, the next step of mRNA processing. The significant increase of components of the tRNA splicing ligase complex, various aminoacyl-tRNA synthetases, ribosomal subunits and eukaryotic translation initiation factors indicate an enhanced translation of spliced mRNAs. Moreover, in post-mortem PD brains, region and stage-dependent alterations in the machinery of protein synthesis have been reported and have been associated with α-synuclein oligomers in remaining neurons (67).

The mTOR kinase is a master regulator of cellular metabolism that functions in two distinct complexes: mTORC1 and mTORC2 (68) with the first implicated in protein and lipid biosynthesis through a signaling cascade that includes SK6 and 4E-BP1 proteins (69). Unlike proliferating cells where this pathway is utilized for growth and division, in neurons it acts as a regulator of healthy metabolism and aging (70) with its restriction being associated with prolonged life span and delay of age-related pathologies. p.A53T neurons have increased RPS6, IQGAP1 and RAG-GTPases, components of mTORC1 pathway and this seems to be associated with an increased translation of a subset of mRNAs that are linked to RNA metabolism and the stress response. Similarly, a quantitative proteomics study of a pre-symptomatic p.A53T-αSyn Drosophila model shows significant upregulation of ribosomal proteins in the p.A53T flies (71). Although the mechanistic link between p.A53T-αSyn and mTORC1 remains to be established, recent evidence shows that genetic variability in the mTOR pathway contributes to SNCA effects in disease pathogenesis (72).

Concomitantly with promoting protein synthesis mTORC1 acts to repress autophagy through ULK1 phosphorylation. Autophagy has a central role in promoting health and

longevity while this process is impaired in neurodegenerative diseases and αSyn pathology (73, 74). The p.A53T-proteome shows that neurons are under stress as proteins involved in the UPR or the heat-shock stress response, proteasome assembly and regulation, known to be orchestrated by mTORC1 in neurons, are significantly upregulated (70). Restoration of numerous components of RNA metabolism and protein translation cascades by BX795 is directly related to the diminished stress response that emerges by the lower levels of UPR and heat-shock-associated proteins also conferred by this molecule. In parallel, a significant number of ubiquitin/proteasome-associated proteins were brought back to near control levels suggesting that BX795 helps misfolded protein clearance by limiting protein synthesis. This is in agreement with its demonstrated ability to decrease protein aggregates in p.A53T-neurons, as shown in this study, along with facilitation of autophagy in SYSH-5Y cells expressing p.A53T.

BX795 is a multi-kinase inhibitor that targets numerous pathways, including the kinases TBK1 and PDK1 (29-31, 35). Although in our system differences in the total or phosphorylated levels of these two kinases were not observed in the presence of BX795 (data not shown), we cannot exclude that its effects are mediated through these two kinases as both are involved in neurodegeneration, mTOR signaling and autophagy (75, 76). Yet four other PDK1 inhibitors that were included in the Selleck library did not emerge as hits during the screening campaign. Interestingly, even though we demonstrated an acute effect of BX795 in mTOR and RPS6 in p.A53T-expressing cells, multiple other inhibitors of mTOR phosphorylation present in the kinase inhibitor library tested (26 in total, including rapamycin), failed to show any protective effects. Considering that BX795 has been proposed to act through distinct mechanisms in different pathologies, future mechanistic studies should reveal its direct targets in p.A53T neurons. Nevertheless, the work presented

here uniquely identifies BX795 as a promising compound that may have therapeutic potential for patients with PD and other protein conformational disorders. Further, our collective data along with previous proteomics and systems approaches shed light into the molecular and cellular pathways of αSyn proteotoxicity unveiling new disease targets for the development of combined therapeutics.

Materials and Methods

iPSC lines. iPSCs used in this study were previously generated and characterized from two Parkinson's disease patients harboring the p.A53T-α-synuclein mutation and a healthy subject (control, wild-type SNCA) (22). All procedures for generation of human iPSCs were approved by the Scientific Council and Ethics Committee of Attikon University Hospital (Athens, Greece), which is one of the Mendelian forms of Parkinson's disease clinical centers, and by the Hellenic Pasteur Institute Ethics Committee overlooking stem cell research. Written informed consent was obtained from all donors before skin biopsy.

Directed neuronal differentiation. For directed differentiation, iPSCs were allowed to form embryoid bodies and neural induction was initiated by applying a dual SMAD inhibition protocol in the presence of Noggin and TGFβ inhibitor for generation of neural precursor cells (NPCs) (22). NPCs were expanded in DMEM/F12/B27/N2-medium supplemented with HEPES, Glutamax, non-essential amino acids [NEAA] and 20ug/ml FGF2. For neuronal differentiation, NPCs were dissociated with accutase and seeded onto poly-L-ornithine (20 µg/ml; Sigma-Aldrich)/laminin (5 µg/ml; Sigma-Aldrich)-coated dishes in DMEM/F12/ B27/N2-medium supplemented with 200 ng/ml human recombinant sonic hedgehog (SHH, R&D Systems) and 100 ng/ml murine recombinant fibroblast growth factor 8b (FGF-8b, R&D Systems) for 7 days in vitro (DIV). Cells were then replated in medium supplemented with 20

ng/ml brain-derived neurotrophic factor (BDNF, R&D Systems), 20 ng/ml glial cell-derived neurotrophic factor (GDNF, R&D Systems), 200 µM ascorbic acid (AA, Sigma-Aldrich) and 0.5 mM cyclic AMP (cAMP, Sigma- Aldrich). The medium was changed every 2 to 3 days for 2 weeks.

iCell Dopa neurons and isogenic iCell DopaNeurons PD SNCA A53T HZ. Commercially available iCell DopaNeurons 01279, Catalog No C1028, and a heterozygous (HZ) A53T allelic variant isogenic to iCell DopaNeurons, PD SNCA A53T HZ 01279, Catalog No C1113, in which the site-specific p.A53T mutation was introduced into the *SNCA* gene by nuclease-mediated SNP alteration, were purchased from Fujifilm Cellular Dynamics International and were maintained according to the User's Guide protocol for two weeks.

Compound screening and High Content image analysis. iPSC-derived NPCs at 7 DIV were dissociated with accutase, seeded (9,000 cells/well) onto poly-L-ornithine/ laminin-coated 384-well optical bottom plates containing the kinase inhibitors (Greiner Bio-One, Kremsmünster, Austria) and cultured in neuronal differentiation medium for two weeks (Fig. 1a). A collection of 273 small molecule kinase inhibitors from Selleck Chemicals was used. The list of inhibitors and their known targets according to the provider, is shown in Table S1. The compounds were dispensed in duplicate in 384-well optical bottom plates at a final concentration of 1µM, followed by NPC seeding. After 2 weeks of neuronal differentiation, cells were fixed in 4% paraformaldehyde for 20 min followed by immunofluorescence for βIII-tubulin (TUJ1) and Tyrosine hydroxylase (TH) at 4^{o}C overnight and incubation with appropriate secondary antibodies (Molecular Probes, Thermo Fisher Scientific) conjugated to AlexaFluor 488 (green) or 546 (red), for at least 1 h at room temperature. Nuclei were stained with Hoechst dye. Images were captured by automated confocal microscopy (Opera High-Content Screening System, Perkin Elmer, Hamburg, Germany). A total of 15 images per

well were acquired using a 10X magnifying objective. Cell nuclei and fluorescence staining were quantified by segmentation on 15 images per well in a duplicate experimental setup. Parameters were set as follows: primary object detection (cell nuclei) was based on Hoechst staining, captured in channel 1. Detection of neurons was based on TUJ1 immunofluorescence signal, captured in channel 2 and on TH immunofluorescence signal, captured in channel 3. For quantification of TUJ1 and TH intensity Image Mining was used, a custom-made image processing and analysis application with an extendable "plug-in" infrastructure (77).

RNA isolation, cDNA Synthesis and qRT-PCR. Total RNA was extracted from cell pellets using the TRIzol® Reagent (Life Technologies). Following digestion with DNaseI, 1 µg of total RNA was used for first strand cDNA synthesis with the ImProm-II Reverse Transcription System (Promega) according to the manufacturer's instructions. Quantitative RT-PCR analyses were carried out in a Light Cycler 96 (Roche) real time PCR detection system using KAPA SYBR FAST qPCR Master Mix (KapaBiosystems). All primers used are listed in Table S2.

Immunofluorescence staining. Cells were paraformaldehyde-fixed, blocked with 5% donkey serum in PBS/ 0.1% Triton X-100 (Sigma-Aldrich) for 30 min and immunofluorescence labelled as above. Coverslips were mounted with ProLong Gold antifade reagent with DAPI (Cell Signaling) and images were acquired using a Leica TCS SP8 confocal microscope (LEICA Microsystems) and analyzed using ImageJ software (NIH).

Neurite analysis. Neurite length was estimated manually by tracing the length of all neurites on TH-labeled neurons at 21 DIV using the NeuronJ plugin of ImageJ (NIH). At least 50 single TH+ neurons per sample were analyzed.

Axon degeneration index. The number of TUJ1+ spots in blebbed or fragmented axons was counted manually (ImageJ) on twenty randomly selected fields and the ratio between the

number of spots and the total TUJ1+ staining area (ImageJ) was defined as axon degeneration index [22].

Protein aggregate quantification. Protein aggregates were detected with the PROTEOSTAT Aggresome Detection Kit (Enzo) followed by immunolabeling for TUJ1 or TH (22, 32). Manual analysis was performed by isolating individual cells from images (ROIs), applying a threshold, and utilizing the 'analyze particles' ImageJ function.

Proteomic Analysis. iPSC-derived neurons at 21 DIV were suspended, lysed and the proteins reduced in 4% SDS, 100 mM DTT, 100 mM Tris pH 7.8 through heating for 5 min. Next, the proteins were alkylated by 100 mM iodoacetamide treatment for 30 min in the dark. Samples were further processed according to the Single-Pot Solid-Phase enhanced Sample Preparation (SP3) method of Hughes et al (78). Digestion was carried out overnight at 37°C using Trypsin/LysC mix (Promega) at a protein/enzyme ratio of 50:1 in a ThermoMixer under continuous mixing at 1000 rpm. After digestion, the tubes were placed on a magnetic rack, and the supernatant containing the peptides was collected and dried down in a centrifugal evaporator (Savant SPD 1010, Thermo scientific). The peptide mixtures were reconstituted in a solution of 2% (v/v) ACN/ 0.1% (v/v) formic acid and incubated for 3 min in a sonication water bath. Peptide concentration was determined by nanodrop absorbance measurement at 280 nm.

Ultra-high pressure nanoLC. 2.5 µg peptides were pre-concentrated with a flow of 3 µL/min for 10 min using a C18 trap column (Acclaim PepMap100, 100 µm x 2 cm, Thermo Scientific) and then loaded onto a 50 cm long C18 column (75 µm ID, particle size 2 µm, 100Å, Acclaim PepMap100 RSLC, Thermo Scientific). The binary pumps of the HPLC (RSLCnano, Thermo Scientific) consisted of Solution A (2% (v/v) ACN in 0.1% (v/v) formic acid) and Solution B (80% (v/v) ACN in 0.1% (v/v) formic acid). The peptides were separated using a linear

gradient of 4% B up to 40% B in 340 min with a flow rate of 300 nL/min. The column was placed in an oven at 35°C.

LC-MS/MS. Eluted peptides were ionized by a nanospray source and detected by an LTQ Orbitrap XL mass spectrometer (Thermo Fisher Scientific, Waltham, MA, USA) operating in a data dependent mode (DDA). Full scan MS spectra were acquired in the orbitrap (m/z 300–1600) in profile mode with resolution set to 60,000 at m/z 400 and automatic gain control target at 106 ions. The six most intense ions were sequentially isolated for collision-induced (CID) MS/MS fragmentation and detection in the linear ion trap. Dynamic exclusion was set to 1 min and activated for 90 sec. Ions with single charge states were excluded. Lockmass of m/z 445,120025 was used for continuous internal calibration. XCalibur (Thermo Scientific) was used to control the system and acquire the raw files.

Protein identification and quantification. The raw mass spectral files were processed using MaxQuant software (version 1.6.9.0) with default parameters for protein identification and quantification. Trypsin specificity was set to allow two missed cleavages and minimum peptide length was set to 7 amino acids. Cysteine carbamidomethylation was set as fixed, and methionine oxidation, deamidation of asparagine and glutamine and N-terminal acetylation were set as variable modifications. A maximum of 5 modifications per peptide was set. The false discovery rate both for peptide and protein was set to 1%. For calculation of protein abundances, label-free quantification (LFQ) was performed with both “second peptides” and “match between run” options enabled. The human FASTA files were from UniProt downloaded on 15 October 2019.

Proteomic data analysis. Statistical analysis was performed using Perseus (1.6.6.0). Proteins identified as contaminants, “reverse” and “only identified by site” were filtered out. The LFQ intensities were transformed to logarithmic values [log2(x)]. The protein groups were

filtered to obtain at least 2 valid values in at least one group. The label-free quantified proteins were subjected to statistical analysis with ANOVA test (permutation-based p-value with 0.05 cutoff). LC-MS/MS data after statistical analysis were plotted in a volcano graph based on the difference between the two samples expressed as log2(x) versus their statistical significance expressed as –Log10(p-value). Hierarchical clustering was carried out on Z-score transformed LFQ values using average linkage of Euclidian distance. For statistical and bioinformatics analysis, as well as for visualization, Perseus, which is part of Maxquant, was used (79). GO Enrichment analysis for biological processes, molecular function and cellular compartment was performed using DAVID functional annotation tools with official gene symbol as identifiers, the Homo sapiens background and the GOTERM_DIRECT annotation categories. A P value of 0.05 was selected as the cutoff criterion. The enrichment of proteins involved in signaling pathways was performed using the Reactome pathway database. A P value of 0.01 was selected as the cutoff criterion.

Western blot. Cells were lysed at 4^{o}C for 15 min in ice cold lysis buffer [150mMNaCl, 50 mM Tris pH 7.5, 1% Triton X-100, 1mM EDTA, 1mM EGTA, 0.1% SDS, 0.5% sodium deoxycholate containing PhosSTOP phosphatase inhibitors and a complete protease inhibitor mixture (Roche Life Science)], and centrifuged at 20,000 g. Protein concentration was estimated in the supernatant by Bradford assay (Applichem). Proteins were separated by SDS-polyacrylamide gel electrophoresis and transferred onto nitrocellulose membranes (Maine Manufacturing). For phospho-(Ser129)-αSyn detection, the membrane was heated at 65 ^{0}C overnight in PBS. Nonspecific binding sites were blocked in TBS/ 0.1% Tween 20/ 5% skimmed milk for 1 hour at 20 ^{0}C followed by overnight incubation with primary antibodies diluted in the same buffer. Incubation with appropriate HRP-conjugated secondary antibodies (Thermo) was for 2 hours at room temperature and protein bands were visualized

using the Clarity Western ECL Substrate (BIO-RAD). Densitometric analysis was performed using ImageJ software (NIH).

Production of CMV.DsRed and CMV.DsRed.A53T lentiviral vectors. Four plasmids were used for lentivirus generation: the lentiviral transfer vector and three lentiviral packaging vectors (pMDL, pRev and pVSVG; provided by Dr. Fred Gage, the Salk Institute for Biological Studies). The lentiviral transfer vectors for expression of either the red fluorescent protein DsRed under the control of CMV promoter (LV.CMV.DsRed) or for co-expression of the red fluorescent protein DsRed, a T2A bicistronic configuration and human p.A53T-αSyn under the control of CMV promoter (LV.CMV.DsRed.T2A.A53T) were constructed by VectorBuilder. The preparation and purification of the lentiviral vectors were performed as previously described (80)**.**

Generation of stably transduced SH-SY5Y cells: SH-SY5Y cells were transduced with the control vector LV.CMV.DsRed or LV.CMV.DsRed.T2A.A53T for expression of DsRed or co-expression of DsRed and human p.A53T-αSyn. Transduced cells were maintained in regular RPMI 1640 medium/ 10% FBS (Gibco)/ 1% penicillin/streptomycin (Life Technologies) for 48h with one change of medium, and were then transferred in selection medium containing 300 µg/ml gentamycin-disulfate G418. After 3 weeks of selection, when 100% of cells expressed the DsRED protein, they were frozen as a polyclonal pool.

Differentiation of SH-SY5Y cells. Cells were plated on PLL/Laminin coated plates ($2x10^4$ cells/cm^2) in regular RPMI 1640 medium/ 5% FBS/ 1% penicillin/streptomycin (DIV 0). The following day, 10 µM Retinoic Acid (RA) was added (DIV1). On DIV3, the medium was changed to Neurobasal supplemented with B27, N2, Glutamax and BDNF (50ng/ml) with fresh medium added every 2-3 days until DIV9.

Cell culture and transfection of an inducible SH-SY5Y line expressing human p.A53T-αSyn. The inducible SH-SY5Y cell line, in which expression of p.A53T-αSyn was switched off in the presence of doxycycline (Dox, 2 µg/mL), was previously reported (58). Transfection with GFP-LC3 or mCherry-GFP-p62 plasmids (provided by Dr Tamotsu Yoshimori, Osaka University, Japan and Dr Terje Johansen, University of Tromso, Norway, respectively) was performed in the absence of Dox using Lipofectamine 2000, according to the manufacturer's protocol (Invitrogen; Thermo Fisher Scientific, Inc.).

Protein synthesis assay. For detection of total protein synthesis, an assay Kit (ab239725; Abcam) was used that utilizes a cell permeable analog of puromycin, which once inside the cell, stops translation by forming covalent conjugates with nascent polypeptide chains. Truncated polypeptides can be detected based on a click reaction with fluorescent azide. Cells were pre-treated with DMSO vehicle or BX795 for different time points and were incubated for 2h with fresh aliquots of media containing either Protein Label or Protein Label and BX795. Cyclohexamide that blocks protein synthesis was used as a negative control. Fluorescence images were acquired using a Leica TCS SP8 confocal microscope (LEICA Microsystems) and analyzed using ImageJ software (NIH).

Statistics. All experiments were replicated at least three times and data from parallel cultures were acquired. Statistical analysis was performed using GraphPad Prism 6 software. Before performing parametric tests, data were assessed for normality with a D'Agostino–Pearson omnibus. Statistical significance was calculated for two groups using Student's t-tests or the Mann-Whitney test for non-parametric distribution. Group comparisons of data were performed by one-way ANOVA test followed by Tukey post hoc test using PRISM (Graph Pad). P-values < 0.05 were considered significant; *p < 0.05, **p < 0.01, ***p < 0.001, ****p<0.0001.

Study approval. All studies on human pluripotent stem cells were approved by the Hellenic Pasteur Institute Ethics Committee overlooking stem cell research.

Data availability

The mass spectrometry proteomics data have been deposited to the ProteomeXchange Consortium via the PRIDE partner repository with the dataset identifier PXD019574.

Acknowledgements

We thank Drs. Tamotsu Yoshimori and Terje Johansen for providing GFP-LC3 and mCherry-GFP-p62 plasmids, respectively. This work was supported by: a Stavros Niarchos Foundation grant to the Hellenic Pasteur Institute as part of the Foundation's initiative to support the Greek Research Center ecosystem; the Greek General Secretariat for Research and Technology (GSRT) grant BIOIMAGING-GR MIS 5002755 implemented under the Action "Reinforcement of Research and Innovation Infrastructure", funded by the Operational Programme "Competitiveness, Entrepreneurship and Innovation" (NSRF 2014-2020) and co-financed by Greece and the European Union (European Regional Development Fund); the GSRT Flagship Action for Neurodegenerative Diseases on the basis of Personalized Medicine; the Hellenic Foundation for Research and Innovation 899-PARKINSynapse grant to G.K; the South Korea Ministry of Science and ICT (MSIT) grant (NRF-2017M3A9G6068257) to RG. N.A. was recipient of a Calmette & Yersin Fellowship for a technology exchange visit to the Institut Pasteur Korea.

Author contributions

NA carried out the experiments, analyzed and interpreted the data, generated the figures, participated in the study design and in writing the manuscript. KP and ET analyzed proteomics data. GK generated the patient-derived p.A53T and control iPSCs used in this study and provided training on iPSC culture and differentiation. MS and GP performed the proteomic analysis. MX and LS provided reagents, analytic tools and guidance for autophagy experiments. NA and RG performed high-content imaging and drug screening on p.A53T neurons. ET and RM conceived, designed and supervised the study, analyzed the data and wrote the paper with contribution from all authors.

Conflict of Interests

The authors declare that they have no conflict of interests.

Figure Legends

Fig 1 Identification of BX795 by high content screening of a kinase inhibitor library

a. Directed differentiation of Pax6+ (green)/ Nestin+ (red) neural precursor cells (NPCs; DIV 0, left) into TUJ1+ (red)/ TH+ (green) neurons (DIV 21, right). The differentiation protocol and timeline of analysis are shown in the drawing in the middle.. FG2 and FGF8, fibroblast growth factors 2 and 8; SHH, Sonic Hedgehog; AA, ascorbic acid; Scale bar represents BDNF, brain-derived neurotrophic factor; GDNF, glial cell-derived neurotrophic factor (GDNF); cAMP, cyclic AMP. Scale bars, 50 µm.

b. Scatter plot showing the ratio of TH versus TUJ1 fluorescence intensity in duplicate upon treatment with 273 small molecule kinase inhibitors. The dots inside the green square correspond to the 4 hit compounds showing significant increase of TH versus TUJ1

fluorescence ratio as compared to the DMSO controls (blue dots). The red arrow indicates BX795.

c. Representative images of patient-derived p.A53T-neurons immunolabelled for TH in 384-well plates. Upper micrograph shows control DMSO-treated cells while lower micrograph represents BX795-treated cells. Scale bar represents 150 µm.

d. Tests of the four hit compounds in a dose-response format. Data are presented as mean ± SEM.(one-way ANOVA, *P<0.05 , n=3 independent experiments).

Fig 2 Rescue of neuropathological features in patient-derived p.A53T neurons by BX795

a. BX795 has a positive effect on neurite length of p.A53T-neurons. Representative confocal images of healthy control (ctl) and p.A53T-neurons immunostained for TH and quantification of total neurite length of TH+ cells. Data represent mean ± SEM. (Comparisons by ANOVA with Tukey correction *P<0.05, **P<0.01, n=4 independent experiments with at least 50 cells analyzed in each experiment). Scale bar, 50µm.

b. BX795 alleviates axonal neuropathology in p.A53T-neurons. Higher magnification at the right (upper, DMSO-treated cells; lower, BX795-treated cells) shows neurites with swollen varicosities or fragmented processes (arrows). Scale bar, 30µm. Quantification of axonal degeneration is estimated in the accompanying graph by measuring the ratio of TUJ1+ spots over the total TUJ1+ area in untreated (p.A53T) or BX795-treated p.A53T-neurons. Data represent mean ± SEM.(Comparisons by ANOVA with Tukey correction, *P< 0.05, **P<0.01, n = 20 randomly selected fields for each condition).

c. BX795 reduces protein aggregates in p.A53T-neurons. Representative confocal images showing protein aggregates in p.A53T TUJ1+ neurons (Scale bar, 10µm) and quantification in

untreated or BX795-treated TUJ1+ cells (Mann–Whitney test; n=at least 50 cells per group; ****P< 0.0001).

d. Detection and quantification of p(Ser129)αSyn by Western blot; Actin shows equal protein loading. Data represent mean ± SEM (*t*-test, *P<0.05, n=4 independent experiments).

Fig 3 BX795 reduces protein aggregates in a gene-edited p.A53T line of mature human iPSC-derived TH neurons

a. Representative confocal images of wild-type (ctl) and isogenic p.A53T iCell Dopa neurons immunolabelled for Nuclei, TUJ1, MAP2 and TH. Scale bar, 30 µm

b. Representative confocal images of wild-type (ctl) and isogenic p.A53T iCellDopa neurons showing immunostaining for tyrosine hydroxylase (TH green) and protein aggregates (red). p.A53T cells were treated or not with BX795, as indicated. Scale bar, 5µm

c. Quantification of aggregates in TH+ neurons. Data represent mean ± SEM. (Comparisons by ANOVA with Tukey correction, ****P<0.0001, n = at least 50 randomly selected TH+ cells for each condition).

Fig 4 Bioinformatics analysis of dysregulated proteins in p.A53T-neurons that are restored by BX795

a. Hierarchical clustering of 118 upregulated proteins in patient-derived p.A53T-neurons that are restored upon treatment with BX795 (one-way ANOVA analysis). Columns in the different groups (control, p.A53T-neurons and p.A53T-neurons treated with BX795) correspond to individual samples tested and rows represent single proteins (blue, low expression; red, high expression; n=3 for control and p.A53T; n=2 for p.A53T+BX795).

b. GO enrichment analysis for biological processes, molecular function and cellular compartments was performed using DAVID software ($p<0.01$).

c. Pathway analysis using Reactome software ($p<0.01$)

Fig 5 Protein network of pathways and processes restored by BX795 treatment

a. Heatmaps illustrating specific proteins upregulated in p.A53T-neurons that are involved in RNA metabolism, protein synthesis, protein modification and transport and response to stress, which are restored after BX795 treatment. High expression is in red and low expression is in blue.

b. STRING-analysis representation of the protein-protein interaction network of the 118 upregulated proteins in p.A53T-neurons that are restored by BX795. Each circular node depicts one protein and the different colors represent the different pathways/processes as indicated. Connecting lines represent protein-protein associations and line intensity represents the confidence score of a functional association.

Fig 6 Restoration of disease-associated proteins by BX795 in p.A53T-neurons

a. Heatmap of proteins associated with neurodegeneration that are restored after BX795 treatment. High expression is in red and low expression is in blue.

b. Disease-associated proteins that are modified by BX795 are either known or associated genetic risk factors for neurodegenerative diseases as revealed by human genetic studies.

c. STRING network analysis of the neurodegeneration-associated proteins restored by BX795 in p.A53T-neurons and their interaction with αSyn. Each αSyn interactor is shown as a colored circle and connecting lines between proteins represent protein-protein

associations. The intensity of lines represents the confidence score of a functional association.

Fig 7 BX795 affects the mTORC1 signaling pathway to attenuate protein synthesis

a. Representative confocal images of control (ctl) and isogenic gene-edited p.A53T iCellDopa neurons, either non-treated or treated with BX795. Cells were immunolabeled for phosphorylated RPS6 (green) and microtubule associated protein 2 (MAP2; red). Nuclei are seen with Hoechst dye (blue). Scale bar, 30µm

b. BX795 reduces phosphorylated RPS6 levels in p.A53T-neurons. Quantification of fluorescence intensity in control, untreated p.A53T or BX795-treated p.A53T neurons. Data represent mean ± SEM (Comparisons by ANOVA with Tukey correction, ***P< 0.001 ****P<0.0001, n = 100 randomly selected cells for each condition).

c. Representative confocal images of control and isogenic gene-edited p.A53T iCellDopa neurons, non-treated or treated with BX795, labeled for total protein synthesis (protein label, green). Nuclei are visualized by Hoechst counterstaining (blue). Scale bar, 30µm

d. BX795 reduces total protein synthesis in p.A53T-neurons. Quantification of fluorescence intensity in non-treated control and p.A53T neurons non-treated or treated with BX795. Cyclohexamide blocks protein synthesis in both genotypes and is used as a negative control. Data represent mean ± SEM (Comparisons by ANOVA with Tukey correction, ****P<0.0001, n = 100 randomly selected cells for each condition).

e. Representative images of SH-SY5Y cells stably transduced to express DsRed only or DsRed and human pA53T-αSyn. After neuronal differentiation, cells were immunolabled for αSyn (SNCA), TUJ1 and pRPS6.

f. Western blot showing that the presence of mutant SNCA in differentiated p.A53T-transduced SH-SY5Y cells, results in an increase in the levels p-mTOR and p-RPS6. Actin shows equal protein loading. Data represent mean ± SEM (*t*-test, *P<0.05, n=3 independent experiments).

g. Western blot showing an acute reduction in the levels of p-mTOR and p-RPS6 in the above stably transduced and differentiated SH-SY5Y cells, in the presence of BX795. Actin shows equal protein loading. Data represent mean ± SEM (Comparisons by ANOVA with Tukey correction, *P<0.05, ****P<0.0001, n=3 independent experiments).

Fig 8 BX795 facilitates autophagy in an inducible SH-SY5Y cell line expressing human p.A53T-αSyn

a. Schema illustrating that cytosolic LC3 is cleaved to yield LC3-I, which is subsequently conjugated to phosphatidylethanolamine (PE) to form membrane-bound LC3-II (green circles). Pre-autophagosomal structures engulfing protein cargo and organelles destined for degradation close to form double membrane spherical autophagosomes. These fuse with lysosomes to yield autolysosomes and their contents are degraded. Bafilomycin blocks autophagic flux by inhibiting autophagosome-lysosome fusion, which results in accumulation of LC3-II+ autophagosomes.

b. Representative immunoblot showing steady-state levels of LC3-II and p62 in lysates of inducible SH-SY5Y cells expressing the human p.A53T-αSyn (-Dox) and quantification relative to actin. Data represent mean ± SEM, *t*-test , *P<0.05 , n=3 independent experiments.

c. Representative confocal images of individual p.A53T SH-SY5Y cells (-Dox) transfected with GFP-LC3 that were treated or not with bafilomycin A1 in the absence or presence of BX795.

d. Quantification of GFP-LC3 puncta per cell. Comparisons by ANOVA with Tukey correction. *P < 0.05, n=72 cells (control DMSO), n=79 cells (BX795), n=67 cells (Bafilomycin A1), n=68 cells BX795+Bafilomycin A1. Data are representative of three independent experiments).

e. Assessment of autophagic flux using mCherry-GFP-LC3 color change between autophagosomes and autolysosomes. Autophagic flux is induced when the GFP:mCherry ratio is reduced.

F, g. Representative confocal images of individual cells [inducible SH-SY5Y cell line expressing p.A53T-αSyn (-Dox)] transfected with GFP-mCherry-p62 that were treated with DMSO (control) or BX795 and quantification of the ratio of GFP+/mCherry+ puncta (*t*-test,n= 60 (control DMSO), n=53 (BX795) **P < 0.01 Data are representative of three independent experiments).

h. Representative immunoblot showing steady-state levels of p62 in cells [inducible SH-SY5Y cell line expressing p.A53T-αSyn (-Dox)] treated or not with BX795, and quantification relative to actin. Data represent mean ± SEM, *t*-test, n=3 independent experiments.

Fig S1 Expression of dopaminergic markers in patient p.A53T-iPSC-derived neurons

a. RT-qPCR analysis of selected domaminergic markers in p.A53T iPSC-derived neurons at 21 DIV: Tyrosine Hydrosylase (TH), Nuclear receptor related 1 protein (Nurr1) and Aromatic L-amino acid decarboxylase (AADC) normalized to GAPDH levels. Data represent mean ± SEM (n = 3). Student's t-test was used .

b. Representative images of p.A53T iPSC-derived neurons at 21 DIV immunostained for Ki67 (red) to label cycling cells. Hoechst+ nuclei are in blue (Scale bar, 50 µm). Quantification of the percentage of Ki67+ cells in the presence or absence of BX795. Data represent mean ± SEM (n = 3). Student's t-test was used.

Fig S2 Identification of toxic compounds in the small molecule library of kinase inhibitors

Summary of total nuclei counts from two screening plates. Compounds in cells with low nuclei counts were considered toxic and where excluded from the analysis. Each assay plate was normalized to DMSO.

Fig S3 Rescue of neuropathological features by BX795 in p.A53T neurons from a second patient

a. BX795 has a positive effect on neurite length of p.A53T-neurons. Representative confocal images of p.A53T-neurons immunostained for TH and quantification of total neurite length of TH+ cells. Data represent mean ± SEM. Student's t-test was used. Scale bar, 50µm.

b. BX795 alleviates axonal neuropathology in p.A53T-neurons as demonstrated by immunostaining for βIII-tubulin (TUJ1; confocal images). Neurites with swollen varicosities or fragmented processes are indicated with arrows. Scale bar, 30µm. Axonal degeneration is estimated in the accompanying graph by measuring the ratio of TUJ1+ spots over the total TUJ1+ area in untreated (DMSO) or BX795-treated p.A53T-neurons. Data represent mean ± SEM. Student's t-test was used.

Fig S4 Identification of the biological processes that are dysregulated in p.A53T neurons

a. Volcano plot of differentially expressed proteins between control and patient-derived p.A53T-neurons assessed by quantitative proteomics analysis. Each point represents the difference in expression (fold-change) between the two groups plotted against the level of statistical significance. Blue dots correspond to proteins downregulated in p.A53T neurons

while red dots show proteins upregulated in p.A53T neurons (FDR=0.05, S0 = 0.1, as indicated by black lines).

b. GO enrichment analysis for biological processes of the differentially expressed proteins was performed using DAVID software ($p<0.05$).

References

1. Baker, M.G., and Graham, L. 2004. The journey: Parkinson's disease. *BMJ* 329:611-614.
2. Olanow, C.W., and Tatton, W.G. 1999. Etiology and pathogenesis of Parkinson's disease. *Annu Rev Neurosci* 22:123-144.
3. Pfeiffer, R.F. 2016. Non-motor symptoms in Parkinson's disease. *Parkinsonism Relat Disord* 22 Suppl 1:S119-122.
4. Gibb, W. 1986. Idiopathic Parkinson's disease and the Lewy body disorders. *Neuropathology and applied neurobiology* 12:223-234.
5. Lewandowsky, M.H. 1914. *Handbuch der neurologie: bd. Spezielle Neurologie IV*: J. Spring.
6. Baba, M., Nakajo, S., Tu, P.H., Tomita, T., Nakaya, K., Lee, V.M., Trojanowski, J.Q., and Iwatsubo, T. 1998. Aggregation of alpha-synuclein in Lewy bodies of sporadic Parkinson's disease and dementia with Lewy bodies. *Am J Pathol* 152:879-884.
7. Breydo, L., Wu, J.W., and Uversky, V.N. 2012. Alpha-synuclein misfolding and Parkinson's disease. *Biochim Biophys Acta* 1822:261-285.
8. Chartier-Harlin, M.C., Kachergus, J., Roumier, C., Mouroux, V., Douay, X., Lincoln, S., Levecque, C., Larvor, L., Andrieux, J., Hulihan, M., et al. 2004. Alpha-synuclein locus duplication as a cause of familial Parkinson's disease. *Lancet* 364:1167-1169.
9. Petrucci, S., Ginevrino, M., and Valente, E.M. 2016. Phenotypic spectrum of alpha-synuclein mutations: New insights from patients and cellular models. *Parkinsonism Relat Disord* 22 Suppl 1:S16-20.
10. Simon-Sanchez, J., Schulte, C., Bras, J.M., Sharma, M., Gibbs, J.R., Berg, D., Paisan-Ruiz, C., Lichtner, P., Scholz, S.W., Hernandez, D.G., et al. 2009. Genome-wide association study reveals genetic risk underlying Parkinson's disease. *Nat Genet* 41:1308-1312.
11. Conway, K.A., Lee, S.J., Rochet, J.C., Ding, T.T., Williamson, R.E., and Lansbury, P.T., Jr. 2000. Acceleration of oligomerization, not fibrillization, is a shared property of both alpha-synuclein mutations linked to early-onset Parkinson's disease: implications for pathogenesis and therapy. *Proc Natl Acad Sci U S A* 97:571-576.
12. Duda, J.E., Giasson, B.I., Mabon, M.E., Miller, D.C., Golbe, L.I., Lee, V.M., and Trojanowski, J.Q. 2002. Concurrence of alpha-synuclein and tau brain pathology in the Contursi kindred. *Acta Neuropathol* 104:7-11.
13. Kotzbauer, P.T., Giasson, B.I., Kravitz, A.V., Golbe, L.I., Mark, M.H., Trojanowski, J.Q., and Lee, V.M. 2004. Fibrillization of alpha-synuclein and tau in familial Parkinson's disease caused by the A53T alpha-synuclein mutation. *Exp Neurol* 187:279-288.
14. Cotzias, G.C., Van Woert, M.H., and Schiffer, L.M. 1967. Aromatic amino acids and modification of parkinsonism. *N Engl J Med* 276:374-379.
15. Ghosh, D., Mehra, S., Sahay, S., Singh, P.K., and Maji, S.K. 2017. alpha-synuclein aggregation and its modulation. *Int J Biol Macromol* 100:37-54.
16. Ghosh, D., Mondal, M., Mohite, G.M., Singh, P.K., Ranjan, P., Anoop, A., Ghosh, S., Jha, N.N., Kumar, A., and Maji, S.K. 2013. The Parkinson's disease-associated H50Q mutation accelerates alpha-Synuclein aggregation in vitro. *Biochemistry* 52:6925-6927.
17. Schulz-Schaeffer, W.J. 2010. The synaptic pathology of alpha-synuclein aggregation in dementia with Lewy bodies, Parkinson's disease and Parkinson's disease dementia. *Acta Neuropathol* 120:131-143.
18. Chen, M., Lee, H.K., Moo, L., Hanlon, E., Stein, T., and Xia, W. 2018. Common proteomic profiles of induced pluripotent stem cell-derived three-dimensional neurons and brain tissue from Alzheimer patients. *J Proteomics* 182:21-33.
19. Cooper, O., Seo, H., Andrabi, S., Guardia-Laguarta, C., Graziotto, J., Sundberg, M., McLean, J.R., Carrillo-Reid, L., Xie, Z., Osborn, T., et al. 2012. Pharmacological rescue of mitochondrial deficits in iPSC-derived neural cells from patients with familial Parkinson's disease. *Sci Transl Med* 4:141ra190.

20. Ryan, S.D., Dolatabadi, N., Chan, S.F., Zhang, X., Akhtar, M.W., Parker, J., Soldner, F., Sunico, C.R., Nagar, S., Talantova, M., et al. 2013. Isogenic human iPSC Parkinson's model shows nitrosative stress-induced dysfunction in MEF2-PGC1alpha transcription. *Cell* 155:1351-1364.
21. Yang, Y.M., Gupta, S.K., Kim, K.J., Powers, B.E., Cerqueira, A., Wainger, B.J., Ngo, H.D., Rosowski, K.A., Schein, P.A., Ackeifi, C.A., et al. 2013. A small molecule screen in stem-cell-derived motor neurons identifies a kinase inhibitor as a candidate therapeutic for ALS. *Cell Stem Cell* 12:713-726.
22. Kouroupi, G., Taoufik, E., Vlachos, I.S., Tsioras, K., Antoniou, N., Papastefanaki, F., Chroni-Tzartou, D., Wrasidlo, W., Bohl, D., Stellas, D., et al. 2017. Defective synaptic connectivity and axonal neuropathology in a human iPSC-based model of familial Parkinson's disease. *Proc Natl Acad Sci U S A* 114:E3679-E3688.
23. Chambers, S.M., Fasano, C.A., Papapetrou, E.P., Tomishima, M., Sadelain, M., and Studer, L. 2009. Highly efficient neural conversion of human ES and iPS cells by dual inhibition of SMAD signaling. *Nat Biotechnol* 27:275-280.
24. Soldner, F., Hockemeyer, D., Beard, C., Gao, Q., Bell, G.W., Cook, E.G., Hargus, G., Blak, A., Cooper, O., Mitalipova, M., et al. 2009. Parkinson's disease patient-derived induced pluripotent stem cells free of viral reprogramming factors. *Cell* 136:964-977.
25. Lovestone, S., Boada, M., Dubois, B., Hull, M., Rinne, J.O., Huppertz, H.J., Calero, M., Andres, M.V., Gomez-Carrillo, B., Leon, T., et al. 2015. A phase II trial of tideglusib in Alzheimer's disease. *J Alzheimers Dis* 45:75-88.
26. Pagan, F.L., Hebron, M.L., Wilmarth, B., Torres-Yaghi, Y., Lawler, A., Mundel, E.E., Yusuf, N., Starr, N.J., Arellano, J., Howard, H.H., et al. 2019. Pharmacokinetics and pharmacodynamics of a single dose Nilotinib in individuals with Parkinson's disease. *Pharmacol Res Perspect* 7:e00470.
27. Cuny, G.D. 2009. Kinase inhibitors as potential therapeutics for acute and chronic neurodegenerative conditions. *Curr Pharm Des* 15:3919-3939.
28. Yu, T., Wang, Z., Jie, W., Fu, X., Li, B., Xu, H., Liu, Y., Li, M., Kim, E., Yang, Y., et al. 2020. The kinase inhibitor BX795 suppresses the inflammatory response via multiple kinases. *Biochem Pharmacol* 174:113797.
29. Clark, K., Plater, L., Peggie, M., and Cohen, P. 2009. Use of the pharmacological inhibitor BX795 to study the regulation and physiological roles of TBK1 and IkappaB kinase epsilon: a distinct upstream kinase mediates Ser-172 phosphorylation and activation. *J Biol Chem* 284:14136-14146.
30. Jaishankar, D., Yakoub, A.M., Yadavalli, T., Agelidis, A., Thakkar, N., Hadigal, S., Ames, J., and Shukla, D. 2018. An off-target effect of BX795 blocks herpes simplex virus type 1 infection of the eye. *Sci Transl Med* 10.
31. Su, A.R., Qiu, M., Li, Y.L., Xu, W.T., Song, S.W., Wang, X.H., Song, H.Y., Zheng, N., and Wu, Z.W. 2017. BX-795 inhibits HSV-1 and HSV-2 replication by blocking the JNK/p38 pathways without interfering with PDK1 activity in host cells. *Acta Pharmacol Sin* 38:402-414.
32. Zygogianni, O., Antoniou, N., Kalomoiri, M., Kouroupi, G., Taoufik, E., and Matsas, R. 2019. In Vivo Phenotyping of Familial Parkinson's Disease with Human Induced Pluripotent Stem Cells: A Proof-of-Concept Study. *Neurochem Res* 44:1475-1493.
33. Ryan, T., Bamm, V.V., Stykel, M.G., Coackley, C.L., Humphries, K.M., Jamieson-Williams, R., Ambasudhan, R., Mosser, D.D., Lipton, S.A., Harauz, G., et al. 2018. Cardiolipin exposure on the outer mitochondrial membrane modulates alpha-synuclein. *Nat Commun* 9:817.
34. Walker, D.G., Lue, L.F., Adler, C.H., Shill, H.A., Caviness, J.N., Sabbagh, M.N., Akiyama, H., Serrano, G.E., Sue, L.I., Beach, T.G., et al. 2013. Changes in properties of serine 129 phosphorylated alpha-synuclein with progression of Lewy-type histopathology in human brains. *Exp Neurol* 240:190-204.
35. Bai, L.Y., Chiu, C.F., Kapuriya, N.P., Shieh, T.M., Tsai, Y.C., Wu, C.Y., Sargeant, A.M., and Weng, J.R. 2015. BX795, a TBK1 inhibitor, exhibits antitumor activity in human oral squamous cell carcinoma through apoptosis induction and mitotic phase arrest. *Eur J Pharmacol* 769:287-296.

36. Cox, J., Hein, M.Y., Luber, C.A., Paron, I., Nagaraj, N., and Mann, M. 2014. Accurate proteome-wide label-free quantification by delayed normalization and maximal peptide ratio extraction, termed MaxLFQ. *Mol Cell Proteomics* 13:2513-2526.
37. Cox, J., and Mann, M. 2008. MaxQuant enables high peptide identification rates, individualized p.p.b.-range mass accuracies and proteome-wide protein quantification. *Nat Biotechnol* 26:1367-1372.
38. Chung, C.Y., Khurana, V., Yi, S., Sahni, N., Loh, K.H., Auluck, P.K., Baru, V., Udeshi, N.D., Freyzon, Y., Carr, S.A., et al. 2017. In Situ Peroxidase Labeling and Mass-Spectrometry Connects Alpha-Synuclein Directly to Endocytic Trafficking and mRNA Metabolism in Neurons. *Cell Syst* 4:242-250 e244.
39. Bowden, H.A., and Dormann, D. 2016. Altered mRNP granule dynamics in FTLD pathogenesis. *J Neurochem* 138 Suppl 1:112-133.
40. Kapur, M., Monaghan, C.E., and Ackerman, S.L. 2017. Regulation of mRNA Translation in Neurons-A Matter of Life and Death. *Neuron* 96:616-637.
41. Chung, C.Y., Khurana, V., Auluck, P.K., Tardiff, D.F., Mazzulli, J.R., Soldner, F., Baru, V., Lou, Y., Freyzon, Y., Cho, S., et al. 2013. Identification and rescue of alpha-synuclein toxicity in Parkinson patient-derived neurons. *Science* 342:983-987.
42. Khurana, V., Peng, J., Chung, C.Y., Auluck, P.K., Fanning, S., Tardiff, D.F., Bartels, T., Koeva, M., Eichhorn, S.W., Benyamini, H., et al. 2017. Genome-Scale Networks Link Neurodegenerative Disease Genes to alpha-Synuclein through Specific Molecular Pathways. *Cell Syst* 4:157-170 e114.
43. Carpanini, S.M., McKie, L., Thomson, D., Wright, A.K., Gordon, S.L., Roche, S.L., Handley, M.T., Morrison, H., Brownstein, D., Wishart, T.M., et al. 2014. A novel mouse model of Warburg Micro syndrome reveals roles for RAB18 in eye development and organisation of the neuronal cytoskeleton. *Dis Model Mech* 7:711-722.
44. Feldmann, A., Bekbulat, F., Huesmann, H., Ulbrich, S., Tatzelt, J., Behl, C., and Kern, A. 2017. The RAB GTPase RAB18 modulates macroautophagy and proteostasis. *Biochem Biophys Res Commun* 486:738-743.
45. Rocca, D.L., Amici, M., Antoniou, A., Blanco Suarez, E., Halemani, N., Murk, K., McGarvey, J., Jaafari, N., Mellor, J.R., Collingridge, G.L., et al. 2013. The small GTPase Arf1 modulates Arp2/3-mediated actin polymerization via PICK1 to regulate synaptic plasticity. *Neuron* 79:293-307.
46. Jean, S., Cox, S., Nassari, S., and Kiger, A.A. 2015. Starvation-induced MTMR13 and RAB21 activity regulates VAMP8 to promote autophagosome-lysosome fusion. *EMBO Rep* 16:297-311.
47. Farley, M.M., and Watkins, T.A. 2018. Intrinsic Neuronal Stress Response Pathways in Injury and Disease. *Annu Rev Pathol* 13:93-116.
48. Maraganore, D.M., Lesnick, T.G., Elbaz, A., Chartier-Harlin, M.C., Gasser, T., Kruger, R., Hattori, N., Mellick, G.D., Quattrone, A., Satoh, J., et al. 2004. UCHL1 is a Parkinson's disease susceptibility gene. *Ann Neurol* 55:512-521.
49. Williams, E.T., Chen, X., and Moore, D.J. 2017. VPS35, the Retromer Complex and Parkinson's Disease. *J Parkinsons Dis* 7:219-233.
50. Chi, B., O'Connell, J.D., Iocolano, A.D., Coady, J.A., Yu, Y., Gangopadhyay, J., Gygi, S.P., and Reed, R. 2018. The neurodegenerative diseases ALS and SMA are linked at the molecular level via the ASC-1 complex. *Nucleic Acids Res* 46:11939-11951.
51. Abramzon, Y.A., Fratta, P., Traynor, B.J., and Chia, R. 2020. The Overlapping Genetics of Amyotrophic Lateral Sclerosis and Frontotemporal Dementia. *Front Neurosci* 14:42.
52. Gonzalez, M.A., Feely, S.M., Speziani, F., Strickland, A.V., Danzi, M., Bacon, C., Lee, Y., Chou, T.F., Blanton, S.H., Weihl, C.C., et al. 2014. A novel mutation in VCP causes Charcot-Marie-Tooth Type 2 disease. *Brain* 137:2897-2902.
53. Aminkeng, F. 2013. HINT1 mutations define a novel disease entity - autosomal recessive axonal neuropathy with neuromyotonia. *Clin Genet* 83:31-32.

54. Haverfield, E.V., Whited, A.J., Petras, K.S., Dobyns, W.B., and Das, S. 2009. Intragenic deletions and duplications of the LIS1 and DCX genes: a major disease-causing mechanism in lissencephaly and subcortical band heterotopia. *Eur J Hum Genet* 17:911-918.
55. Bernert, G., Fountoulakis, M., and Lubec, G. 2002. Manifold decreased protein levels of matrin 3, reduced motor protein HMP and hlark in fetal Down's syndrome brain. *Proteomics* 2:1752-1757.
56. Parekh, P., Sharma, N., Gadepalli, A., Shahane, A., Sharma, M., and Khairnar, A. 2019. A Cleaning Crew: The Pursuit of Autophagy in Parkinson's Disease. *ACS Chem Neurosci* 10:3914-3926.
57. Rabanal-Ruiz, Y., Otten, E.G., and Korolchuk, V.I. 2017. mTORC1 as the main gateway to autophagy. *Essays Biochem* 61:565-584.
58. Xilouri, M., Vogiatzi, T., Vekrellis, K., Park, D., and Stefanis, L. 2009. Abberant alpha-synuclein confers toxicity to neurons in part through inhibition of chaperone-mediated autophagy. *PLoS One* 4:e5515.
59. Kabeya, Y., Mizushima, N., Ueno, T., Yamamoto, A., Kirisako, T., Noda, T., Kominami, E., Ohsumi, Y., and Yoshimori, T. 2000. LC3, a mammalian homologue of yeast Apg8p, is localized in autophagosome membranes after processing. *EMBO J* 19:5720-5728.
60. Jiang, P., and Mizushima, N. 2015. LC3- and p62-based biochemical methods for the analysis of autophagy progression in mammalian cells. *Methods* 75:13-18.
61. Lopez, A., Fleming, A., and Rubinsztein, D.C. 2018. Seeing is believing: methods to monitor vertebrate autophagy in vivo. *Open Biol* 8.
62. Pankiv, S., Clausen, T.H., Lamark, T., Brech, A., Bruun, J.A., Outzen, H., Overvatn, A., Bjorkoy, G., and Johansen, T. 2007. p62/SQSTM1 binds directly to Atg8/LC3 to facilitate degradation of ubiquitinated protein aggregates by autophagy. *J Biol Chem* 282:24131-24145.
63. Spira, P.J., Sharpe, D.M., Halliday, G., Cavanagh, J., and Nicholson, G.A. 2001. Clinical and pathological features of a Parkinsonian syndrome in a family with an Ala53Thr alpha-synuclein mutation. *Ann Neurol* 49:313-319.
64. Yamaguchi, K., Cochran, E.J., Murrell, J.R., Polymeropoulos, M.H., Shannon, K.M., Crowther, R.A., Goedert, M., and Ghetti, B. 2005. Abundant neuritic inclusions and microvacuolar changes in a case of diffuse Lewy body disease with the A53T mutation in the alpha-synuclein gene. *Acta Neuropathol* 110:298-305.
65. Yeo, G., Holste, D., Kreiman, G., and Burge, C.B. 2004. Variation in alternative splicing across human tissues. *Genome Biol* 5:R74.
66. Apicco, D.J., Zhang, C., Maziuk, B., Jiang, L., Ballance, H.I., Boudeau, S., Ung, C., Li, H., and Wolozin, B. 2019. Dysregulation of RNA Splicing in Tauopathies. *Cell Rep* 29:4377-4388 e4374.
67. Garcia-Esparcia, P., Hernandez-Ortega, K., Koneti, A., Gil, L., Delgado-Morales, R., Castano, E., Carmona, M., and Ferrer, I. 2015. Altered machinery of protein synthesis is region- and stage-dependent and is associated with alpha-synuclein oligomers in Parkinson's disease. *Acta Neuropathol Commun* 3:76.
68. Johnson, S.C., Rabinovitch, P.S., and Kaeberlein, M. 2013. mTOR is a key modulator of ageing and age-related disease. *Nature* 493:338-345.
69. Kim, J., and Guan, K.L. 2019. mTOR as a central hub of nutrient signalling and cell growth. *Nat Cell Biol* 21:63-71.
70. Papadopoli, D., Boulay, K., Kazak, L., Pollak, M., Mallette, F., Topisirovic, I., and Hulea, L. 2019. mTOR as a central regulator of lifespan and aging. *F1000Res* 8.
71. Xun, Z., Sowell, R.A., Kaufman, T.C., and Clemmer, D.E. 2008. Quantitative proteomics of a presymptomatic A53T alpha-synuclein Drosophila model of Parkinson disease. *Mol Cell Proteomics* 7:1191-1203.
72. Fernandez-Santiago, R., Martin-Flores, N., Antonelli, F., Cerquera, C., Moreno, V., Bandres-Ciga, S., Manduchi, E., Tolosa, E., Singleton, A.B., Moore, J.H., et al. 2019. SNCA and mTOR Pathway Single Nucleotide Polymorphisms Interact to Modulate the Age at Onset of Parkinson's Disease. *Mov Disord* 34:1333-1344.

73. Arotcarena, M.L., Teil, M., and Dehay, B. 2019. Autophagy in Synucleinopathy: The Overwhelmed and Defective Machinery. *Cells* 8.
74. Menzies, F.M., Fleming, A., Caricasole, A., Bento, C.F., Andrews, S.P., Ashkenazi, A., Fullgrabe, J., Jackson, A., Jimenez Sanchez, M., Karabiyik, C., et al. 2017. Autophagy and Neurodegeneration: Pathogenic Mechanisms and Therapeutic Opportunities. *Neuron* 93:1015-1034.
75. Oakes, J.A., Davies, M.C., and Collins, M.O. 2017. TBK1: a new player in ALS linking autophagy and neuroinflammation. *Mol Brain* 10:5.
76. Pietri, M., Dakowski, C., Hannaoui, S., Alleaume-Butaux, A., Hernandez-Rapp, J., Ragagnin, A., Mouillet-Richard, S., Haik, S., Bailly, Y., Peyrin, J.M., et al. 2013. PDK1 decreases TACE-mediated alpha-secretase activity and promotes disease progression in prion and Alzheimer's diseases. *Nat Med* 19:1124-1131.
77. Dorval, T., Ogier, A., Genovesio, A., Lim, H.K., Kwon, D.Y., Lee, J.H., Worman, H.J., Dauer, W., and Grailhe, R. 2010. Contextual automated 3D analysis of subcellular organelles adapted to high-content screening. *J Biomol Screen* 15:847-857.
78. Hughes, C.S., Moggridge, S., Muller, T., Sorensen, P.H., Morin, G.B., and Krijgsveld, J. 2019. Single-pot, solid-phase-enhanced sample preparation for proteomics experiments. *Nat Protoc* 14:68-85.
79. Tyanova, S., Temu, T., Sinitcyn, P., Carlson, A., Hein, M.Y., Geiger, T., Mann, M., and Cox, J. 2016. The Perseus computational platform for comprehensive analysis of (prote)omics data. *Nat Methods* 13:731-740.
80. Tiscornia, G., Singer, O., and Verma, I.M. 2006. Production and purification of lentiviral vectors. *Nat Protoc* 1:241-245.

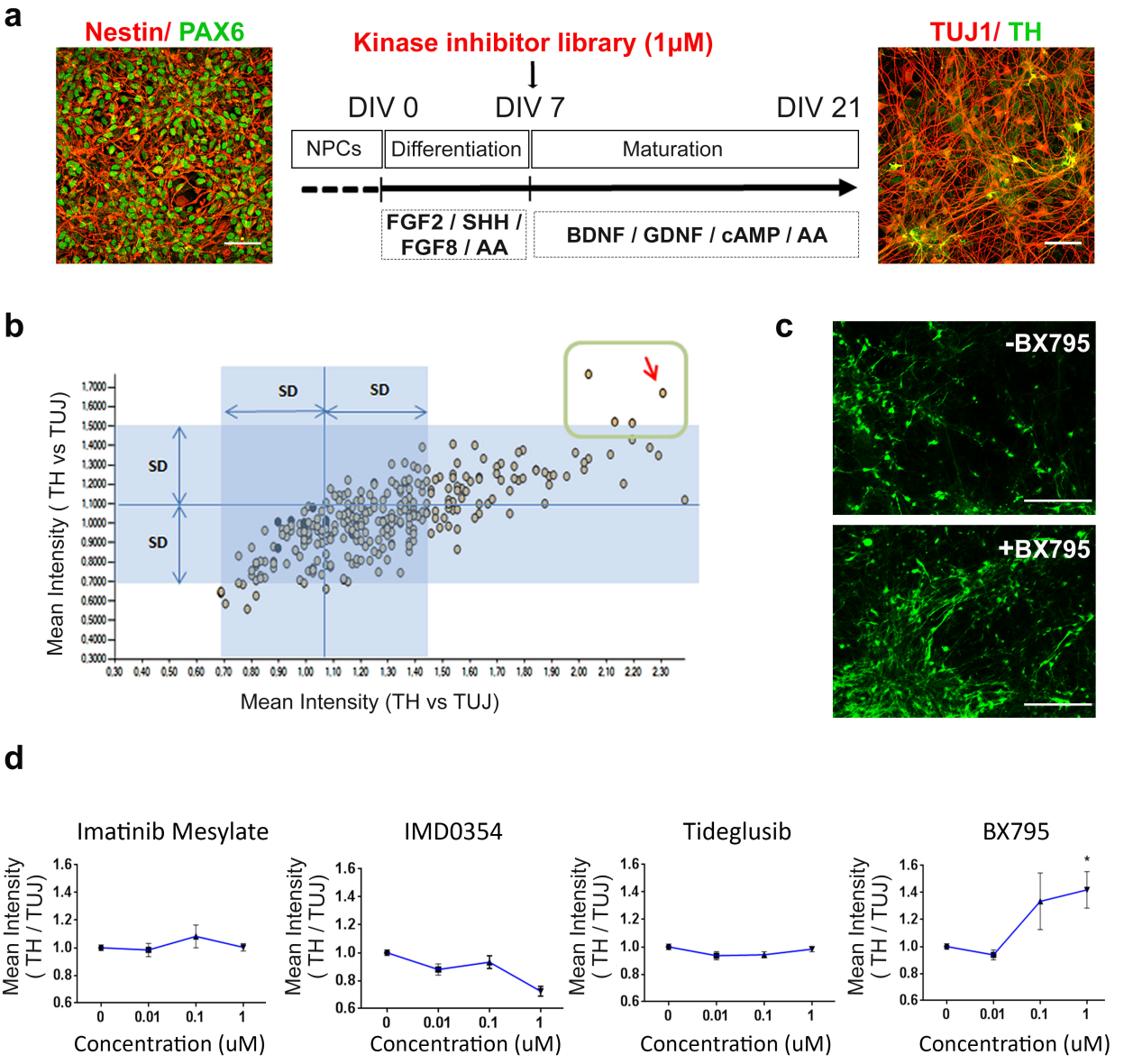
a
Nestin/ PAX6
Kinase inhibitor library (1μM)
DIV 0
DIV 7
DIV 21
NPCs
Differentiation
Maturation
FGF2 / SHH / FGF8 / AA
BDNF / GDNF / cAMP / AA
TUJ1/ TH
b
SD
SD
SD
SD
Mean Intensity (TH vs TUJ)
Mean Intensity (TH vs TUJ)
c
-BX795
+BX795
d
Imatinib Mesylate
IMD0354
Tideglusib
BX795
Mean Intensity (TH / TUJ)
Concentration (uM)
0
0.01
0.1
1
*

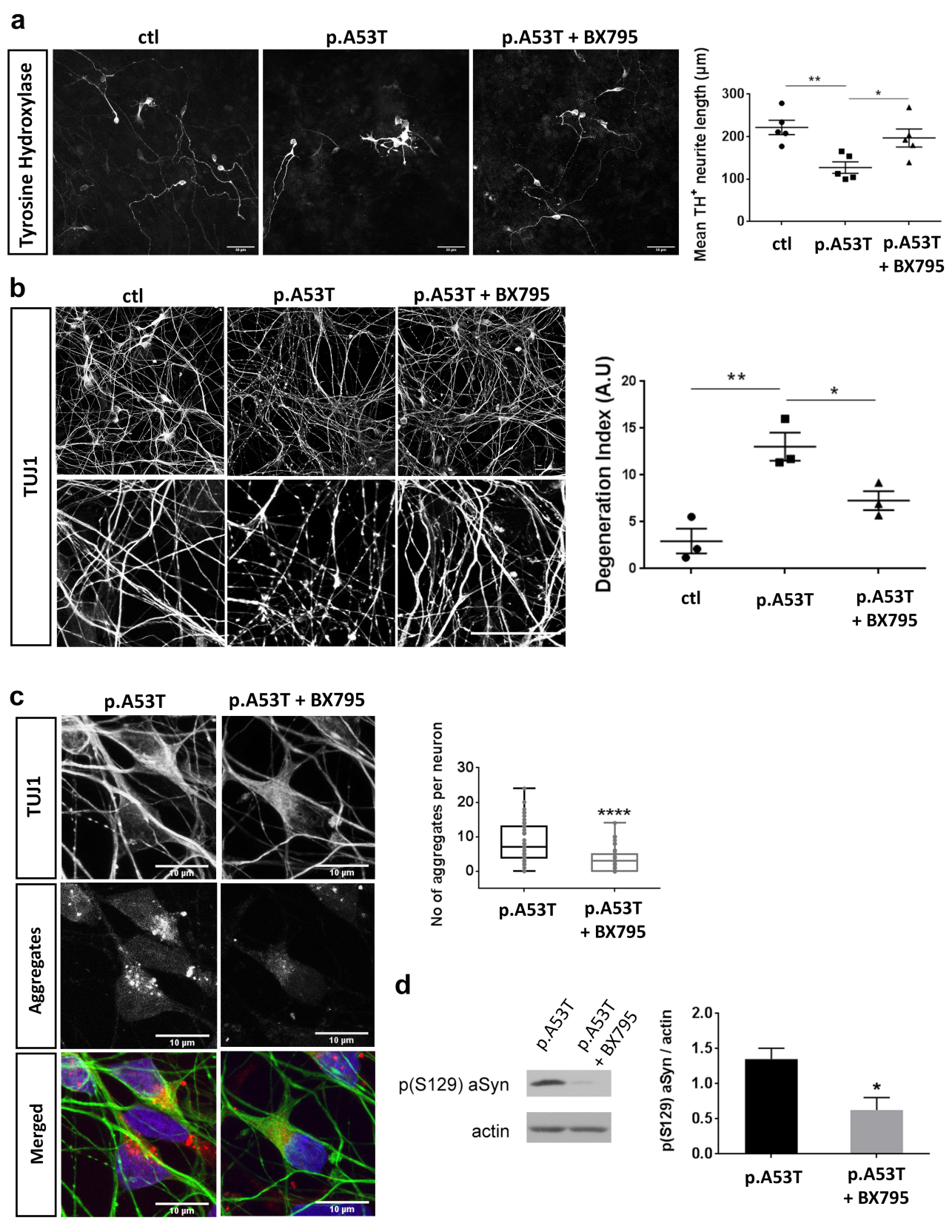
a
ctl
p.A53T
p.A53T + BX795
Tyrosine Hydroxylase
Mean TH+ neurite length (µm)
300
200
100
0
**
*
ctl
p.A53T
p.A53T + BX795
b
ctl
p.A53T
p.A53T + BX795
TUJ1
Degeneration Index (A.U)
20
15
10
5
0
**
*
ctl
p.A53T
p.A53T + BX795
c
p.A53T
p.A53T + BX795
TUJ1
Aggregates
Merged
10 µm
No of aggregates per neuron
30
20
10
0
****
p.A53T
p.A53T + BX795
d
p.A53T
p.A53T + BX795
p(S129) aSyn
actin
p(S129) aSyn / actin
2.0
1.5
1.0
0.5
0.0
*
p.A53T
p.A53T + BX795

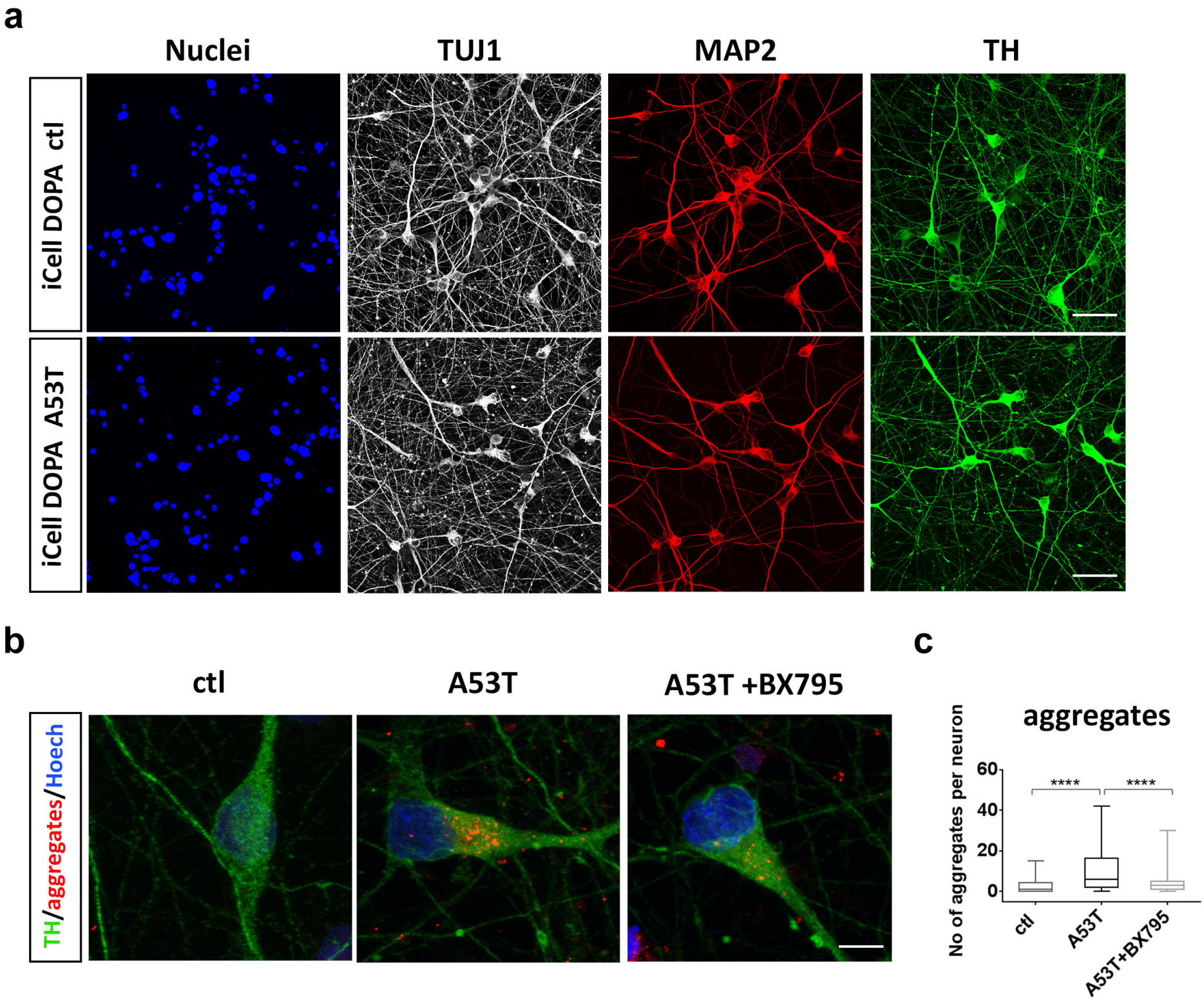
a
Nuclei
TUJ1
MAP2
TH
iCell DOPA ctl
iCell DOPA A53T
b
ctl
A53T
A53T +BX795
TH/aggregates/Hoech
c
aggregates
No of aggregates per neuron
60
40
20
0
****
****
ctl
A53T
A53T+BX795

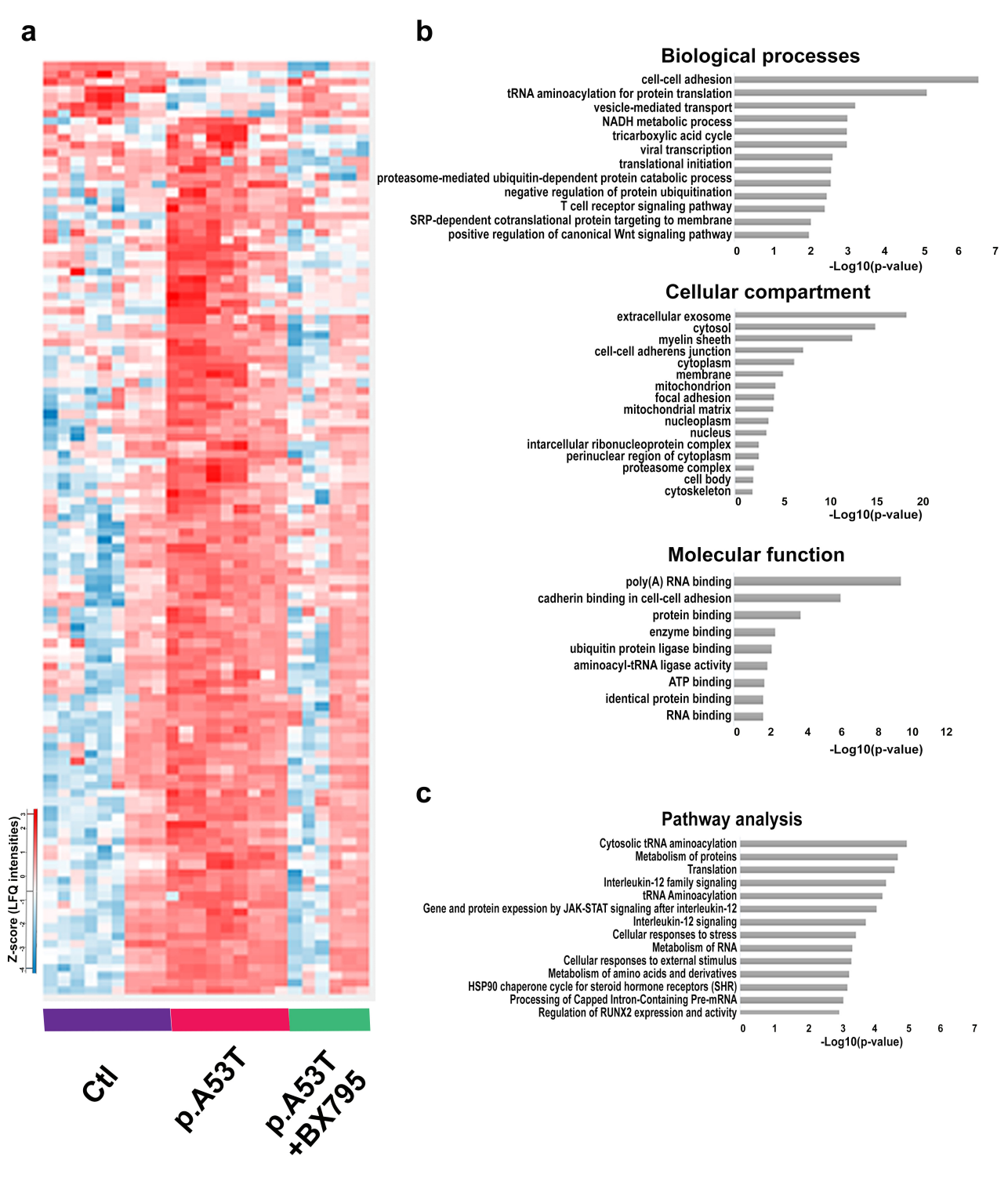
a
Z-score (LFQ intensities)
Ctl
p.A53T
p.A53T +BX795
b
Biological processes
cell-cell adhesion
tRNA aminoacylation for protein translation
vesicle-mediated transport
NADH metabolic process
tricarboxylic acid cycle
viral transcription
translational initiation
proteasome-mediated ubiquitin-dependent protein catabolic process
negative regulation of protein ubiquitination
T cell receptor signaling pathway
SRP-dependent cotranslational protein targeting to membrane
positive regulation of canonical Wnt signaling pathway
0 1 2 3 4 5 6 7
-Log10(p-value)
Cellular compartment
extracellular exosome
cytosol
myelin sheeth
cell-cell adherens junction
cytoplasm
membrane
mitochondrion
focal adhesion
mitochondrial matrix
nucleoplasm
nucleus
intarcellular ribonucleoprotein complex
perinuclear region of cytoplasm
proteasome complex
cell body
cytoskeleton
0 5 10 15 20
-Log10(p-value)
Molecular function
poly(A) RNA binding
cadherin binding in cell-cell adhesion
protein binding
enzyme binding
ubiquitin protein ligase binding
aminoacyl-tRNA ligase activity
ATP binding
identical protein binding
RNA binding
0 2 4 6 8 10 12
-Log10(p-value)
c
Pathway analysis
Cytosolic tRNA aminoacylation
Metabolism of proteins
Translation
Interleukin-12 family signaling
tRNA Aminoacylation
Gene and protein expession by JAK-STAT signaling after interleukin-12
Interleukin-12 signaling
Cellular responses to stress
Metabolism of RNA
Cellular responses to external stimulus
Metabolism of amino acids and derivatives
HSP90 chaperone cycle for steroid hormone receptors (SHR)
Processing of Capped Intron-Containing Pre-mRNA
Regulation of RUNX2 expression and activity
0 1 2 3 4 5 6 7
-Log10(p-value)

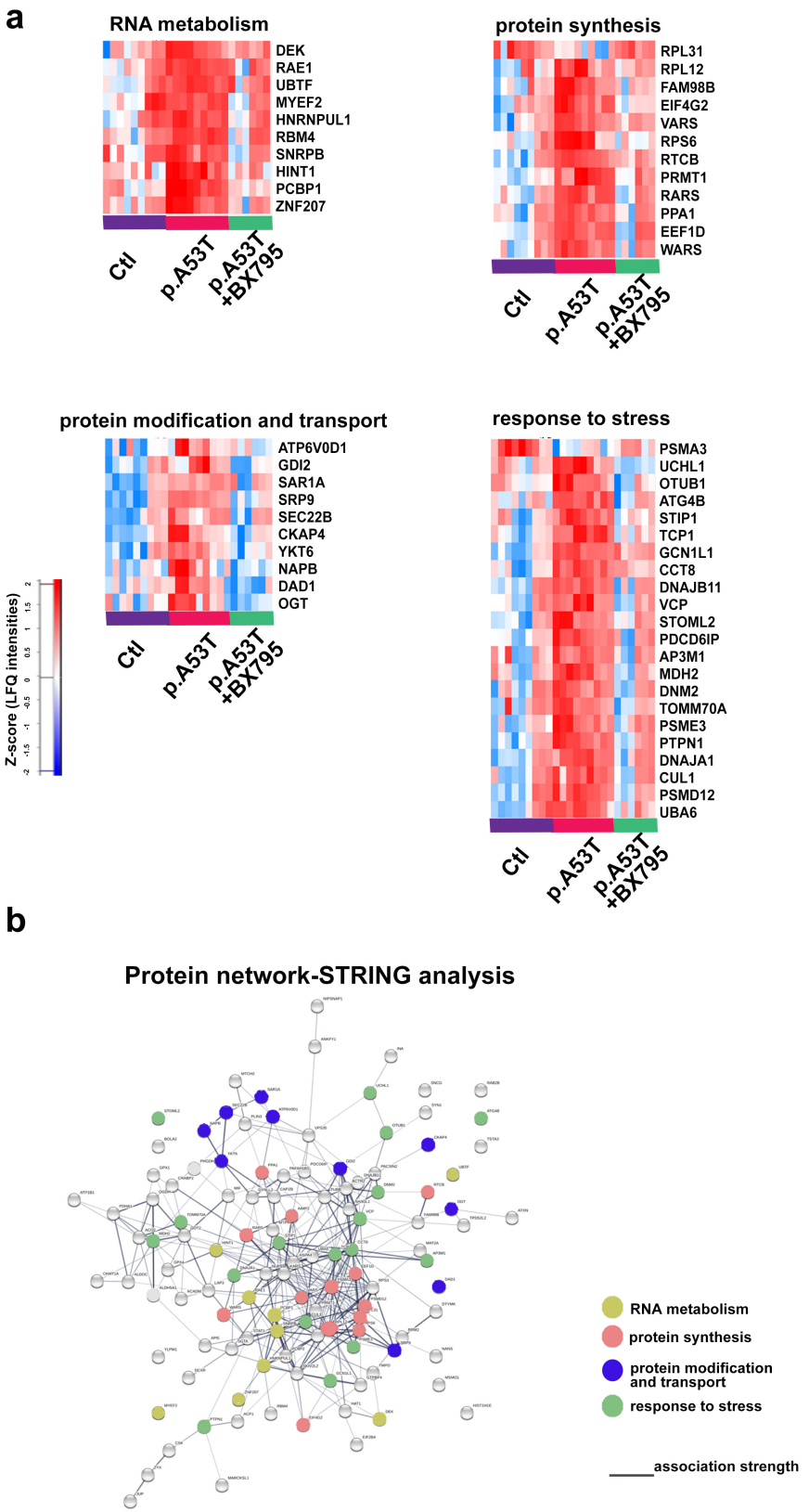
a
RNA metabolism
DEK
RAE1
UBTF
MYEF2
HNRNPUL1
RBM4
SNRPB
HINT1
PCBP1
ZNF207
Ctl
p.A53T
p.A53T +BX795
protein synthesis
RPL31
RPL12
FAM98B
EIF4G2
VARS
RPS6
RTCB
PRMT1
RARS
PPA1
EEF1D
WARS
Ctl
p.A53T
p.A53T +BX795
protein modification and transport
ATP6V0D1
GDI2
SAR1A
SRP9
SEC22B
CKAP4
YKT6
NAPB
DAD1
OGT
Ctl
p.A53T
p.A53T +BX795
response to stress
PSMA3
UCHL1
OTUB1
ATG4B
STIP1
TCP1
GCN1L1
CCT8
DNAJB11
VCP
STOML2
PDCD6IP
AP3M1
MDH2
DNM2
TOMM70A
PSME3
PTPN1
DNAJA1
CUL1
PSMD12
UBA6
Ctl
p.A53T
p.A53T +BX795
Z-score (LFQ intensities)
2
1.5
1
0.5
0
-0.5
-1
-1.5
-2
b
Protein network-STRING analysis
RNA metabolism
protein synthesis
protein modification and transport
response to stress
association strength

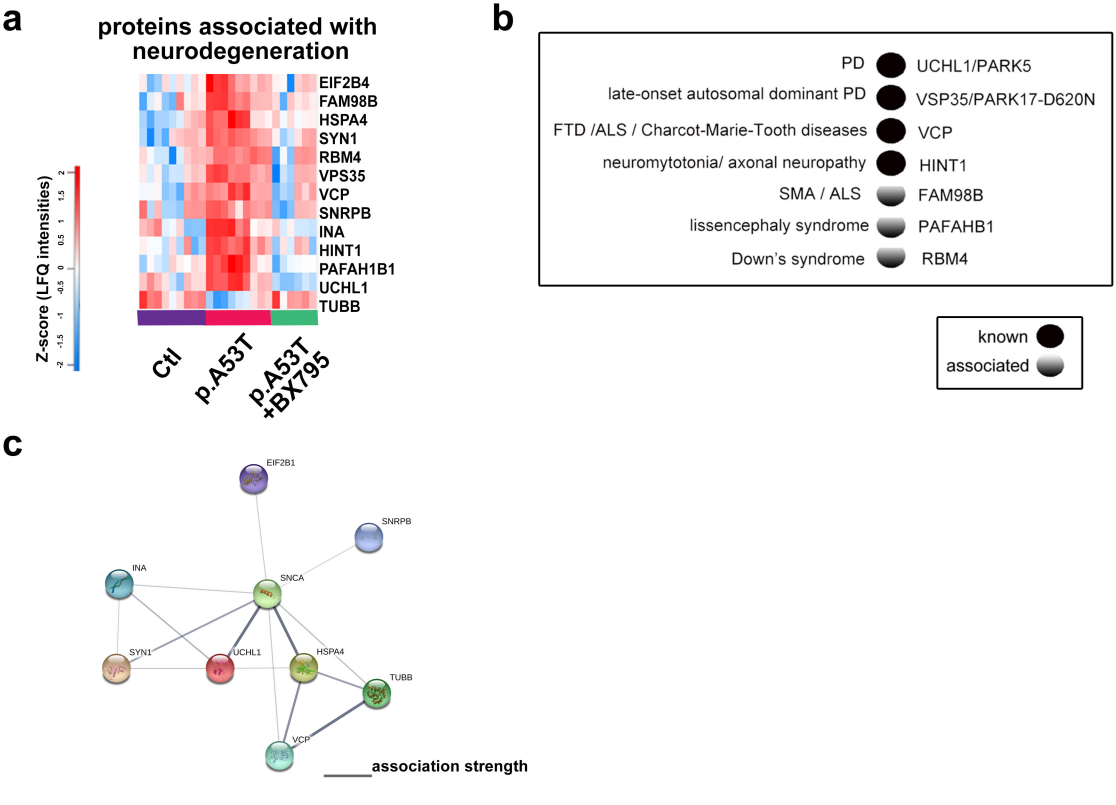
a
proteins associated with neurodegeneration
EIF2B4
FAM98B
HSPA4
SYN1
RBM4
VPS35
VCP
SNRPB
INA
HINT1
PAFAH1B1
UCHL1
TUBB
Z-score (LFQ intensities)
2
1.5
1
0.5
0
-0.5
-1
-1.5
-2
Ctl
p.A53T
p.A53T +BX795
b
PD
UCHL1/PARK5
late-onset autosomal dominant PD
VSP35/PARK17-D620N
FTD /ALS / Charcot-Marie-Tooth diseases
VCP
neuromytotonia/ axonal neuropathy
HINT1
SMA / ALS
FAM98B
lissencephaly syndrome
PAFAHB1
Down's syndrome
RBM4
known
associated
c
EIF2B1
SNRPB
INA
SNCA
SYN1
UCHL1
HSPA4
TUBB
VCP
association strength

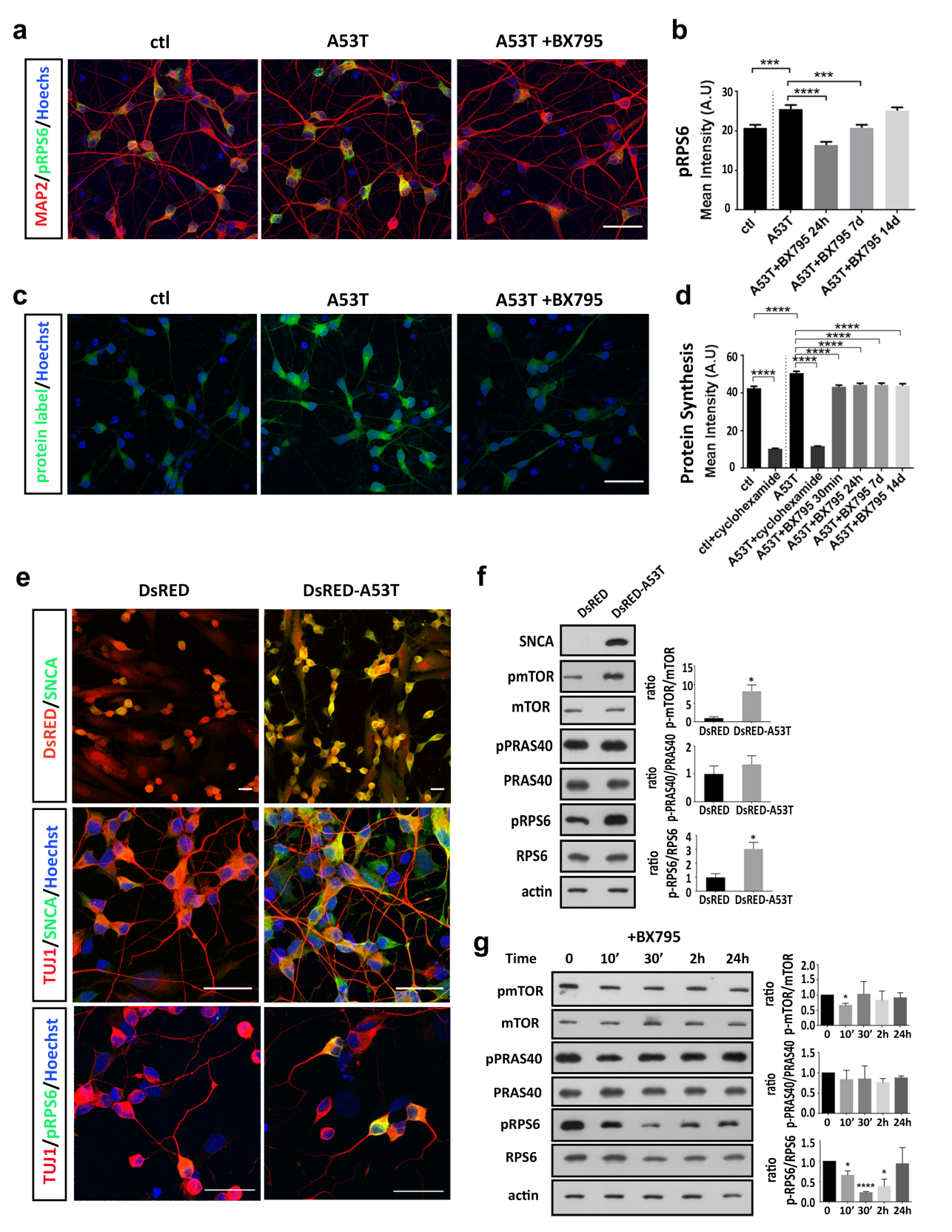
a
ctl
A53T
A53T +BX795
MAP2/pRPS6/Hoechs
b
pRPS6
Mean Intensity (A.U)
ctl
A53T
A53T+BX795 24h
A53T+BX795 7d
A53T+BX795 14d
c
ctl
A53T
A53T +BX795
protein label/Hoechst
d
Protein Synthesis
Mean Intensity (A.U)
ctl
ctl+cyclohexamide
A53T
A53T+cyclohexamide
A53T+BX795 30min
A53T+BX795 24h
A53T+BX795 7d
A53T+BX795 14d
e
DsRED
DsRED-A53T
DsRED/SNCA
TUJ1/SNCA/Hoechst
TUJ1/pRPS6/Hoechst
f
DsRED
DsRED-A53T
SNCA
pmTOR
mTOR
pPRAS40
PRAS40
pRPS6
RPS6
actin
ratio p-mTOR/mTOR
ratio p-PRAS40/PRAS40
ratio p-RPS6/RPS6
g
+BX795
Time
0
10'
30'
2h
24h
pmTOR
mTOR
pPRAS40
PRAS40
pRPS6
RPS6
actin
ratio p-mTOR/mTOR
ratio p-PRAS40/PRAS40
ratio p-RPS6/RPS6

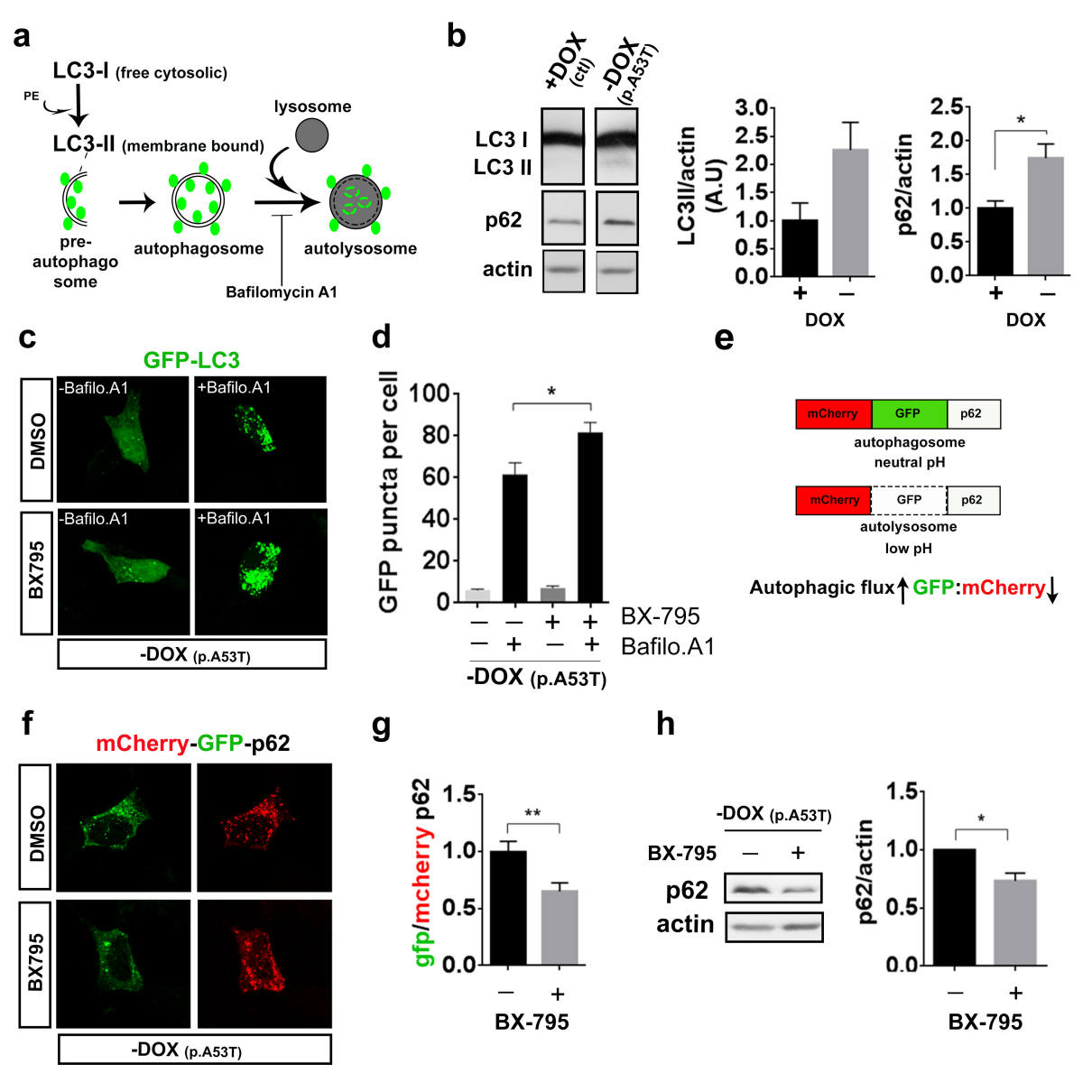
a
LC3-I (free cytosolic)
PE
LC3-II (membrane bound)
lysosome
pre-autophago some
autophagosome
autolysosome
Bafilomycin A1
b
+DOX (ctl)
-DOX (p.A53T)
LC3 I
LC3 II
p62
actin
LC3II/actin (A.U)
p62/actin
DOX
c
GFP-LC3
DMSO
BX795
-Bafilo.A1
+Bafilo.A1
-DOX (p.A53T)
d
GFP puncta per cell
BX-795
Bafilo.A1
-DOX (p.A53T)
e
mCherry
GFP
p62
autophagosome
neutral pH
autolysosome
low pH
Autophagic flux↑ GFP:mCherry↓
f
mCherry-GFP-p62
DMSO
BX795
-DOX (p.A53T)
g
gfp/mcherry p62
BX-795
h
-DOX (p.A53T)
BX-795
p62
actin
p62/actin
BX-795

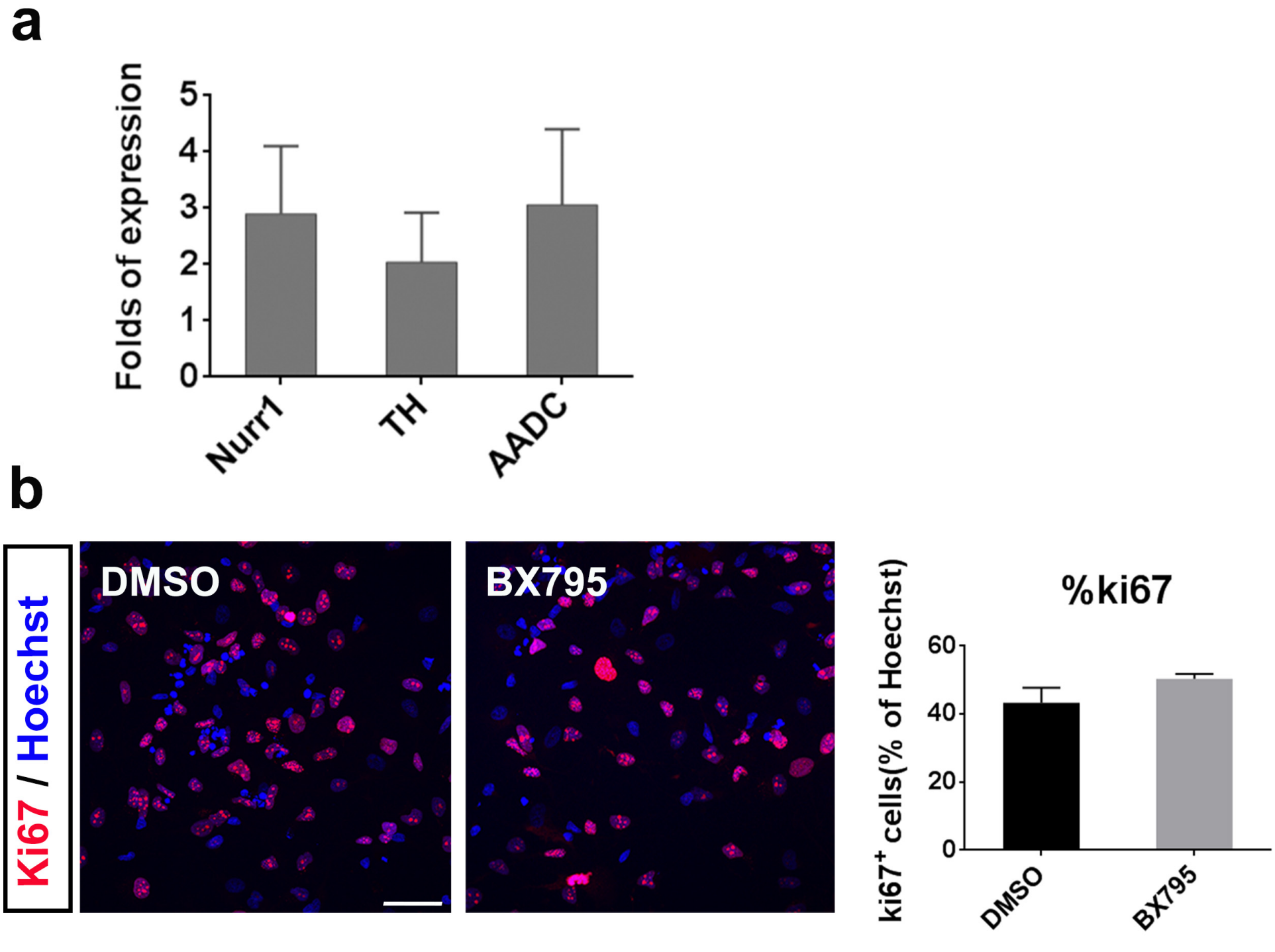
a
Folds of expression
0
1
2
3
4
5
Nurr1
TH
AADC
b
Ki67 / Hoechst
DMSO
BX795
%ki67
ki67+ cells(% of Hoechst)
0
20
40
60
DMSO
BX795

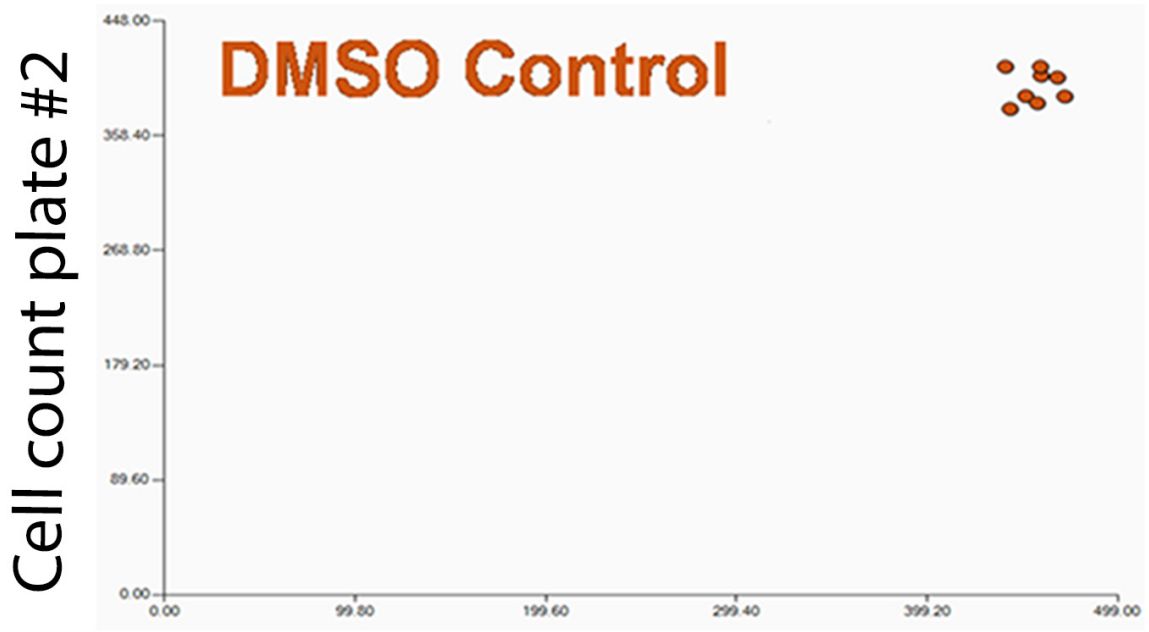
DMSO Control
Cell count plate #2
448.00
358.40
268.80
179.20
89.60
0.00
0.00
99.80
199.60
299.40
399.20
499.00
Cell count plate #1

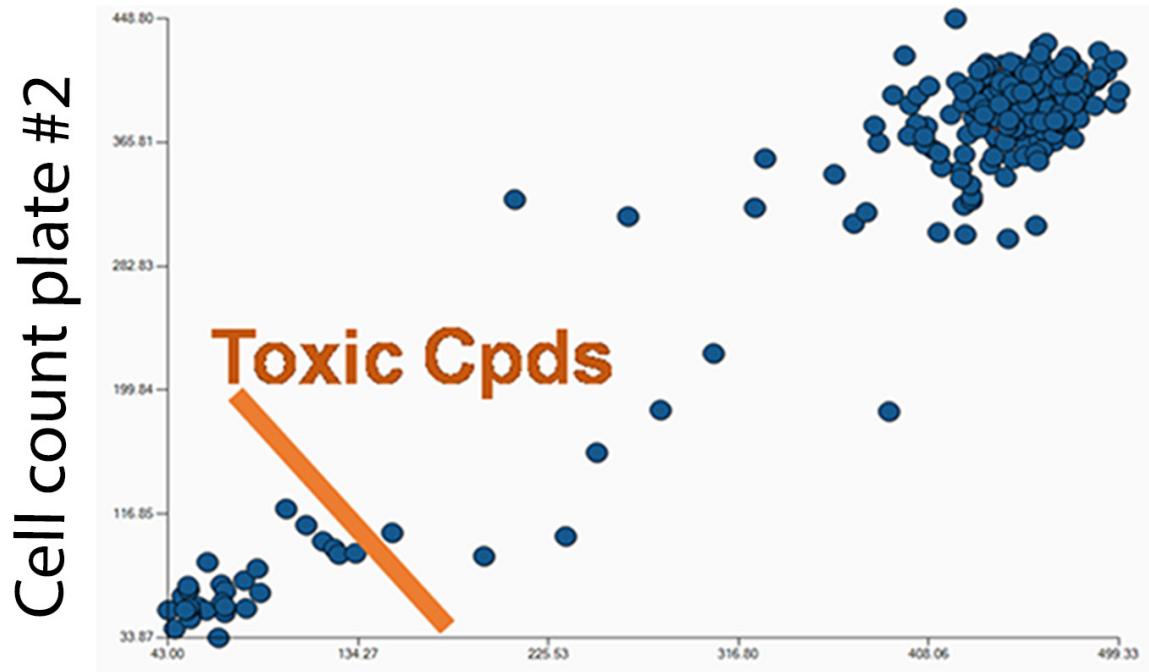
Toxic Cpds
Cell count plate #2
448.80
365.81
282.83
199.84
116.85
33.87
43.00
134.27
225.53
316.80
408.06
499.33
Cell count plate #1

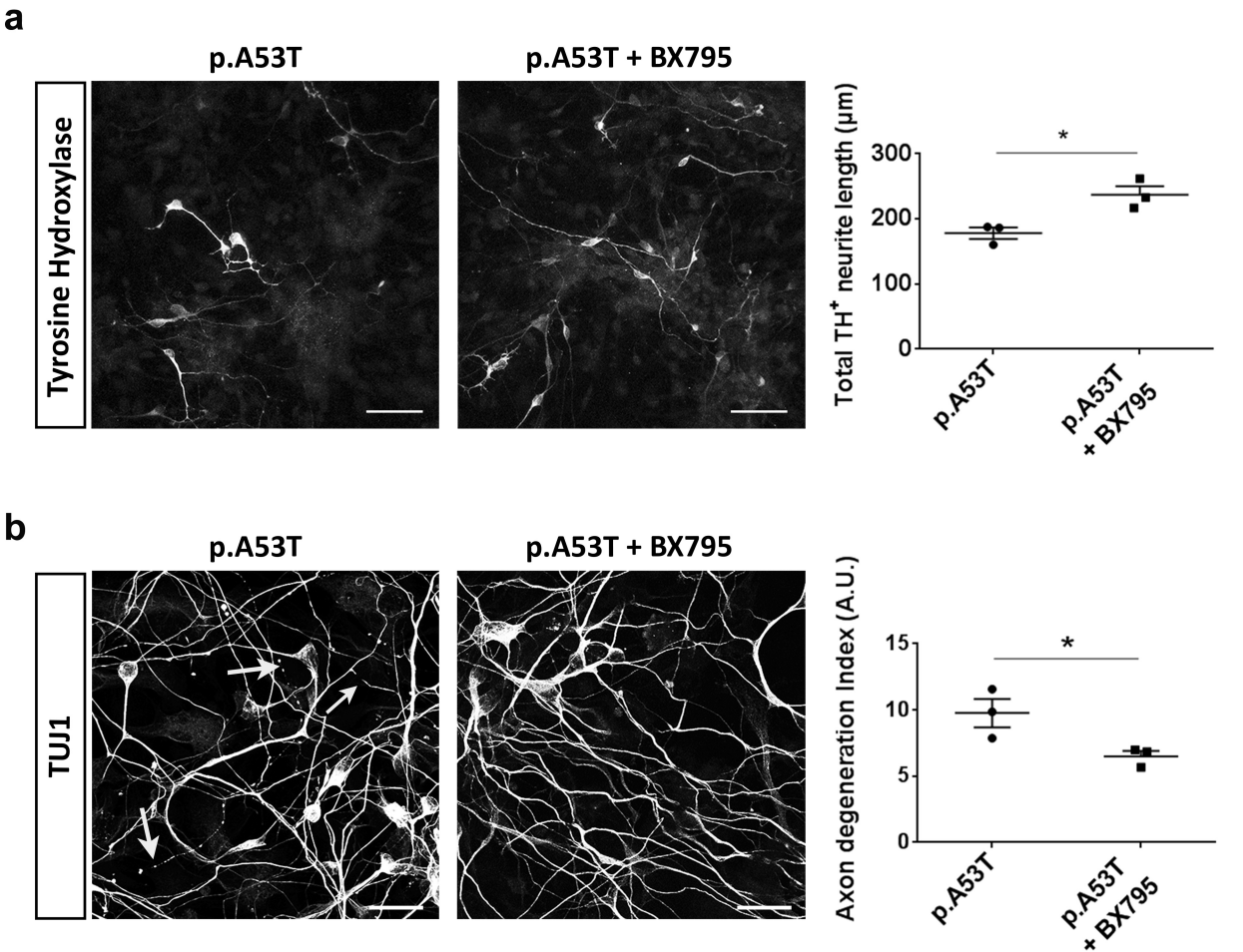
a
p.A53T
p.A53T + BX795
Tyrosine Hydroxylase
Total TH+ neurite length (µm)
300
200
100
0
*
p.A53T
p.A53T + BX795
b
p.A53T
p.A53T + BX795
TUJ1
Axon degeneration Index (A.U.)
15
10
5
0
*
p.A53T
p.A53T + BX795

a

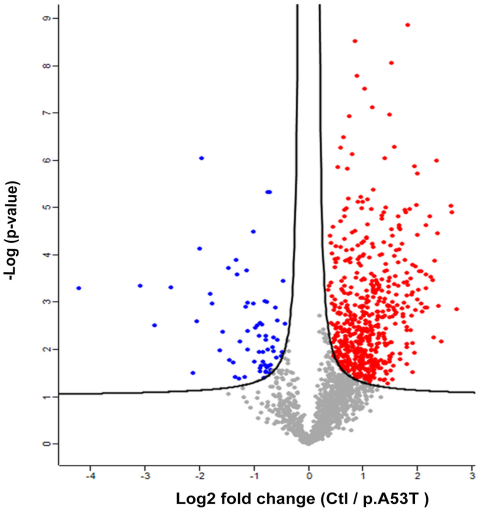
-Log (p-value)
Log2 fold change (Ctl / p.A53T)

b

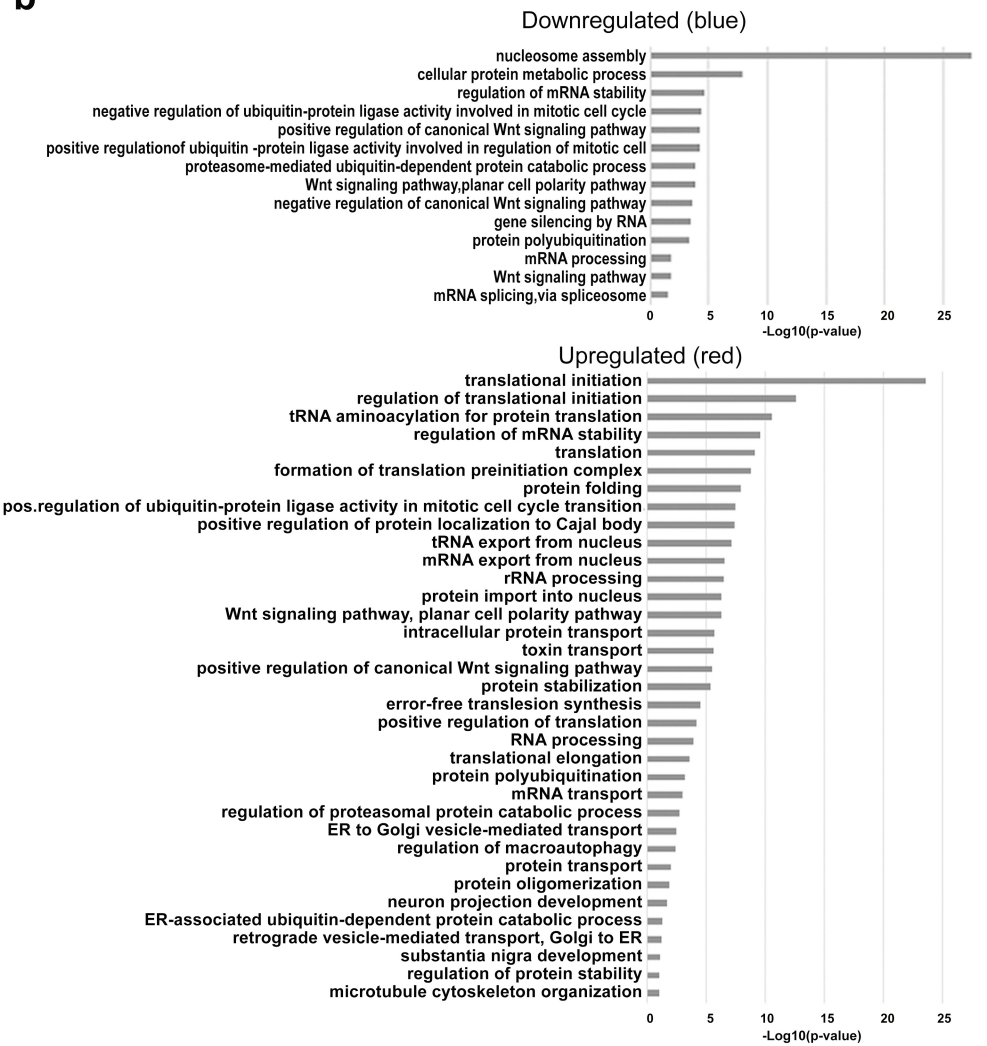
Downregulated (blue)
nucleosome assembly
cellular protein metabolic process
regulation of mRNA stability
negative regulation of ubiquitin-protein ligase activity involved in mitotic cell cycle
positive regulation of canonical Wnt signaling pathway
positive regulationof ubiquitin -protein ligase activity involved in regulation of mitotic cell
proteasome-mediated ubiquitin-dependent protein catabolic process
Wnt signaling pathway,planar cell polarity pathway
negative regulation of canonical Wnt signaling pathway
gene silencing by RNA
protein polyubiquitination
mRNA processing
Wnt signaling pathway
mRNA splicing,via spliceosome
-Log10(p-value)
Upregulated (red)
translational initiation
regulation of translational initiation
tRNA aminoacylation for protein translation
regulation of mRNA stability
translation
formation of translation preinitiation complex
protein folding
pos.regulation of ubiquitin-protein ligase activity in mitotic cell cycle transition
positive regulation of protein localization to Cajal body
tRNA export from nucleus
mRNA export from nucleus
rRNA processing
protein import into nucleus
Wnt signaling pathway, planar cell polarity pathway
intracellular protein transport
toxin transport
positive regulation of canonical Wnt signaling pathway
protein stabilization
error-free translesion synthesis
positive regulation of translation
RNA processing
translational elongation
protein polyubiquitination
mRNA transport
regulation of proteasomal protein catabolic process
ER to Golgi vesicle-mediated transport
regulation of macroautophagy
protein transport
protein oligomerization
neuron projection development
ER-associated ubiquitin-dependent protein catabolic process
retrograde vesicle-mediated transport, Golgi to ER
substantia nigra development
regulation of protein stability
microtubule cytoskeleton organization
-Log10(p-value)

Table S1: Kinase Inhibitor Library (Selleck Chemicals) and targets

Kinase Inhibitor Library (Selleck Chemicals) and targets	
Item Name	**Target**
Linifanib (ABT-869)	PDGFR, VEGFR
Axitinib	VEGFR, PDGFR, c-Kit
Saracatinib (AZD0530)	Src, Bcr-Abl
AZD6244 (Selumetinib)	MEK
BEZ235 (NVP-BEZ235)	mTOR, PI3K
BIBF1120 (Vargatef)	VEGFR, PDGFR, FGFR
Afatinib (BIBW2992)	EGFR, HER2
Bosutinib (SKI-606)	Src
Cediranib (AZD2171)	VEGFR, Flt
CI-1033 (Canertinib)	EGFR, HER2
CI-1040 (PD184352)	MEK
Dasatinib (BMS-354825)	Src, Bcr-Abl, c-Kit
Deforolimus (Ridaforolimus)	mTOR
Gefitinib (Iressa)	EGFR
Imatinib Mesylate	PDGFR, c-Kit, Bcr-Abl
Lapatinib Ditosylate (Tykerb)	EGFR, HER2
Motesanib Diphosphate	VEGFR, PDGFR, c-Kit
Nilotinib (AMN-107)	Bcr-Abl
Pazopanib HCl	VEGFR, PDGFR, c-Kit
PD0325901	MEK
PI-103	DNA-PK, PI3K, mTOR
Rapamycin (Sirolimus)	mTOR
Sorafenib (Nexavar)	VEGFR, PDGFR, Raf
Sunitinib Malate (Sutent)	VEGFR, PDGFR, c-Kit, Flt
Tandutinib (MLN518)	Flt
Temsirolimus (Torisel)	mTOR
Vandetanib (Zactima)	VEGFR
VX-680 (MK-0457, Tozasertib)	Aurora Kinase
Enzastaurin (LY317615)	PKC
BMS-599626 (AC480)	EGFR, HER2
Masitinib (AB1010)	c-Kit, PDGFR, FGFR, FAK
GDC-0941	PI3K
SB 431542	TGF-beta/Smad

Crizotinib (PF-02341066)	c-Met, ALK
ZSTK474	PI3K
SB 216763	GSK-3
SB 203580	p38 MAPK
SB 202190	p38 MAPK
MK-2206 dihydrochloride	Akt
PD153035 HCl	EGFR
SU11274	c-Met
NVP-ADW742	IGF-1R
KU-55933	ATM
PF-04217903	c-Met
U0126-EtOH	MEK
ZM-447439	Aurora Kinase
GDC-0879	Raf
LY294002	PI3K
Danusertib (PHA-739358)	Aurora Kinase, FGFR, Bcr-Abl, c-RET, Src
TAE684 (NVP-TAE684)	ALK
BI 2536	PLK
Foretinib (GSK1363089, XL880)	c-Met, VEGFR
SGX-523	c-Met
JNJ-38877605	c-Met
PD 0332991 (Palbociclib) HCl	CDK
XL147	PI3K
Everolimus (RAD001)	mTOR
MLN8237 (Alisertib)	Aurora Kinase
AT9283	Bcr-Abl, JAK, Aurora Kinase
AG-490	JAK, EGFR
SNS-032 (BMS-387032)	CDK
Barasertib (AZD1152-HQPA)	Aurora Kinase
PLX-4720	Raf
SNS-314	Aurora Kinase
CP-724714	EGFR, HER2
TGX-221	PI3K
WZ3146	EGFR
CYC116	Aurora Kinase, VEGFR
WZ4002	EGFR
PD98059	MEK
Regorafenib (BAY 73-4506)	c-Kit, Raf, VEGFR

WZ8040	EGFR
ENMD-2076	Flt, Aurora Kinase, VEGFR
PIK-90	PI3K
Tivozanib (AV-951)	VEGFR, c-Kit, PDGFR
OSI-930	c-Kit, VEGFR
Ku-0063794	mTOR
Amuvatinib (MP-470)	c-Met, c-Kit, PDGFR, Flt, c-RET
JNJ-7706621	CDK, Aurora Kinase
WYE-354	mTOR
IC-87114	Others
TG100-115	PI3K
GSK1059615	PI3K, mTOR
MGCD-265	c-Met, VEGFR, Tie-2
Rigosertib (ON-01910)	PLK
Ki8751	VEGFR, c-Kit, PDGFR
Pelitinib (EKB-569)	EGFR
AS-605240	PI3K
Aurora A Inhibitor I	Aurora Kinase
PHA-680632	Aurora Kinase
SP600125	JNK
TSU-68	VEGFR, PDGFR , FGFR
AS703026	MEK
SB 525334	TGF-beta/Smad
HMN-214	PLK
AEE788 (NVP-AEE788)	EGFR, Flt, VEGFR, HER2
PHA-793887	CDK
PIK-93	PI3K, VEGFR
Ponatinib (AP24534)	Bcr-Abl, VEGFR, FGFR, PDGFR, Flt
LY2228820	p38 MAPK
CCT129202	Aurora Kinase
XL765	PI3K, mTOR
AT7519	CDK
Quizartinib (AC220)	Flt
Hesperadin	Aurora Kinase
BIX 02188	MEK
BIX 02189	MEK
AZD7762	Chk
R406(free base)	Syk
AZD8055	mTOR

KRN 633	VEGFR, PDGFR
AT7867	Akt, S6 kinase
BMS 777607	c-Met
PD318088	MEK
KU-60019	ATM
BS-181 HCl	CDK
BIRB 796 (Doramapimod)	p38 MAPK
NVP-BSK805	JAK
DCC-2036 (Rebastinib)	Bcr-Abl
AZD8330	MEK
Neratinib (HKI-272)	HER2, EGFR
KW 2449	Flt, Bcr-Abl, Aurora Kinase
LY2784544	JAK
AZD8931	EGFR, HER2
GSK461364	PLK
R406	Syk, Flt
Raf265 derivative	VEGFR, Raf
BMS 794833	c-Met, VEGFR
NVP-BHG712	VEGFR, Src, Raf, Bcr-Abl
OSI-420 (Desmethyl Erlotinib)	EGFR
PIK-293	PI3K
AZ 960	JAK
Mubritinib (TAK 165)	HER2
PP242	mTOR
Cyt387	JAK
Indirubin	GSK-3
Quercetin (Sophoretin)	PI3K, PKC, Src, Sirtuin
Imatinib (Gleevec)	
GSK2126458	PI3K, mTOR
VX-702	p38 MAPK
CAL-101 (GS-1101)	PI3K
BI6727 (Volasertib)	PLK
PIK-294	PI3K
Telatinib (BAY 57-9352)	VEGFR, PDGFR, c-Kit
AZD5438	CDK
OSI-027	mTOR
PP-121	DNA-PK, mTOR, PDGF
WP1130	DUB, Bcr-Abl
BKM120 (NVP-BKM120)	PI3K
cx-4945 (Silmitasertib)	PKC

LDN193189	TGF-beta/Smad
PF-05212384 (PKI-587)	mTOR, PI3K
TAK-733	MEK
CCT128930	Akt
A66	PI3K
A-674563	Akt, CDK, PKA
AS-252424	PI3K
AS-604850	PI3K
PF-00562271	FAK
WAY-600	mTOR
WYE-125132	mTOR
WYE-687	mTOR
Apatinib (YN968D1)	VEGFR
LY2603618 (IC-83)	Chk
GSK1120212 (Trametinib)	MEK
A-769662	AMPK
KX2-391	Src
PCI-32765 (Ibrutinib)	Src
TAK-901	Aurora Kinase
TG101209	Flt, JAK, c-RET
AMG 900	Aurora Kinase
GSK1838705A	IGF-1, ALK
ZM 336372	Raf
GDC-0980 (RG7422)	mTOR, PI3K
NU7441(KU-57788)	DNA-PK, PI3K
Flavopiridol hydrochloride	CDK
PH-797804	p38 MAPK
Crenolanib (CP-868596)	PDGFR
PF-04691502	mTOR, PI3K, Akt
Dovitinib (TKI-258)	c-Kit, FGFR, Flt, VEGFR, PDGFR
Y-27632 2HCl	ROCK
Brivanib (BMS-540215)	VEGFR, FGFR
GSK1904529A	IGF-1R
MLN8054	Aurora Kinase
OSU-03012	PDK-1
PD173074	FGFR, VEGFR
Vemurafenib (PLX4032)	Raf
AMG-208	c-Met
Thiazovivin	ROCK
Palomid 529	mTOR

PHT-427	Akt, PDK-1
Tie2 kinase inhibitor	Tie-2
Baricitinib (LY3009104)	JAK
E7080 (Lenvatinib)	VEGFR
BGJ398 (NVP-BGJ398)	FGFR
SB590885	Raf
R788 (Fostamatinib)	Syk
CAY10505	PI3K
CHIR-124	Chk
Linsitinib (OSI-906)	IGF-1R
GSK690693	Akt
Ruxolitinib (INCB018424)	JAK
PHA-665752	c-Met
GSK1070916	Aurora Kinase
PKI-402	PI3K
TG101348 (SAR302503)	JAK
PF-03814735	Aurora Kinase, FAK
SB 415286	GSK-3
INK 128	mTOR
Dinaciclib (SCH727965)	CDK
MK-5108 (VX-689)	Aurora Kinase
AG-1478 (Tyrphostin AG-1478)	EGFR
AMG458	c-Met
Arry-380	HER2, EGFR
PHA-848125	CDK
AZ628	Raf
CCT137690	Aurora Kinase
CHIR-98014	GSK-3
NVP-BGT226	PI3K, mTOR
YM201636	PI3K
3-Methyladenine	PI3K
BX-795	PDK-1, IKK
BX-912	PDK-1
CH5424802	ALK
NVP-BVU972	c-Met
AST-1306	EGFR
BMS-265246	CDK
MK-2461	c-Met, FGFR, PDGFR
AZD2014	mTOR
TAK-285	EGFR, HER2

INCB28060	c-Met
WP1066	JAK
Piceatannol	Others
Sotrastaurin (AEB071)	PKC
AZD4547	FGFR
GDC-0068	Akt
Dabrafenib (GSK2118436)	Raf
Tyrphostin AG 879 (AG 879)	HER2
Torin 2	mTOR
BYL719	PI3K
CEP33779	JAK
NVP-TAE226	FAK
CP 673451	Others
PHA-767491	CDK
Torin 1	mTOR
TPCA-1	IKK
Wortmannin	PI3K
Staurosporine	PKC
ARRY334543	EGFR
Tideglusib	GSK-3
Semaxanib (SU5416)	VEGFR
SAR131675	VEGFR
IMD0354	IKK
TG 100713	PI3K
WHI-P154	JAK, EGFR
ARQ 197 (Tivantinib)	c-Met
TWS119	GSK-3

Table S2: Differentially expressed proteins between pA53T and control neurons

Differentially expressed proteins between pA53T and control neurons		
Protein names	**Gene names**	**Difference**
Prothymosin alpha;Prothymosin alpha, N-terminally processed;Thymosin alpha-1	PTMA	-4,22058974
Protein transport protein Sec61 subunit alpha isoform 1	SEC61A1	-3,09643152
Histone H3.3;Histone H3.2;Histone H3.1t;Histone H3.1	H3f3a;H3F3A;HIST2H3A;HIST3H3;Hist1h3b;Hist1h3a;HIST1H3A	-2,83120812
Fibronectin;Anastellin;Ugl-Y1;Ugl-Y2;Ugl-Y3	FN1	-2,52735837
60S ribosomal protein L31	RPL31	-2,12383503
Glial fibrillary acidic protein	GFAP	-2,05050193
Golgi-associated plant pathogenesis-related protein 1	GLIPR2	-1,997111
Histone H1.4	HIST1H1E	-1,96522289
Transgelin	TAGLN	-1,80209096
Radixin	RDX	-1,77318255
Collagen alpha-1(I)	COL1A1	-1,63404274

chain		
Ubiquitin-conjugating enzyme E2 variant 2	UBE2V2	-1,57051065
Histone H2A type 2-C;Histone H2A type 2-A	Hist2h2ac;HIST2H2AC;Hist2h2aa1;HIST2H2AA3	-1,46609285
MARCKS-related protein	MARCKSL1	-1,45300293
Chromobox protein homolog 1	CBX1	-1,35597377
Histone H2B type 1-L;Histone H2B type 1-M;Histone H2B type 1-N;Histone H2B type 1-H;Histone H2B type 1-P;Histone H2B type 1-K;Histone H2B type 1-C/E/G;Histone H2B type 2-B;Histone H2B type 1-B;Histone H2B type 2-F;Histone H2B type 1-C/E/F/G/I;Histone H2B type 1-D;Histone H2B type 1-F/J/L;Histone	HIST1H2BL;HIST1H2BM;HIST1H2BN;HIST1H2BH;Hist1h2bp;Hist1h2bk;Hist1h2bc;Hist2h2bb;Hist1h2bh;Hist1h2bb;HIST2H2BF;HIST1H2BC;HIST1H2BD;Hist1h2bm;Hist1h2bf;HIST1H2BK;H2BFS;hist2h2l;Hist1h2ba;HIST1H2BA	-1,32357407

H2B type F-S;Histone H2B 3;Histone H2B type 1-A		
Histone H1.5	HIST1H1B	-1,32074398
TAR DNA-binding protein 43	TARDBP	-1,28565174
Neutral amino acid transporter A	SLC1A4	-1,26124043
Clathrin light chain A	CLTA	-1,16397328
Cytoplasmic dynein 1 intermediate chain 2	DYNC1I2;Dync1i2	-1,15378104
CDKN2A-interacting protein	CDKN2AIP	-1,13875198
Tropomyosin alpha-4 chain	TPM4	-1,1163631
Tropomyosin alpha-1 chain	TPM1	-1,11481222
Soluble lamin-associated protein of 75 kDa	FAM169A	-1,11439917
Ribosome-binding protein 1	RRBP1	-1,01449564
Histone H1.2;Histone H1.3	HIST1H1C;Hist1h1d;Hist1h1c	-1,00663524
Zinc finger RNA-binding protein	ZFR	-1,00062116
Cellular retinoic acid-binding protein 1	CRABP1	-0,97820261

45 kDa calcium-binding protein	SDF4	-0,93680615
Eukaryotic translation initiation factor 4 gamma 3	EIF4G3	-0,91687775
Protein phosphatase 1B	PPM1B	-0,90773561
Caldesmon	CALD1	-0,89930958
Proteasome subunit alpha type-3	PSMA3	-0,89364327
Tubulin beta chain	TUBB	-0,89241261
Protein canopy homolog 2	CNPY2	-0,86795319
Nuclear pore complex protein Nup153	NUP153	-0,85966153
Transmembrane emp24 domain-containing protein 10	TMED10;Tmed10	-0,84096781
Rho GTPase-activating protein 21	ARHGAP21	-0,83467611
Brain acid soluble protein 1	BASP1	-0,82571665
Heterochromatin protein 1-binding protein 3	HP1BP3	-0,81141747
Peroxiredoxin-2	PRDX2	-0,80545298
Plasma	ATP2B1	-0,78781933

membrane calcium-transporting ATPase 1		
Band 4.1-like protein 3;Band 4.1-like protein 3, N-terminally processed	EPB41L3	-0,78772333
Actin, alpha cardiac muscle 1;Actin, alpha skeletal muscle	ACTC1;ACTA1	-0,77967135
Polypyrimidine tract-binding protein 2	PTBP2;Ptbp2	-0,77931235
Putative phospholipase B-like 2;Putative phospholipase B-like 2 32 kDa form;Putative phospholipase B-like 2 45 kDa form	PLBD2	-0,76606115
Heterogeneous nuclear ribonucleoprotein A1;Heterogeneous nuclear ribonucleoprotein A1, N-terminally processed;Heterogeneous	HNRNPA1;HNRNPA1L2	-0,76263936

nuclear ribonucleoprotein A1-like 2		
Acyl-CoA dehydrogenase family member 9, mitochondrial	ACAD9	-0,7569809
Kinectin	KTN1	-0,74694803
UBX domain-containing protein 1	UBXN1	-0,72750621
ATP synthase subunit d, mitochondrial	ATP5H	-0,72205056
Reticulon-4	RTN4	-0,71967845
Amyloid beta A4 protein;N-APP;Soluble APP-alpha;Soluble APP-beta;C99;Beta-amyloid protein 42;Beta-amyloid protein 40;C83;P3(42);P3(40);C80;Gamma-secretase C-terminal fragment 59;Gamma-secretase C-terminal fragment 57;Gamma-secretase C-	APP;App	-0,70541975

terminal fragment 50;C31		
Formin-binding protein 1-like	FNBP1L	-0,69941372
Ubiquitin-40S ribosomal protein S27a;Ubiquitin;40S ribosomal protein S27a;Ubiquitin-60S ribosomal protein L40;Ubiquitin;60S ribosomal protein L40;Polyubiquitin-B;Ubiquitin;Polyubiquitin-C;Ubiquitin;Polyubiquitin-A;Ubiquitin;Ubiquitin-related	RPS27A;Rps27a;UBA52;Uba52;RpL40;RpS27A;UBB;Ubb;UBC;ubq-2;ubq-1	-0,66847505
Prelamin-A/C;Lamin-A/C	LMNA	-0,66254658
N(G),N(G)-dimethylarginine dimethylaminohydrolase 2	DDAH2	-0,64632734
U4/U6.U5 tri-snRNP-associated protein 1	SART1;Sart1	-0,63747215
Splicing	SFPQ	-0,61198764

factor, proline- and glutamine-rich		
Delta-1-pyrroline-5-carboxylate dehydrogenase, mitochondrial	ALDH4A1	-0,58621025
Pre-mRNA-processing factor 40 homolog A	PRPF40A	-0,57962841
Zyxin	ZYX	-0,56851408
Histone H4	Hist1h4a;HIST1H4A	-0,49797291
Catenin delta-1	CTNND1	-0,48542023
Lamin-B1	LMNB1	-0,47633659
Reticulocalbin-1	RCN1	-0,44097794
Polyadenylate-binding protein 1	PABPC1	0,36678696
T-complex protein 1 subunit eta	CCT7	0,37164391
ELAV-like protein 1	ELAVL1	0,38943545
Nitric oxide synthase-interacting protein	NOSIP	0,40467771
Lamina-associated polypeptide 2, isoform alpha;Thymopoietin;Thymopentin	TMPO	0,41073651
Chromobox protein	CBX5;Cbx5	0,41383574

homolog 5		
Elongation factor 2	EEF2;Eef2	0,42066256
60S ribosomal protein L4	RPL4	0,4245472
Cell cycle and apoptosis regulator protein 2	CCAR2	0,43223847
Pre-mRNA-splicing factor ATP-dependent RNA helicase DHX15	DHX15	0,44824028
Ubiquitin thioesterase OTUB1	OTUB1	0,44847086
Myosin-10	MYH10	0,44919946
Platelet-activating factor acetylhydrolase IB subunit alpha	PAFAH1B1;Pafah1b1	0,46440866
MICOS complex subunit MIC60	IMMT	0,47223282
General transcription factor II-I	GTF2I;Gtf2i	0,47717624
Voltage-dependent anion-selective channel protein 2	VDAC2	0,47729916
DNA topoisomerase 1	TOP1	0,47934278
60 kDa heat	HSPD1	0,48447143

shock protein, mitochondrial		
Far upstream element-binding protein 2	KHSRP	0,48472828
Stress-70 protein, mitochondrial	HSPA9	0,48504872
Dynamin-2	DNM2	0,48548105
Hydroxymethylglutaryl-CoA synthase, cytoplasmic	HMGCS1	0,48664877
Sarcoplasmic/endoplasmic reticulum calcium ATPase 2	ATP2A2	0,49363581
Multifunctional protein ADE2;Phosphoribosylaminoimidazole-succinocarboxamide synthase;Phosphoribosylaminoimidazole carboxylase	PAICS	0,49574788
Bifunctional purine biosynthesis protein PURH;Phosphoribosylaminoimidazolecarboxamide formyltransfe	ATIC	0,49794049

rase;IMP cyclohydrolase		
Isocitrate dehydrogenase [NADP], mitochondrial	IDH2	0,49905989
Adenosylhomocysteinase	AHCY	0,50178507
Methionine--tRNA ligase, cytoplasmic	MARS	0,50235918
Eukaryotic initiation factor 4A-III;Eukaryotic initiation factor 4A-III, N-terminally processed	EIF4A3	0,50351991
Coatomer subunit alpha;Xenin;Proxenin	COPA	0,50397809
Rab GDP dissociation inhibitor beta	GDI2	0,5050727
Oxysterol-binding protein 1	OSBP	0,50976329
Ras-related protein Rab-2A	RAB2A	0,51790598
NADPH--cytochrome P450 reductase	POR	0,52251604
Aspartate aminotransferase, mitochondrial	GOT2	0,52831353

Eukaryotic translation initiation factor 3 subunit E	EIF3E	0,53256332
40S ribosomal protein SA	Rpsa;RPSA	0,53590287
Stress-induced-phosphoprotein 1	STIP1	0,53696569
Serine-threonine kinase receptor-associated protein	STRAP	0,53877873
2,4-dienoyl-CoA reductase, mitochondrial	DECR1	0,54022598
Malate dehydrogenase, mitochondrial	MDH2	0,54088974
Malectin	MLEC	0,54325846
Coatomer subunit beta	COPB2	0,54395019
Septin-9	SEPT9	0,54734124
CTP synthase 1	CTPS1	0,55151049
Signal transducer and activator of transcription 3	STAT3	0,55413225
Cysteine protease ATG4B	ATG4B;Atg4b	0,55785137

Flap endonuclease 1	FEN1	0,56196107
ATP-dependent RNA helicase DDX19A;ATP-dependent RNA helicase DDX19B	DDX19A;DDX19B	0,56328519
Nuclear pore membrane glycoprotein 210	NUP210	0,56637213
Heat shock 70 kDa protein 4	HSPA4	0,566942
Phosphoserine aminotransferase	PSAT1	0,57374679
Pyruvate dehydrogenase E1 component subunit beta, mitochondrial	PDHB	0,57605701
Transitional endoplasmic reticulum ATPase	Vcp;VCP	0,58135562
Arginine--tRNA ligase, cytoplasmic	RARS	0,58195093
X-ray repair cross-complementing protein 6	XRCC6	0,58255429
Bifunctional glutamate/proline--tRNA ligase;Glutam	EPRS	0,58510844

ate--tRNA ligase;Proline--tRNA ligase		
Peroxiredoxin-6	PRDX6	0,58962144
CAD protein;Glutamine-dependent carbamoyl-phosphate synthase;Aspartate carbamoyltransferase;Dihydroorotase	CAD	0,59100299
Farnesyl pyrophosphate synthase	FDPS	0,59512181
Cyclin-dependent-like kinase 5	CDK5	0,60137918
Ran GTPase-activating protein 1	RANGAP1	0,60225423
Heterogeneous nuclear ribonucleoprotein D-like	HNRNPDL	0,60320918
NEDD8-activating enzyme E1 catalytic subunit	UBA3	0,60380046
T-complex protein 1 subunit beta	CCT2	0,60664368
Cytoskeleton-associated protein 5	CKAP5	0,60961533
Prohibitin	PHB	0,61144045
Unconventional myosin-VI	MYO6	0,61296166

Cleavage stimulation factor subunit 3	CSTF3	0,61377652
Importin-5	IPO5	0,61648496
Very-long-chain (3R)-3-hydroxyacyl-CoA dehydratase 3	HACD3	0,61995697
Glycine--tRNA ligase	GARS	0,62528377
Thioredoxin-like protein 1	TXNL1	0,62663396
Isoleucine--tRNA ligase, cytoplasmic	IARS	0,62683529
Pyruvate carboxylase, mitochondrial	PC	0,63483853
T-complex protein 1 subunit gamma	CCT3	0,6354794
40S ribosomal protein S10;Putative 40S ribosomal protein S10-like	RPS10;RPS10P5	0,63819567
182 kDa tankyrase-1-binding protein	TNKS1BP1	0,64544317
ATP-citrate synthase	ACLY;Acly	0,64815733
Inositol-3-phosphate synthase 1	ISYNA1	0,65151003

Guanine nucleotide-binding protein subunit beta-2-like 1;Guanine nucleotide-binding protein subunit beta-2-like 1, N-terminally processed	GNB2L1	0,6532597
Probable ATP-dependent RNA helicase DDX6;ATP-dependent RNA helicase ddx6	DDX6;Ddx6;ddx6	0,65331353
Gem-associated protein 5	GEMIN5	0,65372573
Mitochondrial-processing peptidase subunit alpha	PMPCA	0,65491528
ATP-dependent RNA helicase DDX1	DDX1	0,65614933
Neurofilament light polypeptide	NEFL	0,65656302
40S ribosomal protein S6	RPS6	0,65667152
Methylmalonate-semialdehyde dehydrogena	ALDH6A1	0,65771061

se [acylating], mitochondrial		
Heterogeneous nuclear ribonucleoprotein L	HNRNPL	0,65942128
Exportin-1	XPO1;Xpo1	0,66231028
T-complex protein 1 subunit theta	CCT8	0,66265233
Heterogeneous nuclear ribonucleoprotein M	HNRNPM	0,66267946
T-complex protein 1 subunit epsilon	CCT5	0,66413583
Lysine--tRNA ligase	KARS	0,66436916
Carboxymethylenebutenolidase homolog	CMBL	0,66666497
Uncharacterized protein C7orf50	C7orf50	0,66734335
Neurofilament medium polypeptide	NEFM	0,6674739
Dynamin-1-like protein	DNM1L	0,66997189
Nuclear pore complex protein Nup50	NUP50	0,67132717
Peroxiredoxin-1	PRDX1	0,67464023
Ubiquitin carboxyl-terminal hydrolase 5	USP5	0,67514716

Chloride intracellular channel protein 1	CLIC1	0,67566193
T-complex protein 1 subunit delta	CCT4	0,6770969
Elongation factor 1-beta	EEF1B2	0,67718993
AP-2 complex subunit alpha-2	AP2A2	0,68129052
Septin-2	SEPT2	0,68638208
High mobility group protein B1;Putative high mobility group protein B1-like 1	HMGB1;Hmgb1;HMGB1P1	0,6891399
Replication factor C subunit 1	RFC1	0,69490157
MICOS complex subunit MIC19	CHCHD3	0,69938045
Alpha-internexin	INA	0,7001809
RNA polymerase II-associated factor 1 homolog	PAF1	0,70027139
60S ribosomal protein L5	RPL5	0,7005859
Sideroflexin-1	SFXN1	0,701732
Poly(rC)-binding protein 2	PCBP2	0,70254792
Protein crumbs homolog 2	CRB2	0,70587688

39S ribosomal protein L22, mitochondrial	MRPL22	0,70988634
Cytoskeleton-associated protein 4	CKAP4	0,70989778
Tumor protein D54	TPD52L2	0,71015655
Metastasis-associated protein MTA2	MTA2;Mta2	0,71304385
mRNA cap guanine-N7 methyltransferase	RNMT	0,71329859
Ubiquitin carboxyl-terminal hydrolase isozyme L1	UCHL1	0,71483188
Cytochrome b-c1 complex subunit 2, mitochondrial	UQCRC2	0,715438
YLP motif-containing protein 1	YLPM1	0,71668392
ATP-dependent DNA helicase Q1	RECQL	0,71730084
Vacuolar protein sorting-associated protein 35	VPS35;Vps35	0,71786329
Chromobox protein homolog 3	CBX3	0,71830495
60S	RPL12	0,72048357

ribosomal protein L12		
Sodium/potassium-transporting ATPase subunit beta-1	ATP1B1	0,72105302
Protein LSM14 homolog B	LSM14B	0,72187487
C-1-tetrahydrofolate synthase, cytoplasmic;Methylenetetrahydrofolate dehydrogenase;Methenyltetrahydrofolate cyclohydrolase;Formyltetrahydrofolate synthetase;C-1-tetrahydrofolate synthase, cytoplasmic, N-terminally processed	MTHFD1	0,72321616
40S ribosomal protein S25	RPS25	0,72731739
FACT complex subunit SSRP1	SSRP1	0,72842047
Huntingtin-interacting protein 1	HIP1	0,72859001
Pyrroline-5-carboxylate	PYCR1	0,72987959

reductase 1, mitochondrial		
Pre-mRNA-processing-splicing factor 8	PRPF8	0,7321896
HBS1-like protein	HBS1L	0,73350504
Adenylosuccinate synthetase isozyme 2	ADSS	0,73512416
Protein arginine N-methyltransferase 1	PRMT1	0,7378042
Alanine--tRNA ligase, cytoplasmic	AARS	0,73953523
O-acetyl-ADP-ribose deacetylase 1	OARD1	0,74088754
SUMO-activating enzyme subunit 2	UBA2	0,74310282
Nuclear pore complex protein Nup205	NUP205	0,74427859
Ataxin-10	ATXN10	0,75490401
Glutathione peroxidase 1	GPX1	0,75532087
Calcyclin-binding protein	CACYBP	0,75540161
F-actin-capping protein subunit beta	CAPZB	0,75865576
Alpha-aminoadipic	ALDH7A1	0,76025094

semialdehyde dehydrogenase		
Calcium-binding mitochondrial carrier protein Aralar1	SLC25A12	0,76159901
Aconitate hydratase, mitochondrial	ACO2	0,76345507
Sorting nexin-6;Sorting nexin-6, N-terminally processed	SNX6	0,76497332
Heat shock 70 kDa protein 12A	HSPA12A	0,76612684
Basic leucine zipper and W2 domain-containing protein 1	BZW1	0,77025922
Enhancer of mRNA-decapping protein 4	EDC4	0,78210153
Nuclear protein localization protein 4 homolog	NPLOC4	0,78391669
Tyrosine-protein kinase CSK	CSK	0,78742769
Translation initiation factor eIF-2B subunit delta	EIF2B4	0,78922335
E3 ubiquitin-	UHRF1	0,78940964

protein ligase UHRF1		
60S ribosomal protein L27a	RPL27A;Rpl27a	0,79095183
26S proteasome non-ATPase regulatory subunit 4	PSMD4	0,79130618
FACT complex subunit SPT16	SUPT16H	0,79339176
Trifunctional purine biosynthetic protein adenosine-3;Phosphoribosylamine--glycine ligase;Phosphoribosylformylglycinamidine cyclo-ligase;Phosphoribosylglycinamide formyltransferase	GART	0,79848162
Eukaryotic translation initiation factor 4 gamma 2	EIF4G2	0,80582746
E2/E3 hybrid ubiquitin-protein ligase UBE2O	UBE2O	0,80629285
Eukaryotic translation initiation	EIF3C;EIF3CL	0,80635749

factor 3 subunit C;Eukaryotic translation initiation factor 3 subunit C-like protein		
DNA ligase 3	LIG3	0,80947198
ATP-binding cassette sub-family F member 1	ABCF1	0,81026226
Nuclear pore complex protein Nup88	NUP88	0,8166737
Adipocyte plasma membrane-associated protein	APMAP	0,81971105
Cysteine and glycine-rich protein 1	CSRP1	0,8229582
Nucleoporin p54	NUP54	0,82570903
ATP-dependent 6-phosphofructokinase, muscle type	PFKM	0,83510272
Protein kinase C and casein kinase substrate in neurons protein 2	PACSIN2	0,83510399
DNA repair protein XRCC1	XRCC1	0,83597565
Succinate-semialdehyde	ALDH5A1	0,83830134

dehydrogenase, mitochondrial		
Aflatoxin B1 aldehyde reductase member 2	AKR7A2	0,8383984
E3 ubiquitin-protein ligase BRE1A	RNF20	0,83881548
PHD finger protein 6	PHF6	0,8417937
28S ribosomal protein S31, mitochondrial	MRPS31	0,8446863
Probable global transcription activator SNF2L1	SMARCA1;Smarca1	0,84491963
Regulator of chromosome condensation	RCC1	0,84653388
Cyclin-dependent kinase 11A;Cyclin-dependent kinase 11B	CDK11A;CDK11B	0,84698232
39S ribosomal protein L1, mitochondrial	MRPL1	0,84698423
Pinin	PNN	0,8496774
Fatty acid synthase;[Acyl-carrier-protein] S-acetyltransfer	FASN	0,85016759

ase;[Acyl-carrier-protein] S-malonyltransferase;3-oxoacyl-[acyl-carrier-protein] synthase;3-oxoacyl-[acyl-carrier-protein] reductase;3-hydroxyacyl-[acyl-carrier-protein] dehydratase;Enoyl-[acyl-carrier-protein] reductase;Oleoyl-[acyl-carrier-protein] hydrolase		
Protein transport protein Sec31A	SEC31A	0,85054546
Structural maintenance of chromosomes protein 1A	SMC1A;smc1a	0,85207791
Protein transport protein Sec23A	SEC23A	0,85275926
Kinesin-like protein KIF1A	KIF1A	0,8551178
Squalene synthase	FDFT1	0,85576375
Eukaryotic	EIF2S3;Eif2s3;EIF2S3L;Eif2s3x;Eif2s3y	0,85691494

translation initiation factor 2 subunit 3;Putative eukaryotic translation initiation factor 2 subunit 3-like protein;Eukaryotic translation initiation factor 2 subunit 3, X-linked;Eukaryotic translation initiation factor 2 subunit 3, Y-linked		
Heterogeneous nuclear ribonucleoprotein F;Heterogeneous nuclear ribonucleoprotein F, N-terminally processed	HNRNPF	0,85778597
Squalene monooxygenase	SQLE	0,85792033
T-complex protein 1 subunit alpha	TCP1;Tcp1	0,86092822
10 kDa heat shock protein, mitochondrial	HSPE1	0,86157121

Quinone oxidoreductase	CRYZ	0,86160787
Glycylpeptide N-tetradecanoyltransferase 1	NMT1	0,87303861
Glutaredoxin-3	GLRX3	0,8834112
Heat shock protein 105 kDa	HSPH1	0,88477092
Probable glutathione peroxidase 8	GPX8	0,88546732
Intraflagellar transport protein 27 homolog	IFT27	0,88639641
Protein O-GlcNAcase	MGEA5;Mgea5	0,8876614
Importin-4	IPO4	0,8891076
Exosome complex component RRP43	EXOSC8	0,89599164
Protein DEK	DEK	0,89820035
ADP-ribosylation factor-like protein 8A	ARL8A	0,89923392
Synaptobrevin homolog YKT6	YKT6	0,89995914
Eukaryotic initiation factor 4A-I	EIF4A1	0,90034993
N-acetylserotonin O-methyltransferase-like protein	ASMTL	0,90054046

Histidine--tRNA ligase, cytoplasmic	HARS	0,90092129
Glutamine--tRNA ligase	QARS	0,90180757
Apoptosis regulator BAX	BAX	0,90222761
Cysteine and histidine-rich domain-containing protein 1	CHORDC1	0,90228123
Calcium-binding mitochondrial carrier protein Aralar2	SLC25A13	0,90638924
Atlastin-1	ATL1	0,90722953
26S proteasome non-ATPase regulatory subunit 8	PSMD8	0,90734715
Uridine 5-monophosphate synthase;Orotate phosphoribosyltransferase;Orotidine 5-phosphate decarboxylase	UMPS	0,91802639
Ras-related protein Rab-18	RAB18	0,92116186
26S proteasome non-ATPase regulatory subunit 10	PSMD10	0,921548

Lanosterol 14-alpha demethylase	CYP51A1	0,92195278
Membrane-associated progesterone receptor component 2	PGRMC2	0,92723952
THO complex subunit 4	ALYREF	0,92735121
Filamin-C	FLNC	0,92777104
Valine--tRNA ligase	VARS	0,92905405
Cleavage and polyadenylation specificity factor subunit 5	NUDT21	0,93198013
Heterogeneous nuclear ribonucleoprotein U-like protein 1	HNRNPUL1	0,93243514
Eukaryotic translation initiation factor 3 subunit F	EIF3F	0,93482166
Septin-5	SEPT5	0,93491491
Eukaryotic translation initiation factor 3 subunit H	EIF3H	0,9407408
NEDD8-activating enzyme E1 regulatory subunit	NAE1	0,94177945
Sideroflexin-3	SFXN3	0,94284206
Alcohol dehydrogenase class-3	ADH5	0,94287194

Dolichyl-diphosphooligosaccharide--protein glycosyltransferase subunit STT3B	STT3B	0,94328859
40S ribosomal protein S9	RPS9	0,945062
Poly(rC)-binding protein 1	PCBP1	0,94605361
Nuclear pore complex protein Nup85	NUP85	0,95299551
Lysine-specific histone demethylase 1A	KDM1A	0,95578766
Sister chromatid cohesion protein PDS5 homolog B	PDS5B	0,95589892
26S proteasome non-ATPase regulatory subunit 11	PSMD11	0,95619117
Histone acetyltransferase type B catalytic subunit	HAT1	0,95839225
Nuclear pore complex protein Nup155	NUP155;Nup155	0,95919906
Vacuolar protein	VPS4B	0,95933194

sorting-associated protein 4B		
Eukaryotic translation initiation factor 3 subunit M	EIF3M	0,95983484
Spermine synthase	SMS	0,95988231
Actin-related protein 2;Actin-related protein 2-B	ACTR2;actr2b	0,96049881
Adenine phosphoribosyltransferase	APRT	0,96247821
Ankycorbin	RAI14	0,96523158
Transmembrane protein 33	TMEM33	0,96590932
40S ribosomal protein S3	RPS3	0,96805848
Eukaryotic translation initiation factor 3 subunit B	EIF3B	0,96913613
Myosin regulatory light chain 12A;Myosin regulatory light chain 12B	MYL12A;MYL12B	0,97154744
Eukaryotic translation initiation factor 3 subunit D	EIF3D	0,97200288
Protein	PPME1	0,9724297

phosphatase methylesterase 1		
DNA replication licensing factor MCM6	MCM6	0,97616132
Anamorsin	CIAPIN1	0,9777209
ADP-sugar pyrophosphatase	NUDT5	0,97962591
Cullin-1	Cul1;CUL1	0,98065461
Splicing factor 45	RBM17	0,98133341
Syntaxin-12	STX12	0,9816316
Hsc70-interacting protein;Putative protein FAM10A5;Putative protein FAM10A4	ST13;ST13P5;ST13P4	0,98399353
V-type proton ATPase subunit d 1	ATP6V0D1	0,98763635
Methionine adenosyltransferase 2 subunit beta	MAT2B	0,98799621
Probable ATP-dependent RNA helicase DDX5	DDX5	0,9885966
Nucleoside diphosphate kinase B	NME2	0,98965306
Mycophenolic acid acyl-glucuronide esterase, mitochondria	ABHD10	0,99094348

l		
Ubiquitin-conjugating enzyme E2 E3;Ubiquitin-conjugating enzyme E2 E2	UBE2E3;Ube2e3;UBE2E2	0,99097697
Nuclear pore complex protein Nup133	NUP133	0,99205356
5-3 exoribonuclease 2	XRN2	0,99258635
GDP-L-fucose synthase	TSTA3	0,99589411
Syntenin-1	SDCBP	0,99601788
U2 snRNP-associated SURP motif-containing protein	U2SURP	0,99694697
UDP-N-acetylglucosamine--peptide N-acetylglucosaminyltransferase 110 kDa subunit	OGT	0,99701733
Proteasome subunit alpha type-1	PSMA1	0,99923706
Myosin light polypeptide 6	MYL6	0,99941953
Condensin complex subunit 3	NCAPG	1,00285445
Agrin;Agrin N-terminal 110 kDa subunit;Agrin C-terminal	AGRN	1,00335926

110 kDa subunit;Agrin C-terminal 90 kDa fragment;Agrin C-terminal 22 kDa fragment		
Exportin-2	CSE1L	1,00356144
Fanconi anemia group I protein	FANCI	1,00651783
Isopentenyl-diphosphate Delta-isomerase 1	IDI1	1,0073897
Mitochondrial import receptor subunit TOM70	TOMM70A	1,00825564
Selenide, water dikinase 1	SEPHS1	1,0087293
Synaptic vesicle membrane protein VAT-1 homolog-like	VAT1L	1,01057137
Laminin subunit gamma-1	LAMC1	1,0107265
DnaJ homolog subfamily C member 7	DNAJC7	1,01387151
Nucleolar GTP-binding protein 1	GTPBP4	1,01682303
Mesencephalic astrocyte-derived neurotrophic	MANF	1,02139431

factor		
Proliferating cell nuclear antigen	PCNA	1,02184698
Signal recognition particle receptor subunit beta	SRPRB	1,0224639
Casein kinase II subunit alpha	CSNK2A2	1,0233061
Ephrin type-A receptor 2	EPHA2	1,02584394
Ubiquitin-conjugating enzyme E2 K	UBE2K	1,03290727
ELAV-like protein 3	ELAVL3	1,03751861
Apoptosis inhibitor 5	API5	1,03793229
Peptidyl-prolyl cis-trans isomerase FKBP10	FKBP10	1,04088169
Translocon-associated protein subunit delta	SSR4	1,04090563
AP-3 complex subunit delta-1	AP3D1	1,04234166
Ubiquitin carboxyl-terminal hydrolase 14	USP14	1,04278119
28 kDa heat- and acid-stable phosphoprotein	PDAP1	1,04491382
Serine/threo	PPP2CA	1,04501343

nine-protein phosphatase 2A catalytic subunit alpha isoform		
NADH dehydrogenase [ubiquinone] iron-sulfur protein 2, mitochondrial	NDUFS2	1,04504479
Electron transfer flavoprotein subunit beta	ETFB	1,04917781
NADH dehydrogenase [ubiquinone] iron-sulfur protein 3, mitochondrial	NDUFS3	1,05075328
Serine/threonine-protein phosphatase 2A activator	PPP2R4	1,0543357
Golgi-specific brefeldin A-resistance guanine nucleotide exchange factor 1	GBF1	1,05519549
Acetyl-CoA carboxylase 1;Biotin carboxylase	ACACA	1,05589909
Replication factor C subunit 5	RFC5	1,05746905

NAD-dependent malic enzyme, mitochondrial	ME2	1,06008848
Protein PBDC1	PBDC1	1,06041993
Regulator of nonsense transcripts 1	UPF1	1,0617307
Methylmalonyl-CoA mutase, mitochondrial	MUT	1,06339433
ATP-binding cassette sub-family D member 3	ABCD3	1,06370862
Structural maintenance of chromosomes protein 4	SMC4	1,06396378
Alcohol dehydrogenase [NADP(+)]	AKR1A1	1,06649611
BTB/POZ domain-containing protein KCTD12	KCTD12;Kctd12	1,06699498
DNA polymerase delta catalytic subunit	POLD1	1,06902334
Band 4.1-like protein 2	EPB41L2	1,07153087
26S protease regulatory subunit 10B	PSMC6	1,07276196

Regulation of nuclear pre-mRNA domain-containing protein 1B	RPRD1B	1,07551363
Cyclin-dependent kinase 1	CDK1	1,08203782
Synapsin-1	SYN1	1,08556345
Ornithine aminotransferase, mitochondrial;Ornithine aminotransferase, hepatic form;Ornithine aminotransferase, renal form	OAT	1,08617592
28S ribosomal protein S22, mitochondrial	MRPS22	1,08682378
tRNA-splicing ligase RtcB homolog	RTCB;rtcb	1,08863449
Succinate dehydrogenase [ubiquinone] flavoprotein subunit, mitochondrial	SDHA	1,08875423
SUMO-activating enzyme subunit 1;SUMO-	SAE1	1,08953815

activating enzyme subunit 1, N-terminally processed		
3-mercaptopyruvate sulfurtransferase	MPST	1,09141858
cAMP-dependent protein kinase catalytic subunit alpha	PRKACA	1,09949705
Inosine-5-monophosphate dehydrogenase 2	IMPDH2	1,10493978
Glucosamine-6-phosphate isomerase 1	GNPDA1	1,10534392
Endoplasmic reticulum resident protein 44	ERP44	1,1056508
ER membrane protein complex subunit 1	EMC1	1,10666614
Delta-1-pyrroline-5-carboxylate synthase;Glutamate 5-kinase;Gamma-glutamyl phosphate reductase	ALDH18A1	1,10695733
26S	PSMD1	1,10745769

proteasome non-ATPase regulatory subunit 1		
Replication factor C subunit 4	RFC4	1,1082628
Glutathione S-transferase omega-1	GSTO1	1,10830943
Cytoplasmic dynein 1 light intermediate chain 1	DYNC1LI1	1,10837788
NADH-ubiquinone oxidoreductase 75 kDa subunit, mitochondrial	NDUFS1	1,10967467
Endophilin-A2	SH3GL1	1,11236042
Elongation factor 1-delta	EEF1D	1,11504322
Calpain-2 catalytic subunit	CAPN2	1,11789682
Cytosol aminopeptidase	LAP3	1,11820115
Probable ATP-dependent RNA helicase DDX46	DDX46	1,11878671
Copine-3	CPNE3	1,12190289
Nucleolar transcription factor 1	UBTF	1,12599924
GTPase NRas	NRAS	1,13142776
60S ribosomal	RPL19	1,13175625

protein L19		
Ras-related protein Rab-21	RAB21	1,13661808
Polyadenylate-binding protein 4	PABPC4	1,13796128
DNA replication licensing factor MCM4	MCM4	1,14170096
Low molecular weight phosphotyrosine protein phosphatase	ACP1	1,14384058
Protein RER1	RER1	1,14668761
Nuclear cap-binding protein subunit 1	NCBP1	1,14675395
Sorting and assembly machinery component 50 homolog	SAMM50	1,14759827
Serine/threonine-protein kinase 26	STK26	1,14860047
Aminopeptidase B	RNPEP	1,15134536
Diablo homolog, mitochondrial	DIABLO	1,15148841
Cleft lip and palate transmembrane protein 1	CLPTM1	1,15618854
Bleomycin hydrolase	BLMH	1,15647719
RNA-binding	RNPS1	1,15653102

protein with serine-rich domain 1		
Coronin-1A	CORO1A;Coro1a	1,15791215
Sialic acid synthase	NANS	1,15846146
DNA replication licensing factor MCM2	MCM2;Mcm2	1,1607009
Transaldolase	TALDO1	1,16363313
Synaptotagmin-1	Syt1;SYT1	1,16573736
Eukaryotic translation initiation factor 5B	EIF5B	1,16850323
Glycine cleavage system H protein, mitochondrial	GCSH	1,16958915
Vacuolar protein sorting-associated protein 29	VPS29;vps29	1,17153422
Exportin-T	XPOT	1,17379231
Stomatin-like protein 2, mitochondrial	STOML2	1,17472013
Nck-associated protein 1	NCKAP1;nckap1	1,17568694
Chloride intracellular channel protein 4	CLIC4	1,17719523
26S protease regulatory subunit 8	PSMC5	1,17812665

Importin subunit alpha-1	KPNA2	1,1813221
DNA (cytosine-5)-methyltransferase 1	DNMT1	1,18229421
Calcium-binding mitochondrial carrier protein SCaMC-1	SLC25A24	1,1828732
Proteasome activator complex subunit 3	PSME3	1,18618562
Serine/threonine-protein phosphatase PGAM5, mitochondrial	PGAM5	1,18735949
C-terminal-binding protein 1	CTBP1	1,18810251
Ubiquitin-like modifier-activating enzyme 6	UBA6	1,18917169
Mitochondrial carrier homolog 2	MTCH2	1,18970256
Ribonucleoside-diphosphate reductase subunit M2	RRM2	1,19053099
S-phase kinase-associated protein 1	SKP1	1,19096947
Coatomer	COPG1	1,19160737

subunit gamma-1		
Exportin-5	XPO5	1,19247754
Histidine triad nucleotide-binding protein 1	HINT1	1,19640308
Transforming protein RhoA	Rhoa;RHOA;rhoab	1,20195495
Structural maintenance of chromosomes protein 2	SMC2	1,20228174
LETM1 and EF-hand domain-containing protein 1, mitochondrial	LETM1	1,20574273
Double-stranded RNA-binding protein Staufen homolog 1	STAU1	1,21546872
SWI/SNF complex subunit SMARCC1	SMARCC1;Smarcc1	1,21738921
Macrophage migration inhibitory factor	MIF;Mif	1,21811401
Trifunctional enzyme subunit beta, mitochondrial;3-ketoacyl-CoA thiolase	HADHB	1,21991603
E3 ubiquitin-	UBR4	1,22438007

protein ligase UBR4		
Mitochondrial import receptor subunit TOM40 homolog	TOMM40	1,22960154
Structural maintenance of chromosomes flexible hinge domain-containing protein 1	SMCHD1	1,23066839
SUMO-conjugating enzyme UBC9	Ube2i;UBE2I	1,23218918
Eukaryotic translation initiation factor 5	EIF5	1,2381293
1-phosphatidylinositol 4,5-bisphosphate phosphodiesterase gamma-1	PLCG1	1,24022484
Methylsterol monooxygenase 1	MSMO1	1,24659877
Tryptophan--tRNA ligase, cytoplasmic;T1-TrpRS;T2-TrpRS	WARS	1,24817318
Microtubule-associated protein RP/EB family	MAPRE2	1,24869453

member 2		
Symplekin	SYMPK	1,24962786
Glyoxylate reductase/hydroxypyruvate reductase	GRHPR	1,24965096
4-trimethylaminobutyraldehyde dehydrogenase	ALDH9A1	1,25107638
N-alpha-acetyltransferase 15, NatA auxiliary subunit	NAA15	1,26060253
tRNA (cytosine(34)-C(5))-methyltransferase	NSUN2	1,26419301
Ribose-phosphate pyrophosphokinase 1	PRPS1	1,26651658
Eukaryotic translation initiation factor 5A-1;Eukaryotic translation initiation factor 5A-1-like;Eukaryotic translation initiation factor 5A-2	EIF5A;EIF5AL1;EIF5A2;Eif5a2	1,26715575
Gamma-glutamyl hydrolase	GGH	1,26757537
Rab GTPase-activating	RABGAP1	1,26782735

protein 1		
CUGBP Elav-like family member 1	CELF1;Celf1	1,27082994
Nuclear pore complex protein Nup93	NUP93	1,27744166
Tubulin polymerization-promoting protein family member 3	TPPP3	1,27820799
Importin subunit alpha-4	Kpna3;KPNA3	1,27962981
Double-stranded RNA-binding protein Staufen homolog 2	STAU2	1,28062312
Small nuclear ribonucleoprotein Sm D1	SNRPD1	1,28078588
26S proteasome non-ATPase regulatory subunit 7	PSMD7	1,29013634
SH3 and PX domain-containing protein 2B	SH3PXD2B	1,29430347
EH domain-containing protein 1	EHD1	1,29486889
Creatine kinase U-type, mitochondrial	CKMT1A	1,29677412

AP-1 complex subunit beta-1	AP1B1;Ap1b1	1,29709562
Echinoderm microtubule-associated protein-like 4	EML4	1,29756249
Transportin-1	TNPO1	1,2988063
Junction plakoglobin	JUP	1,30739339
Polyadenylate-binding protein-interacting protein 1	PAIP1	1,3093124
Spermidine synthase	SRM	1,31046973
Superoxide dismutase [Mn], mitochondrial	SOD2	1,31601312
Calponin-2	CNN2	1,32280413
Proline-, glutamic acid- and leucine-rich protein 1	PELP1	1,32325384
Nodal modulator 2;Nodal modulator 3;Nodal modulator 1	NOMO2;NOMO3;NOMO1	1,33712133
DNA replication licensing factor MCM5	MCM5	1,34007666
Fructose-bisphosphate aldolase C	ALDOC	1,34261025
Phosphomevalonate	PMVK	1,3451182

kinase		
Leucine--tRNA ligase, cytoplasmic	LARS	1,3463548
GMP synthase [glutamine-hydrolyzing]	GMPS	1,34731123
Vacuolar protein sorting-associated protein 26A	VPS26A	1,34943602
Acylglycerol kinase, mitochondrial	AGK	1,35339419
Sterol-4-alpha-carboxylate 3-dehydrogenase, decarboxylating	NSDHL	1,35563893
Replication factor C subunit 2	RFC2;Rfc2	1,36727333
Phosphoribosyl pyrophosphate synthase-associated protein 2	PRPSAP2	1,37010574
Translationally-controlled tumor protein	TPT1	1,37118318
L-lactate dehydrogenase A chain	LDHA	1,37382317
Serotransferrin	TF	1,37452168

rRNA 2-O-methyltransferase fibrillarin	FBL	1,37890095
Cilia- and flagella-associated protein 20	CFAP20	1,38244353
Asparagine synthetase [glutamine-hydrolyzing]	ASNS	1,38304392
Myelin expression factor 2	MYEF2	1,38640277
Ubiquitin carboxyl-terminal hydrolase isozyme L5	UCHL5	1,3929437
NAD(P) transhydrogenase, mitochondrial	NNT	1,39506065
Serine/threonine-protein kinase VRK1	VRK1	1,3966287
BolA-like protein 2	BOLA2	1,39900398
Serine/threonine-protein phosphatase PP1-alpha catalytic subunit	PPP1CA	1,40087403
40S ribosomal protein S15a	RPS15A	1,40176688
DNA replication licensing factor MCM3	MCM3	1,4035812

Programmed cell death 6-interacting protein	PDCD6IP	1,40365707
Aldose reductase	AKR1B1	1,40620316
Protein ERGIC-53	LMAN1	1,40865495
Amidophosphoribosyltransferase	PPAT	1,40898344
AP-3 complex subunit beta-1	AP3B1	1,40919198
V-type proton ATPase 116 kDa subunit a isoform 1	ATP6V0A1	1,4100469
Dihydrofolate reductase	DHFR	1,41320165
60S ribosomal protein L10	RPL10	1,42001449
Casein kinase II subunit alpha;Casein kinase II subunit alpha 3	Csnk2a1;CSNK2A1;CSNK2A3	1,42455716
Rabankyrin-5	ANKFY1	1,430201
Lactoylglutathione lyase	GLO1	1,44422616
ATP-dependent 6-phosphofructokinase, liver type	PFKL	1,44787788
DnaJ homolog subfamily B member 11	DNAJB11	1,44850201
Cytochrome	CYB5B	1,4577891

b5 type B		
ATP-binding cassette sub-family E member 1	ABCE1	1,46688165
Neural cell adhesion molecule L1	L1CAM	1,46708934
Beta-soluble NSF attachment protein	NAPB	1,46821361
Superkiller viralicidic activity 2-like 2	SKIV2L2	1,47076183
Histone-arginine methyltransferase CARM1	CARM1	1,47321447
AP-3 complex subunit mu-1	AP3M1	1,47604307
Signal transducer and activator of transcription 1-alpha/beta	STAT1	1,4764542
Copine-1	CPNE1	1,48263359
Single-stranded DNA-binding protein, mitochondrial	SSBP1	1,48416011
Thioredoxin reductase 1, cytoplasmic	TXNRD1	1,48630291
Lethal(2) giant larvae protein homolog 1	LLGL1;Llgl1	1,48706245
Glutamine--	GFPT1	1,4924433

fructose-6-phosphate aminotransferase [isomerizing] 1		
Plastin-3	PLS3	1,49344381
Ankyrin-2	ANK2	1,49850718
3-ketoacyl-CoA thiolase, mitochondrial	ACAA2	1,49996482
Dolichyl-diphosphooligosaccharide--protein glycosyltransferase subunit DAD1	Dad1;DAD1	1,50628026
Cysteine and glycine-rich protein 2	CSRP2	1,51664988
Ribonucleoside-diphosphate reductase large subunit	RRM1	1,51934963
Ras-related protein Rab-2B	RAB2B	1,52369372
Small nuclear ribonucleoprotein Sm D3	SNRPD3	1,52862612
Vesicle-trafficking protein SEC22b	SEC22B	1,53125276
Ubiquitin carboxyl-terminal hydrolase 10	USP10	1,53869883
Eukaryotic peptide chain	ETF1	1,54195086

release factor subunit 1		
Ras GTPase-activating-like protein IQGAP1	IQGAP1	1,54405997
Aminoacyl tRNA synthase complex-interacting multifunctional protein 1;Endothelial monocyte-activating polypeptide 2	AIMP1	1,55432426
ADP-ribosylation factor 1;ADP-ribosylation factor 3	Arf1;ARF1;ARF3	1,562301
ATPase family AAA domain-containing protein 1;ATPase family AAA domain-containing protein 1-B	ATAD1;atad1b	1,56366009
Condensin complex subunit 1	NCAPD2	1,57342254
Putative ATP-dependent RNA helicase DHX30	DHX30	1,57458687
DnaJ homolog subfamily A member 1	DNAJA1;Dnaja1	1,57503446

Transcription elongation factor B polypeptide 1	TCEB1	1,58280585
2-oxoglutarate dehydrogenase, mitochondrial	OGDH	1,59054989
RNA-binding protein 4	RBM4	1,59804175
CDGSH iron-sulfur domain-containing protein 2	CISD2;Cisd2	1,60473484
COP9 signalosome complex subunit 2	COPS2	1,61503855
Four and a half LIM domains protein 1	FHL1;Fhl1	1,61602105
26S proteasome non-ATPase regulatory subunit 12	PSMD12	1,61712053
Eukaryotic translation initiation factor 3 subunit I	EIF3I	1,63669247
NHP2-like protein 1;NHP2-like protein 1, N-terminally processed	NHP2L1	1,64543682
mRNA export factor	RAE1	1,64564217

Cancer-related nucleoside-triphosphatase	NTPCR	1,65407817
Serine/threonine-protein phosphatase 2A 56 kDa regulatory subunit epsilon isoform	PPP2R5E	1,65412649
DNA replication licensing factor MCM7	MCM7	1,66373634
60S ribosomal protein L27	RPL27	1,66913626
26S proteasome non-ATPase regulatory subunit 5	PSMD5	1,67783546
Acetyl-CoA acetyltransferase, cytosolic	ACAT2	1,68484137
Solute carrier family 2, facilitated glucose transporter member 1	SLC2A1	1,7083274
Perilipin-3	PLIN3	1,71646457
Delta(24)-sterol reductase	DHCR24	1,73236232
FAS-associated factor 2	FAF2	1,73505211
Heat shock 70 kDa	HSPA4L	1,7407928

protein 4L		
Glypican-4;Secreted glypican-4	GPC4	1,75487497
Small nuclear ribonucleoprotein-associated proteins B and B	SNRPB	1,75680796
Importin subunit alpha-5;Importin subunit alpha-5, N-terminally processed	KPNA1;Kpna1	1,76424514
Myotrophin	MTPN	1,7719858
Aminoacyl tRNA synthase complex-interacting multifunctional protein 2	AIMP2	1,78462558
Thioredoxin	TXN	1,79231008
Actin-related protein 2/3 complex subunit 4	Arpc4;ARPC4	1,79283778
40S ribosomal protein S27-like	RPS27L	1,79476293
Eukaryotic initiation factor 4A-II;Eukaryotic initiation factor 4A-II, N-terminally processed	EIF4A2	1,8018411

S-adenosylmethionine synthase isoform type-2	MAT2A	1,80378787
Leucine-rich repeat-containing protein 40	LRRC40	1,80677817
LIM and SH3 domain protein 1	LASP1	1,80794885
Elongation factor 1-alpha 2	EEF1A2;Eef1a2	1,80938085
Small glutamine-rich tetratricopeptide repeat-containing protein alpha	SGTA	1,82048522
D-3-phosphoglycerate dehydrogenase	PHGDH	1,82128949
Actin-like protein 6A	ACTL6A;Actl6a	1,82179472
Histone-binding protein RBBP7	RBBP7	1,86049122
Ran-specific GTPase-activating protein	RANBP1;Ranbp1	1,8705438
BUB3-interacting and GLEBS motif-containing	ZNF207	1,87806087

protein ZNF207		
Unconventional myosin-Ib	MYO1B	1,88188214
Pyruvate dehydrogenase E1 component subunit alpha, somatic form, mitochondrial	PDHA1	1,88665432
Ras-related protein Rab-6B	RAB6B	1,91266653
Mitochondrial glutamate carrier 1;Mitochondrial glutamate carrier 2	SLC25A22;SLC25A18	1,91282908
Gamma-synuclein	SNCG	1,91344664
Tyrosine-protein phosphatase non-receptor type 1	PTPN1	1,91481972
Ras-related protein Rab-10	RAB10	1,94398859
Translational activator GCN1	GCN1L1	1,94721307
DNA mismatch repair protein Msh6	MSH6	1,95109749
Activator of 90 kDa heat shock protein ATPase	AHSA1	1,95730146

homolog 1		
Aldehyde dehydrogenase family 16 member A1	ALDH16A1	1,98171404
Phosphoribosylformylglycinamidine synthase	PFAS	1,99841309
Thymidylate synthase	TYMS	1,99952147
Medium-chain specific acyl-CoA dehydrogenase, mitochondrial	ACADM	2,0000568
Peptidyl-prolyl cis-trans isomerase-like 1	PPIL1	2,01126713
Inorganic pyrophosphatase	PPA1	2,02653122
Protein FAM98B	FAM98B	2,05904028
Phospholipid hydroperoxide glutathione peroxidase, mitochondrial	GPX4	2,06965658
Protein NipSnap homolog 1	NIPSNAP1;Nipsnap1	2,08286815
Histone deacetylase 2	HDAC2;Hdac2	2,13791275
Cellular retinoic acid-binding protein 2	CRABP2	2,14412202

Eukaryotic translation initiation factor 2 subunit 2	EIF2S2	2,14471118
26S proteasome non-ATPase regulatory subunit 6	PSMD6	2,15996827
Adenylate kinase isoenzyme 1	AK1	2,16386965
Dynein light chain 2, cytoplasmic	DYNLL2	2,23186874
GTP-binding protein SAR1a	SAR1A	2,24796465
Tricarboxylate transport protein, mitochondrial	SLC25A1	2,28178279
Ubiquitin-conjugating enzyme E2 N;Ubiquitin-conjugating enzyme E2 35;Ubiquitin-conjugating enzyme E2 36;Putative ubiquitin-conjugating enzyme E2 N-like	UBE2N;Ube2n;UBC35;UBC36;UBE2NL	2,29580328
Signal recognition particle 9 kDa protein	SRP9	2,31755235
DNA	TOP2A	2,34728707

topoisomerase 2-alpha		
Saccharopine dehydrogenase-like oxidoreductase	SCCPDH	2,37124464
Peroxiredoxin-4	PRDX4;Prdx4	2,38741154
60S ribosomal protein L26;60S ribosomal protein L26-like 1	RPL26;RPL26L1	2,44196616
Thymidylate kinase	DTYMK	2,60647668
L-xylulose reductase	DCXR	2,62080744
Tubulin alpha-1B chain;Tubulin alpha-4A chain	TUBA1B;TUBA4A	2,72059165

Table S3: List of the 118 dysregulated proteins in p.A53T neurons that were restored upon treatment with BX795

List of the 118 dysregulated proteins in p.A53T neurons that were restored upon treatment with BX795				
Gene Name	Protein Name	Biological Process	-Log ANOVA p value	ANOVA q-value
SH3GL1	Endophilin-A2	Cell Membrane	256.133	0,011476
MIF	Macrophage migration inhibitory factor	Cytokine	180.931	0,0363767
ACTR2	Actin-related protein 2	Cytoskeleton	194.818	0,030058
CAPZB	F-actin-capping protein subunit beta	Cytoskeleton	46.958	0,000648649
DYNLL2	Dynein light chain 2, cytoplasmic	Cytoskeleton	278.624	0,00791795
JUP	Junction plakoglobin	Cytoskeleton	184.446	0,0338618
MARCKSL1	MARCKS-related protein	Cytoskeleton	182.146	0,0355364
SNCG	Gamma-synuclein	Cytoskeleton	369.107	0,0025
TUBB	Tubulin beta chain	Cytoskeleton	328.033	0,004
HAT1	Histone acetyltransferase type B catalytic subunit	DNA Organization	193.087	0,0303367
ACO2	Aconitate hydratase, mitochondrial	Metabolism	239.553	0,0147068
ACP1	Low molecular weight phosphotyrosine protein phosphatase	Metabolism	223.884	0,0187195
ALDOC	Fructose-bisphosphate aldolase C	Metabolism	19.283	0,0305445
DCXR	L-xylulose reductase	Metabolism	450.627	0,000888889
DTYMK	Thymidylate kinase	Metabolism	429.648	0,00128302
GPX4	Phospholipid hydroperoxide glutathione peroxidase, mitochondrial	Metabolism	313.215	0,00468571
MSMO1	Methylsterol monooxygenase 1	Metabolism	23.571	0,0159706
NANS	Sialic acid synthase	Metabolism	197.987	0,0284313
OGDH	2-oxoglutarate dehydrogenase, mitochondrial	Metabolism	189.588	0,0314673
TSTA3	GDP-L-fucose synthase	Metabolism	471.268	0,00066666 7
ALDH5A1	Succinate-semialdehyde dehydrogenase, mitochondrial	Neuronal	281.456	0,00780645
ATXN10	Ataxin-10	Neuronal	36.278	0,00266667

INA	Alpha-internexin	Neuronal	261.725	0,0103014
NIPSNAP1	Protein NipSnap homolog 1	Neuronal	201.319	0,0272045
PAFAH1B1	Platelet-activating factor acetylhydrolase IB subunit alpha	Neuronal	416.529	0,00144262
SYN1	Synapsin-1	Neuronal	282.487	0,00773913
HIST1H1E	Histone H1.4	Nuclear Assembly	462.922	0,000682927
TMPO	Lamina-associated polypeptide 2, isoform alpha;Thymopoietin;Thymopentin	Nuclear Assembly	273.826	0,00829268
ACADM	Medium-chain specific acyl-CoA dehydrogenase, mitochondrial	Oxidative Stress	361.925	0,00273684
CKMT1A	Creatine kinase U-type, mitochondrial	Oxidative Stress	169.957	0,0433538
GOT2	Aspartate aminotransferase, mitochondrial	Oxidative Stress	195.739	0,0293862
GPX1	Glutathione peroxidase 1	Oxidative Stress	256.414	0,0115088
MDH2	Malate dehydrogenase, mitochondrial	Oxidative Stress	325.647	0,00410256
MTCH2	Mitochondrial carrier homolog 2	Oxidative Stress	2.402	0,0146818
PDHA1	Pyruvate dehydrogenase E1 component subunit alpha, somatic form, mitochondrial	Oxidative Stress	222.971	0,0189673
STOML2	Stomatin-like protein 2, mitochondrial	Oxidative Stress	313.378	0,00475362
TOMM70A	Mitochondrial import receptor subunit TOM70	Oxidative Stress	181.295	0,0362534
ATP1B1	Sodium/potassium-transporting ATPase subunit beta-1	Plasma Membrane	192.654	0,0305888
ANKFY1	Rabankyrin-5	Protein Modification and Transport	23.323	0,0163
AP3M1	AP-3 complex subunit mu-1	Protein Modification and Transport	178.641	0,0375263
ATP6V0D1	V-type proton ATPase subunit d 1	Protein Modification and Transport	186.993	0,0326792
CCT8	T-complex protein 1 subunit theta	Protein Modification and Transport	449.206	0,000956522
CKAP4	Cytoskeleton-associated protein 4	Protein Modification	271.468	0,00867308

		and Transport		
DAD1	Dolichyl-diphosphooligosaccharide--protein glycosyltransferase subunit DAD1	Protein Modification and Transport	270.969	0,00872381
GDI2	Rab GDP dissociation inhibitor beta	Protein Modification and Transport	194.495	0,0300524
LAP3	Cytosol aminopeptidase	Protein Modification and Transport	19.891	0,0281967
NAPB	Beta-soluble NSF attachment protein	Protein Modification and Transport	263.779	0,00978802
OGT	UDP-N-acetylglucosamine--peptide N-acetylglucosaminyltransferase 110 kDa subunit	Protein Modification and Transport	216.824	0,0208777
PACSIN2	Protein kinase C and casein kinase substrate in neurons protein 2	Protein Modification and Transport	286.533	0,00715556
PLIN3	Perilipin-3	Protein Modification and Transport	167.058	0,0455219
RAB2B	Ras-related protein Rab-2B	Protein Modification and Transport	377.583	0,00245783
SAR1A	GTP-binding protein SAR1a	Protein Modification and Transport	227.985	0,0173559
SEC22B	Vesicle-trafficking protein SEC22b	Protein Modification and Transport	189.207	0,0317391
SRP9	Signal recognition particle 9 kDa protein	Protein Modification and Transport	357.866	0,00273469
YKT6	Synaptobrevin homolog YKT6	Protein Modification and Transport	201.411	0,0271685
AIMP2	Aminoacyl tRNA synthase complex-interacting multifunctional protein 2	Protein Synthesis	540.207	0,00032
EEF1D	Elongation factor 1-delta	Protein Synthesis	24.002	0,0146566
EIF2B4	Translation initiation factor eIF-2B subunit delta	Protein Synthesis	277.038	0,00814141

EIF4G2	Eukaryotic translation initiation factor 4 gamma 2	Protein Synthesis	325.565	0,00403361
FAM98B	Protein FAM98B	Protein Synthesis	302.174	0,00571795
GTPBP4	Nucleolar GTP-binding protein 1	Protein Synthesis	178.873	0,0375154
KARS	Lysine--tRNA ligase	Protein Synthesis	359.204	0,00272165
MAT2A	S-adenosylmethionine synthase isoform type-2	Protein Synthesis	350.993	0,00290196
PHGDH	D-3-phosphoglycerate dehydrogenase	Protein Synthesis	106.486	0
PPA1	Inorganic pyrophosphatase	Protein Synthesis	203.525	0,0261486
PRMT1	Protein arginine N-methyltransferase 1	Protein Synthesis	558.198	0,000190476
RARS	Arginine--tRNA ligase, cytoplasmic	Protein Synthesis	34.511	0,00316981
RPL12	60S ribosomal protein L12	Protein Synthesis	236.748	0,0156444
RPL31	60S ribosomal protein L31	Protein Synthesis	241.579	0,0145385
RPS3	40S ribosomal protein S3	Protein Synthesis	321.674	0,0043252
RPS6	40S ribosomal protein S6	Protein Synthesis	295.529	0,0064878
RTCB	tRNA-splicing ligase RtcB homolog	Protein Synthesis	347.921	0,00303846
VARS	Valine--tRNA ligase	Protein Synthesis	302.941	0,00571429
WARS	Tryptophan--tRNA ligase, cytoplasmic;T1-TrpRS;T2-TrpRS	Protein Synthesis	233.632	0,0162437
DEK	Protein DEK	RNA Metabolism	19.105	0,0308276
HINT1	Histidine triad nucleotide-binding protein 1	RNA Metabolism	417.925	0,00135593
HNRNPUL1	Heterogeneous nuclear ribonucleoprotein U-like protein 1	RNA Metabolism	213.047	0,0220917
MYEF2	Myelin expression factor 2	RNA Metabolism	178.281	0,0377856
NHP2L1	NHP2-like protein 1;NHP2-like protein 1, N-terminally processed	RNA Metabolism	395.001	0,00191781
NUP93	Nuclear pore complex protein	RNA	290.302	0,00691954

	Nup93	Metabolism		
PCBP1	Poly(rC)-binding protein 1	RNA Metabolism	617.692	0
PCBP2	Poly(rC)-binding protein 2	RNA Metabolism	242.141	0,0143938
RAE1	mRNA export factor	RNA Metabolism	231.102	0,0169645
RBM4	RNA-binding protein 4	RNA Metabolism	23.421	0,0162464
RRM2	Ribonucleoside-diphosphate reductase subunit M2	RNA Metabolism	311.101	0,00472222
SKIV2L2	Superkiller viralicidic activity 2-like 2	RNA Metabolism	395.007	0,00194444
SNRPB	Small nuclear ribonucleoprotein-associated proteins B and B	RNA Metabolism	19.464	0,0300842
UBTF	Nucleolar transcription factor 1	RNA Metabolism	252.596	0,0123729
YLPM1	YLP motif-containing protein 1	RNA Metabolism	347.249	0,00304762
ZNF207	BUB3-interacting and GLEBS motif-containing protein ZNF207	RNA Metabolism	280.434	0,00785263
API5	Apoptosis inhibitor 5	Signal Transduction	192.253	0,03041
BOLA2	BolA-like protein 2	Signal Transduction	243.992	0,0139765
CRABP2	Cellular retinoic acid-binding protein 2	Signal Transduction	652.555	0
CSK	Tyrosine-protein kinase CSK	Signal Transduction	302.647	0,00570323
MTPN	Myotrophin	Signal Transduction	536.379	0,000307692
STAT1	Signal transducer and activator of transcription 1-alpha/beta	Signal Transduction	250.904	0,0127197
ZYX	Zyxin	Signal Transduction	323.528	0,00406557
ATG4B	Cysteine protease ATG4B	Stress Response	30.765	0,00512752
CUL1	Cullin-1	Stress Response	205.844	0,0253684
DNAJA1	DnaJ homolog subfamily A member 1	Stress Response	264.155	0,00980465
DNAJB11	DnaJ homolog subfamily B member 11	Stress Response	234.026	0,0161727
DNM2	Dynamin-2	Stress Response	185.961	0,0332459
GCN1L1	Translational activator GCN1	Stress Response	57.176	0

HSPA4	Heat shock 70 kDa protein 4	Stress Response	325.383	0,004
OTUB1	Ubiquitin thioesterase OTUB1	Stress Response	351.675	0,00289109
PDCD6IP	Programmed cell death 6-interacting protein	Stress Response	300.728	0,00585987
PSMA3	Proteasome subunit alpha type-3	Stress Response	318.164	0,00443077
PSMD12	26S proteasome non-ATPase regulatory subunit 12	Stress Response	269.053	0,00904265
PSME3	Proteasome activator complex subunit 3	Stress Response	331.891	0,00378947
PTPN1	Tyrosine-protein phosphatase non-receptor type 1	Stress Response	349.068	0,00291262
SGTA	Small glutamine-rich tetratricopeptide repeat-containing protein alpha	Stress Response	191.864	0,0304814
STIP1	Stress-induced-phosphoprotein 1	Stress Response	303.961	0,00565789
TCP1	T-complex protein 1 subunit alpha	Stress Response	480.438	0,000685714
UBA6	Ubiquitin-like modifier-activating enzyme 6	Stress Response	226.136	0,0179532
UCHL1	Ubiquitin carboxyl-terminal hydrolase isozyme L1	Stress Response	555.947	0,000181818
VCP	Transitional endoplasmic reticulum ATPase	Stress Response	263.882	0,00983333
VPS35	Vacuolar protein sorting-associated protein 35	Stress Response	303.784	0,00564706
TPD52L2	Tumor protein D54	Unknown	19.239	0,0305592

Table S4: GO analysis for cellular compartment between pA53T and control neurons

GO analysis for cellular compartment between pA53T and control neurons

Cellular Compartment	No of genes	P-Value	Bonferroni
extracellular exosome	299	1,6E-75	1,0E-72
membrane	204	2,8E-38	1,7E-35
nucleoplasm	230	7,9E-36	4,8E-33
cytoplasm	334	2,2E-32	1,3E-29
mitochondrion	118	1,6E-19	9,5E-17
nucleus	292	6,3E-15	3,9E-12
nuclear pore	22	6,7E-14	4,1E-11
intracellular ribonucleoprotein complex	29	7,5E-14	4,6E-11
nucleosome	23	2,4E-12	1,4E-9
nuclear chromosome, telomeric region	26	8,1E-12	4,9E-9
nuclear nucleosome	16	2,1E-11	1,3E-8
nuclear envelope	28	2,5E-11	1,5E-8
proteasome complex	18	2,8E-11	1,7E-8
focal adhesion	43	4,4E-10	2,7E-7
eukaryotic translation initiation factor 3 complex	10	2,1E-9	1,3E-6
proteasome accessory complex	9	5,6E-8	3,4E-5
chaperonin-containing T-complex	7	1,8E-7	1,1E-4
nuclear membrane	27	3,3E-7	2,0E-4
cell body	14	3,6E-7	2,2E-4
proteasome regulatory particle	7	9,3E-7	5,7E-4
eukaryotic translation initiation factor 3 complex, eIF3m	6	1,3E-6	7,8E-4
axon cytoplasm	10	3,40E-06	7,3E-5

Table S5: Nucleosome assembly proteins

Nucleosome assembly proteins		
Protein Name	**Gene Name**	**Difference**
H3 histone family member 3A(H3F3A)	H3F3A	-2,8312081
histone cluster 1 H3 family member a(HIST1H3A)	HIST1H3A	-2,8312081
histone cluster 1 H3 family member b(HIST1H3B)	Hist1h3b	-2,8312081
histone cluster 2 H3 family member a(HIST2H3A)	HIST2H3A	-2,8312081
histone cluster 3 H3(HIST3H3)	HIST3H3	-2,8312081
histone cluster 1 H1 family member e(HIST1H1E)	HIST1H1E	-1,9652229
H2B histone family member S(H2BFS)	H2BFS	-1,3235741
histone cluster 1 H2B family member a(HIST1H2BA)	HIST1H2BA	-1,3235741
histone cluster 1 H2B family member b(HIST1H2BB)	Hist1h2bb	-1,3235741
histone cluster 1 H2B family member c(HIST1H2BC)	HIST1H2BC	-1,3235741
histone cluster 1 H2B family member d(HIST1H2BD)	HIST1H2BD	-1,3235741
histone cluster 1 H2B family member f(HIST1H2BF)	Hist1h2bf	-1,3235741
histone cluster 1 H2B family member h(HIST1H2BH)	Hist1h2bh	-1,3235741
histone cluster 1 H2B family member k(HIST1H2BK)	HIST1H2BK	-1,3235741
histone cluster 1 H2B family member l(HIST1H2BL)	HIST1H2BL	-1,3235741
histone cluster 1 H2B family member m(HIST1H2BM)	Hist1h2bm	-1,3235741
histone cluster 1 H2B family member n(HIST1H2BN)	HIST1H2BN	-1,3235741
histone cluster 2 H2B family member f(HIST2H2BF)	HIST2H2BF	-1,3235741
histone cluster 1 H1 family member b(HIST1H1B)	HIST1H1B	-1,320744
histone cluster 1 H1 family member c(HIST1H1C)	Hist1h1c	-1,0066352
histone cluster 1 H1 family member d(HIST1H1D)	Hist1h1d	-1,0066352
heterochromatin protein 1 binding protein 3(HP1BP3)	HP1BP3	-0,8114175
histone cluster 1 H4 family member a(HIST1H4A)	HIST1H4A	-0,4979729

Table S6: Primers used in the current study

Primers used in the current study						
Gene name	Application	Forward	Reverse			
TH	RT-PCR	TGTCTGAGGAGCCTGAGATTCG	GCTTGTCCTTGGCGTCACTG			
Nurr1	RT-PCR	TCGACATTTCTGCCTTCTCCTG	GGTTCCTTGAGCCCGTGTCT			
AADC	RT-PCR	TGCGAGCAGAGAGGGAGTAG	TGAGTTCCATGAAGGCAGGATG			

Table S7: Primary antibodies used in the current study

Primary antibodies used in the current study				
Name	Host	Dilution	Vendor	Catalog#
Anti-GAPDH	Mouse	1/1000	Santa Cruz Biotechnology	sc-365062
Anti-beta actin	Mouse	1/5000	Abcam	ab8227
Anti-MAP2	Mouse	1/200	Merck-Millipore	MAB3418
Anti-NESTIN	Rabbit	1/200	Merck-Millipore	ABD69
Anti-α-Synuclein (αSyn)	Mouse	1/500	BD Biosciences	610787
Anti-phosphorylated α-Synuclein (Ser129)	Mouse	1/10000	WAKO	015-25191
Anti-TH	Rabbit	1/500	Merck-Millipore	AB152
Anti-VGLUT1	Mouse	1/1000	Merck-Millipore	MAB5502
Anti-TUJ1	Mouse	1/1000	Biolegend	801202
Anti-PAX6	Mouse	1/100	DSHB	AB 528427
Anti-ki67	Rabbit	1/400	Abcam	ab15580
Anti-Phospho-S6 Ribosomal Protein (Ser235/236)	Rabbit	1/1000	Cell Signalling	4858
Anti-S6 Ribosomal Protein (5G10)	Rabbit	1/1000	Cell Signalling	2217
Anti-Phospho-mTOR (Ser2448) (D9C2)	Rabbit	1/1000	Cell Signalling	5536
Anti- mTOR (7C10)	Rabbit	1/1000	Cell Signalling	2983
Anti-Phospho-PRAS40 (Thr246) (C77D7)	Rabbit	1/1000	Cell Signalling	2997
Anti-PRAS40 (D23C7)	Rabbit	1/1000	Cell Signalling	2691
Anti-TBK1/NAK	Rabbit	1/1000	Cell Signalling	3013
Anti-Phospho-TBK1/NAK (Ser172) (D52C2)	Rabbit	1/1000	Cell Signalling	5483
Anti-Phospho-PDK1 (Ser241)	Rabbit	1/1000	Cell Signalling	3061
Anti-PDK1 (D37A7)	Rabbit	1/1000	Cell Signalling	5662